Development of a Converter-Based Testing Platform and Battery Energy Storage System (BESS) Emulator for Microgrid Controller Function Evaluation

A Thesis Presented for the
Master of Science
Degree
The University of Tennessee, Knoxville

Dingrui Li
May 2021

ACKNOWLEDGEMENTS

First, I would like to thank my advisor Dr. Fred Wang, who gives me support and guidance in my study and research. I appreciate Dr. Wang for guiding me to find scientific methodologies and systematical ways of doing research. His insight and experience in power electronics also assisted me to focus on meaningful and practical topics in the research. I am grateful to Dr. Leon M. Tolbert for his instructions in my research. His suggestions and encouragement help me establish confidence at the beginning of my study. I would like to thank Dr. Kevin Bai for kindly accepting my invitation as a committee member. I also appreciate Dr. Daniel Costinett for his great patience and generous help on my course study. I also appreciate Dr. Yilu Liu and Mr. William Giewont for their great suggestions in my research.

Particularly, I would like to thank Drs. Yiwei Ma and Xingru Yan for their help and instructions on both research and daily life. Thanks to their help, I could get used to my life in UTK. I also want to thank Dr. Shiqi Ji for his instructing me on creating good research habits. I am grateful to all the project teammates who are Dr. Lin Zhu, Dr. He Yin, Dr. Jiaojiao Dong, Dr. Xiaojie Shi, Dr. Cheng Nie, Dr. Ruirui Chen, Dr. Li Zhang, Dr. Shida Gu, Mr. Chengwen Zhang, Mr. Yu Su, Mr. Xiaotong Hu, Mr. Montie Smith, Mr. James Palmer, Mr. John Meadors, and Ms. Min Lin. By cooperating and discussing with them, I gained a lot of valuable experience and new knowledge in doing research. It was a pleasure to work with them.

Meanwhile, I want to appreciate the mentorship and help from all the colleagues and friends in CURENT, which include but are not limited to Mr. Zhihao Jiang, Mr. Wen Zhang, Dr. Yunting Liu, Dr. Jingxin Wang, Mr. Zhou Dong, Mr. Haiguo Li, Ms. Le Kong, Mr. Liang Qiao, Ms. Jingjing Sun, Mr. Ruiyang Qing, Mr. Zhe Yang, Dr. Handong Gui, Dr. Ren Ren, Mr. Zihan Gao, Ms. Shuyao Wang, Mr. Jiahao Niu, Mr. Yang Huang, Mr. Liyan Zhu, Mr. Yu Yan, Mr. Nattapatt Praisuwanna, Ms. Paychuda Kritprajun, Mr. Hoang Phuc T Pham, Mr. Jie Li, Dr. Bo Liu, Dr. Pengfei Yao, Dr. Chongwen Zhao. With their support and assistance, I make a lot of progress in both research and enjoying life.

I also owe my gratitude to all the CURENT and EECE staff members, including but not limited to, Mr. Robert Martin, Mr. Jay Cooley, Ms. Wendy Smith, Ms. Anne Skutnik, Mr. Ryan Smiley, Ms. Lisa Beard, Ms. Kimberly Anne Cox, and Ms. Dana Bryson.

Most importantly, I would like to thank my family, especially my grandfather Kaiyue Li, for his unconditional love in 24 years. I want to thank my father Guoqing Li, my mother Qingling Xue, and my grandmother Suqing Tang for their love and belief. Last but not the least, I want to thank my dearest girlfriend, Jiangyun Qi, for her presence, company, and love.

ABSTRACT

The microgrid has attracted increasing research attention in the last two decades. Due to the development of renewable energy resources and power electronics technologies, the future microgrid will trend to be smarter and more complicated. The microgrid controller performs a critical role in the microgrid operation, which will also become more and more sophisticated to support the future microgrid. Before final field deployment and test, the evaluation and testing of the controller is an indispensable step in the controller development, which requires a proper testing platform.

However, existing simulation-based platforms have issues with potential numerical oscillation and may require huge computation resources for complex microgrid controllers. Meanwhile, field test-based controller evaluation is limited to the test conditions. Existing digital simulation-based platforms and field test-based platforms have limitations for microgrid controller testing. To provide a practical and flexible controller evaluation, a converter-based microgrid hardware testbed is designed and implemented considering the actual microgrid architecture and topology information. Compared with the digital simulation-based platforms, the developed microgrid testing platform can provide a more practical testing environment. Compared to the direct field test, the developed platform is more flexible to emulate different microgrids.

As one of the key components, a converter-based battery energy storage system (BESS) emulator is proposed to complete the developed testing platform

based on the testing requirements of microgrid controller functions. Meanwhile, the microgrid controller testing under different microgrid conditions is also considered.

Two controllers for the microgrid with dynamic boundaries are tested to demonstrate the capability of the developed platform as well as the BESS emulator. Different testing cases are designed and tested to evaluate the controller performance under different microgrid conditions.

TABLE OF CONTENTS

Chapter 1. Introduction 1

1.1 Microgrid Concepts 1

1.1.1 Microgrid Operation 1

1.1.2 Microgrid with Dynamic Boundaries 2

1.2 Microgrid Central Controller Testing 4

1.3 BESS in Microgrids 7

1.4 Motivation and Objectives 9

1.5 Organization of the Thesis 11

Chapter 2. Literature Review 14

2.1 Converter-based HTB emulation 14

2.1.1 Converter-Based HTB Architecture 14

2.1.2 Grid Components Emulation 17

2.1.3 System-Level Study 21

2.2 BESS Operation (BMS Functions) 24

2.2.1 BESS Cell Voltage Balancing 24

2.2.2 BESS SOC Estimation 26

2.3 BESS Interaction with Power Grids 28

2.3.1 Grid Frequency Regulation 28

2.3.2 Grid Voltage Support 30

2.3.3 Grid-Forming Operation for Islanded Microgrid 31

2.4 Summary and Research Objectives 33

Chapter 3. Converter-Based Microgrid Controller Testing Platform 35

3.1 Control Architecture Design 35

3.1.1 Actual Microgrid Control Architecture 35

3.1.2 Microgrid HTB Control Architecture Design 36

3.2 Example Microgrid Topology 38

3.2.1 Microgrid with Dynamic Boundaries 38

3.2.1 Microgrid with Multiple Sources at Different Locations 39

3.3 Microgrid HTB Emulation 40

3.3.1 Microgrid Line Emulation 43

3.3.2 Microgrid Smart Switch Emulation 47

3.3.3 Microgrid Component Emulators 50

3.3.4 Experimental Results of Emulators 55

3.3.5 HTB Reconfiguration Design 58

3.3.6 Hardware Implementation 58

3.4 Summary 61

Chapter 4. Microgrid Controller HTB Testing Required BESS Functions 63

4.1 Microgrid Controller Functions 63

4.1.1 Functions for Microgrid Information Input 63

4.1.2 Functions for Recording 64

4.1.3 Functions for Long-Time Microgrid Operation 64

4.1.4 Functions for Real-Time Microgrid Operation 65

4.2 BESS Emulator Functions 68

4.2.1 SOC Indication 71
4.2.2 BESS Functions in Grid-Connected Mode 73
4.2.3 BESS Functions in Islanded Mode 76
4.2.4 BESS Functions in Transitions 83
4.3 Experimental results 86
4.3.1 BESS in Grid-Connected Mode with Grid Suddenly Unavailable 86
4.3.2 BESS in Grid-Connected Mode with Fault Occurred 86
4.3.3 BESS Startup and Steady-State Islanded Operation 88
4.3.4 BESS in Islanded Mode with Fault Occurred 90
4.3.5 BESS in Islanded Mode with Secondary Control 90
4.4 Summary 92
Chapter 5. Demonstration of Microgrid Controller HTB Testing 93
5.1 Controller for Microgrid with Dynamic Boundaries 93
5.1.1 Black Start Test 93
5.1.2 Steady-State Islanded Operation Test 94
5.1.3 Reconnection Test 97
5.1.4 Islanding Test 101
5.1.5 Steady-State Grid-Connected Operation Test 101
5.1.6 Protection Coordination Test 104
5.2 Controller for Microgrids with Dynamic Boundaries and Multiple Sources at Different Locations 105
5.2.1 Black Start Test 107

5.2.2 Steady-State Islanded Operation Test 107
5.2.3 Reconnection Test 107
5.2.4 Islanding Test 109
5.2.5 Steady-State Grid-Connected Operation Test 112
5.3 Summary 115
Chapter 6. Conclusions and Future Work 116
6.1 Conclusions 116
6.2 Future Work 118
References 120
Vita 129

LIST OF TABLES

Table 3 - 1 Line impedance in the microgrid HTB 46

Table 3 - 2. Microgrid HTB parameters. 49

Table 3 - 3. Grid components' rating in HTB testing. 49

Table 4 - 1. Summary of microgrid central controller functions..... 66

Table 4 - 2. Microgrid central controller modes and transitions 70

Table 5 - 1. Summary of testing cases for the controller of microgrid with dynamic boundaries 95

Table 5 - 2. Testing scenarios for the controller of microgrid with dynamic boundaries and multiple sources 106

LIST OF FIGURES

Fig. 1 - 1. Microgrid concept. 3

Fig. 1 - 2. Microgrid transition logic [6]. 3

Fig. 1 - 3. BESS structure. 8

Fig. 2 - 1. HTB architecture [38]....15

Fig. 2 - 2. Converter connection structure in HTB. 15

Fig. 2 - 3. HTB converter emulator. 19

Fig. 2 - 4. Existing HTB grid emulators. 19

Fig. 2 - 5. System level emulation and study. 23

Fig. 2 - 6. Active cell balancing methods for BESSs [54]. 23

Fig. 2 - 7. Battery SOC estimation methods [59]. 27

Fig. 2 - 8. BESS active transferring. 32

Fig. 2 - 9. BESS reactive support. 32

Fig. 3 - 1. Control architecture of an actual microgrid [13]....37

Fig. 3 - 2. Control architecture for microgrid HTB. 37

Fig. 3 - 3. Example topology 1: microgrid with dynamic boundaries. 41

Fig. 3 - 4. Example topology 2: microgrid with dynamic boundaries and multiple sources. 42

Fig. 3 - 5. Series RL model for microgrid lines. 45

Fig. 3 - 6. Line emulator design. 45

Fig. 3 - 7. Smart switch emulator and control structure. 48

Fig. 3 - 8. Testing results of smart switch emulators. 48

Fig. 3 - 9. Main distribution grid emulator. 52
Fig. 3 - 10. Control of the generator emulator. 52
Fig. 3 - 11. Control diagram of the load emulator. 52
Fig. 3 - 12. Control of the PV emulator 54
Fig. 3 - 13. Control of the fault emulator 54
Fig. 3 - 14. Test waveforms of grid and load emulators. 57
Fig. 3 - 15. Test waveforms of the generator emulator. 57
Fig. 3 - 16. Test waveforms of the PV emulator. 57
Fig. 3 - 17. Test waveforms of the fault emulator. 59
Fig. 3 - 18. HTB reconfiguration design. 59
Fig. 3 – 19. Emulating cabinet of microgrid HTB. 60
Fig. 4 – 1. Finite state machine. 69
Fig. 4 - 2. BESS emulator functions for microgrid central controller testing. 69
Fig. 4 - 3. BESS SOC indication function. 72
Fig. 4 - 4. BESS emulator control algorithms in grid-connected mode. 77
Fig. 4 - 5. BESS emulator control algorithms in islanded mode. 79
Fig. 4 - 6. Power transferring for two grid-forming BESS emulators 79
Fig. 4 - 7. Primary and secondary droop control. 82
Fig. 4 - 8. Merged island black start control. 82
Fig. 4 - 9. PLL-based startup control method. 85
Fig. 4 - 10. Control mode transition of BESS emulator. 85

Fig. 4 - 11. Experimental waveforms when grid suddenly becomes unavailable in grid-connected mode. 87
Fig. 4 - 12. Experimental waveforms when the grid is unavailable, and fault still occurs. 87
Fig. 4 - 13. Experimental waveforms of BESS emulator's startup and operation in islanded mode. 89
Fig. 4 - 14. Experimental waveforms of BESS fault ride through in the islanded mode. 89
Fig. 4 - 15. Experimental waveforms BESS emulator operation in islanded mode. 91
Fig. 5 - 1. Testing results of steady-state islanded operation..... 95
Fig. 5 - 2. Testing results of steady-state islanded operation. 96
Fig. 5 - 3. Detailed information of steady-state islanded operation. 96
Fig. 5 - 4. Oscilloscope waveforms of the reconnection transition. 99
Fig. 5 - 5. Detailed information of reconnection transition. 99
Fig. 5 - 6. Experimental results of reconnection process through switch 0608 acquired from controller data logging function. 100
Fig. 5 - 7. Oscilloscope waveforms of the unplanned islanding transition. 102
Fig. 5 - 8. Detailed information of the unplanned islanding transition. 102
Fig. 5 - 9. Waveforms of grid-connected mode with dynamic boundary operation 103
Fig. 5 - 10. Fault applied at load L6 in the grid-connected mode. 103

Fig. 5 - 11. Protection coordination testing results in grid-connected mode. 106
Fig. 5 - 12. Protection coordination testing results in islanded mode. 106
Fig. 5 - 13. Black start for a microgrid with multiple sources at different locations. 108
Fig. 5 - 14. Testing results for the islanded operation of two separate islands. . 108
Fig. 5 - 15. Process of two separate islands reconnected to the main grid. 110
Fig. 5 - 16. Testing waveforms of two separate islands reconnecting to the main grid. 110
Fig. 5 - 17. Process of two separate islands merging to a large microgrid and reconnected to the grid. 111
Fig. 5 - 18. Testing waveforms of two separate islands merging to a large microgrid and reconnecting to the grid. 111
Fig. 5 - 19. Testing waveforms of the planned island separating from one merged island to multiple separate islands. 113
Fig. 5 - 20. Testing waveforms of planned islanding grid-connected mode to one merged island. 113
Fig. 5 - 21. Testing waveforms of energy management in the grid-connected mode. 114

CHAPTER 1. INTRODUCTION

1.1 Microgrid Concepts

1.1.1 Microgrid Operation

Nowadays, with the development of distributed energy resources (DERs) and power electronics technologies, microgrids have been rapidly developed. Compared with traditional distribution grids, microgrids have demonstrated advantages in increasing local grid resiliency [1], promoting renewable energy integration [2], etc.

A microgrid can be formed by a group of loads and localized generation, which can either be connected to the main distribution grid or disconnect from the main grid to work as an island [3]. A simple microgrid is shown in Fig. 1 - 1. There are two main steady-state operation modes for a microgrid, which are grid-connected mode and islanded mode [4].

In the grid-connected mode, the microgrid is connected to the main grid and shares the power with the main grid. In the islanded mode, the microgrid has no power sharing with the main grid. However, there may be some critical loads that cannot lose power such as hospitals, airports, etc. The microgrid should keep the critical loads operating. Therefore, in the islanded mode, DERs in the microgrid establish stable voltage and frequency and provide power to support critical loads [5].

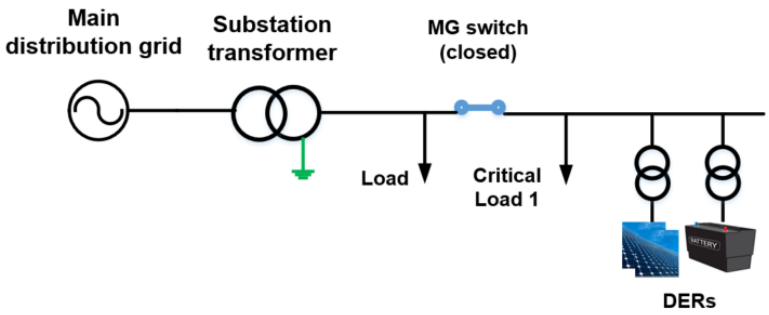
A microgrid can switch the operation mode and the switching processes are defined as transitions. According to reference [6], microgrid transitions are

summarized in Fig. 1 - 2. For a microgrid, there are four types of transitions including unplanned islanding, planned islanding, black start, and reconnection. Planned islanding describes the transition from grid-connected mode to islanded mode Planned islanding normally happens during equipment maintenance. Unplanned islanding usually happens during grid fault conditions [7]. During fault conditions in grid-connected mode, the grid protection detects and isolates the fault, which results in islanding transition. During unplanned islanding, the transients of voltage and power can be large because the microgrid controller cannot determine the islanding information in advance.

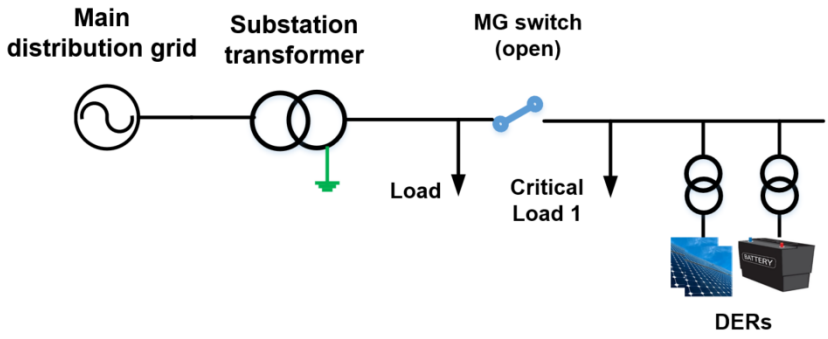
Black start is the start-up transition. The microgrid starts from shutdown to steady-state islanded operation with generation ramping up to support critical loads. Reconnection is the transition from islanded mode to grid-connected mode [8], which usually requires specific reconnection control for the transition.

1.1.2 Microgrid with Dynamic Boundaries

As shown in Fig. 1 - 1, the switch where the microgrid connects or disconnects to the main grid is defined as the microgrid boundary. For a microgrid with a fixed boundary, the DERs in the microgrid can only support the loads within the microgrid boundary, which may limit the usage of renewable energies in the microgrid. Due to the development of automation technologies and the application of smart switches, the loads become sectionalized in the distribution grid, which enables the dynamic boundary capability of microgrids [9].



(a) Grid-connected mode



(b) Islanded mode

Fig. 1 - 1. Microgrid concept.

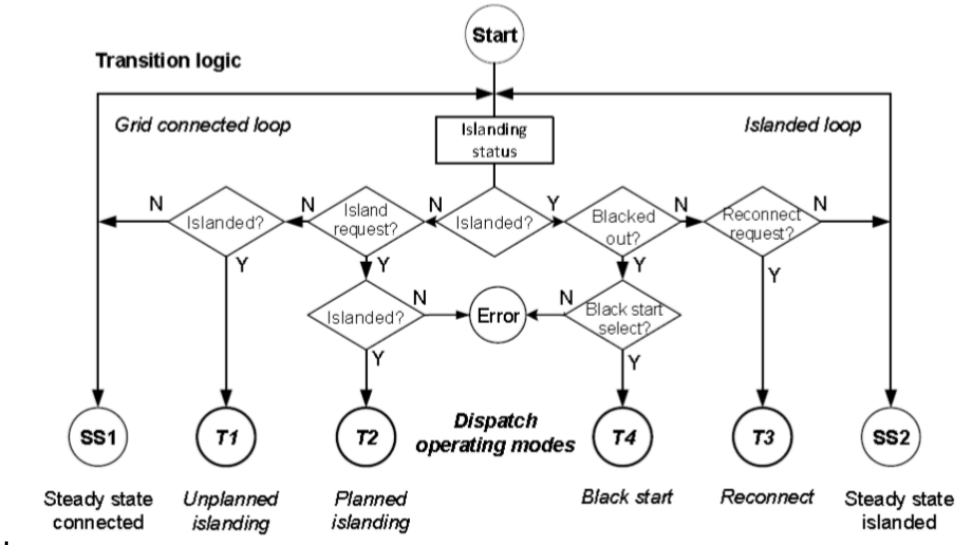


Fig. 1 - 2. Microgrid transition logic [6].

A microgrid with dynamic boundaries can fully utilize the DER generation by shrinking or expanding microgrid boundaries to shed or pick up non-critical loads in the microgrid. By fully utilizing the DER generation, more renewable energy can be integrated for load support. Moreover, the microgrid with dynamic boundaries can provide better fault isolation capability as the fault at non-critical load sections can be isolated by changing the boundary of the microgrid [10].

However, as a future microgrid concept, the microgrid with dynamic boundary is also faced with lots of challenges, especially on the control and operation, including the real-time power management [11], topology identification [10], protection strategies design and coordination [12]. To realize the reliable and stable operation of the microgrid with dynamic boundaries, one solution is to apply a centralized controller to control the whole microgrid and coordinate different operation-required functions [13], which requires thorough testing and evaluation of the controller performance before field implementation.

1.2 Microgrid Central Controller Testing

For a microgrid with a centralized control structure, the microgrid controllers include the central controller and local controllers. The central controller is the main controller of the whole microgrid while the local controller is the controller for a specific microgrid component. The microgrid central controller plays an important role in a microgrid, which can coordinate different DERs, keep the microgrid power flow balanced, and coordinate with the grid fault protection functions. Meanwhile, the operational objective for a microgrid should be realized through the central

controller, which can achieve high energy usage efficiency, ensure system stability and safety, or realize economic operation.

An actual microgrid may have different and complicated operation modes and conditions, especially for the future microgrid such as a microgrid with dynamic boundaries. To ensure normal and safe operation before field deployment, the evaluation and testing of microgrid controller performances are critical [14]. To realize efficient microgrid controller evaluation, the testing platform is one of the key parts. Existing microgrid controllers are normally tested or verified on pure simulation platforms [15], hardware in-the-loop testing platforms [16], or in the actual field [17].

Pure simulation can be realized in MATLAB Simulink, PSCAD, etc., which is an easy and cost-effective way of implementing the testing. However, in the pure simulation, the controller needs to be modeled in the simulation, which may have numerical instability and lose accuracy. The whole microgrid model can be very complex, which increases the computation burden of the processor. Moreover, in a purely digital simulation, real-time testing cannot be realized, and it is hard to test the controller for a relatively long-time scale.

To overcome these disadvantages, HIL testing is applied for the microgrid controller verification [18-20]. The controller HIL testing represents that the actual microgrid controller is implemented in the testing while other parts of the microgrid are modeled through digital simulations. The platform of HIL testing includes Real Time Digital Simulator (RTDS), RT-Lab, etc. In the HIL testing, real-time testing

results can be adopted, which can realize long-timescale verification. However, since the rest of the microgrid is modeled in the digital simulation, several critical factors of the microgrid may not be taken into consideration, including delays, measurement errors, non-linearity, etc. If practical factors were considered for all the components in microgrids, the models would become extremely complicated and cause a heavy computational burden. Moreover, numerical oscillations caused by the discontinuities or interpolation in digital simulation can also impact the testing results.

To improve the microgrid model accuracy, some researchers combined the controller HIL with equipment power hardware in-the-loop (PHIL) by applying actual equipment in the controller HIL testing [21-23]. Reference [21] added the actual DER controller in the microgrid controller HIL testing. Reference [22] provided an actual power interface to test the energy management system of the controller. Reference [23] implemented actual DER inverters in the microgrid controller HIL testing. However, the numerical oscillation issues still may occur in this hybrid HIL testing.

To avoid the numerical oscillation, one direct solution is the actual field testing [24-25]. Actual field testing can achieve the most accurate testing results while this is also the most expensive way. In the meantime, some community microgrids are built on existing utility grids, and the controller testing may impact the grid operation and cause disturbance to the customer. Therefore, finding a

proper testing platform to balance the model accuracy and cost is still a challenge for microgrid controller testing.

1.3 BESS in Microgrids

A microgrid is a great scenario for integrating high penetration renewable energies such as wind [26-27], solar [28-29], etc. Renewable energies are usually affected by weather or other natural factors, which cannot continuously meet the real-time load demand in microgrids. To realize reliable support to loads especially critical loads, applying BESSs is usually a solution in microgrids.

Compared with other energy storage equipment like flywheels, BESSs can achieve both high energy density and high efficiency. BESSs can bring numerous benefits to microgrids, including reducing energy losses, increasing usage efficiency of generation sources [30], promoting microgrid reliability, etc. As shown in Fig. 1 - 3, a BESS in the microgrid usually consists of battery packs, battery management systems (BMSs), control circuits, and the power converter interface.

The BMS monitors and manages the battery packs to realize voltage balancing and battery protection [31]. The energy conversion between battery packs and microgrids is realized through interface converters. Interface converters are usually composed of a dc/dc converter and dc/ac inverter where the dc/ac inverter is directly connected to the microgrid. The battery packs share active power with the microgrid through interface power converters. Moreover, the interface dc/ac inverter can also provide the microgrid with reactive power to support the microgrid voltage [32].

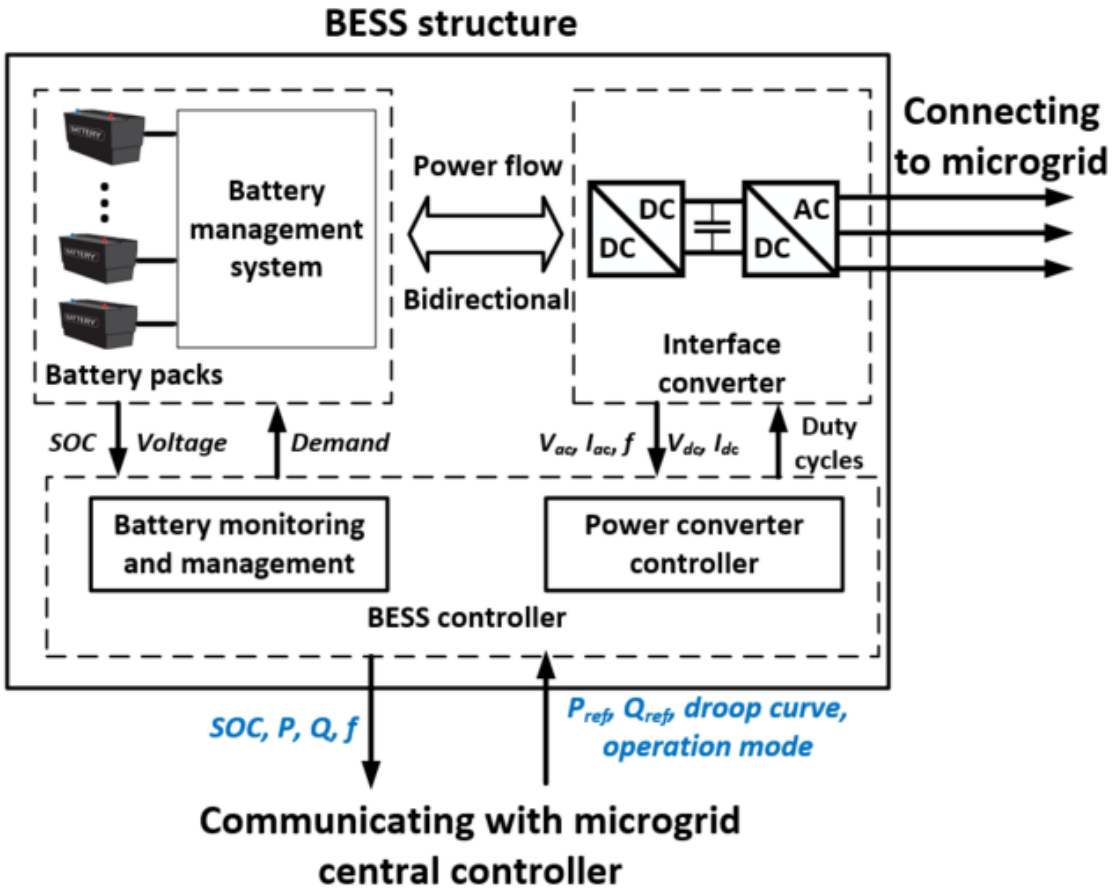


Fig. 1 - 3. BESS structure.

Each BESS requires a local controller which can coordinate with the BMS, control interface converters, and communicate with the microgrid central controller. The BESS local controller normally receives power references, secondary droop control commands [33], and system operation mode information from the microgrid central controller. In the meantime, to support microgrid operation, the local controller can provide the central controller with actual battery output power, battery state of charge (SOC) [34], etc.

BESSs are one of the key components in microgrids. In order to test the microgrid central controller, based on the testing requirements, a well-modeled and well-emulated BESS is needed. The emulation should at least include both the ac outputs characteristics (voltage, current, frequency), local controller functions, and communication with microgrid central controllers.

1.4 Motivation and Objectives

Central controller testing is a significant part of microgrid development. However, the challenges of testing a microgrid central controller come from two perspectives which are the testing platform and microgrid model. From the testing platform perspective, existing microgrid controllers are usually realized through HIL or actual field testing. Using the former platform usually has potential numerical oscillation issues and requires significant computation resources when the microgrid operation is complex. Moreover, it is also easy to ignore some practical but necessary factors in digital simulation models, which leads to inaccurate evaluation of the testing results. For the latter platform, although field testing is the

straightforward way of testing the controller, it still has challenges in coordinating with the utility customers, inconvenience on data monitoring, and difficulties of function debugging. In the meantime, field testing is also a costly approach for microgrid controller testing.

From the microgrid model perspective, a relatively accurate and comprehensive microgrid model is the prerequisite of central controller testing. Compared with traditional distribution grids, microgrids have different operation modes (grid-connected, islanded, etc.) and transitions among different modes. To support these operations and transitions, one of the key components is the BESS.

BESS can increase energy usage in the grid-connected mode and can also work as the voltage source in islanded mode to provide the microgrid with stable voltage and frequency [33]. However, the existing study of BESS focuses on modeling the actual physical characteristics [35] or realizing one function for a certain microgrid operation scenario [36]. There is no specific BESS model that is designed based on microgrid central controller testing requirements. Therefore, developing a comprehensive and accurate BESS model is important in microgrid central controller testing.

The first motivation of this work is to develop a new testing platform for the microgrid central controller testing. The challenge of this work is to develop a new testing platform that can achieve relative practical testing and avoid numerical oscillation issues. Then the second motivation is to propose a comprehensive BESS emulating model that is specific for the proposed controller testing platform.

The challenges are to define the requirements of microgrid central controller testing and coordinate among different functions. Furthermore, for future microgrids such as microgrids with dynamic boundaries or multiple sources, the topology and operation conditions can be much more complicated than existing microgrids. The proposed testing platform and BESS model should be able to serve future microgrids.

This thesis first designs and realizes a converter-based microgrid controller testing platform. The developed testing platform is reconfigurable to test different microgrid topologies. Then, a BESS emulator is proposed by considering different microgrid central controller function requirements and microgrid conditions. By realizing the platform and BESS emulator as well as coordinating with other microgrid emulators, two microgrid central controllers are tested. The first one is the controller for microgrids with dynamic boundaries, and tests are realized under both normal and fault conditions. The second one is the controller for microgrids with multiple sources. The testing focuses on the steady-state operation and mode transitions.

1.5 Organization of the Thesis

The goal of this thesis is to develop a flexible and practical testing platform and a BESS emulator for microgrid controller testing. From exploring actual microgrid control and operation conditions, a converter-based microgrid hardware testbed (HTB) is designed and implemented. A BESS emulator for the microgrid HTB is proposed considering the requirements of microgrid central controller

functions as well as different microgrid conditions. The developed microgrid HTB with the proposed BESS emulator is applied for the testing of two example microgrid controllers.

Chapter 2 reviews the previous emulation of the converter-based HTB, including component-level emulation and system-level emulations. The control functions of BESSs are also reviewed, including the control functions of the BMS system as well as the interface controller. Based on the review, the research gaps and objectives are defined.

Chapter 3 introduces the details of the design and implementation of converter microgrid HTB. The design is based on an actual microgrid considering the control architecture and microgrid topology. The microgrid HTB emulation is discussed, including line emulation, smart switch emulation, microgrid source and load emulation, and reconfiguration design. The hardware implementation of the designed microgrid HTB is also introduced.

Chapter 4 introduces the BESS emulator functions based on microgrid controller testing requirements, including the requirements of different controller functions as well as different microgrid operation modes and conditions. Experimental results of the proposed BESS emulator functions are also provided.

Chapter 5 demonstrates the controller testing of the developed microgrid HTB with the proposed BESS emulator. Two microgrid controllers are tested, which are the controller for the microgrid with dynamic boundaries and the

controller for a microgrid with dynamic boundaries and multiple sources at different locations.

Chapter 6 concludes the work in this thesis and the future work about the microgrid HTB development and BESS emulator function improvement is stated.

CHAPTER 2. LITERATURE REVIEW

The converter-based hardware testbed (HTB) has been widely applied for transmission-level systems emulation. In the HTB, power converters emulate grid components by emulating the output electrical characteristics of the components. BESS is one of the key components in power grids. There are numerous efforts on exploring the control and operation of BESSs. In this chapter, first, the research of transmission level emulation of converter-based HTB will be reviewed, including the HTB architecture, the component emulation, as well as the system operation emulation. Meanwhile, existing research on BESS control and emulating in power grids will also be summarized.

2.1 Converter-based HTB emulation

The converter-based HTB is a power grid emulation platform [37] and has demonstrated its capability in transmission system study [38]. A power grid is composed of diverse components such as generators, loads, DERs, power lines, etc. Therefore, it is required for the HTB to emulate different grid components correctly. After all the emulators are prepared, the HTB can be used for the system level study such as damping control [39], stability analysis [40], etc.

2.1.1 Converter-Based HTB Architecture

The overall architecture of the existing HTB is shown in Fig. 2 - 1. There are three layers in the HTB architecture, which are the system-level controller, local processors, and converter hardware [37]. The system-level controller is composed of a visualization interface and a central controller programmed with LabVIEW.

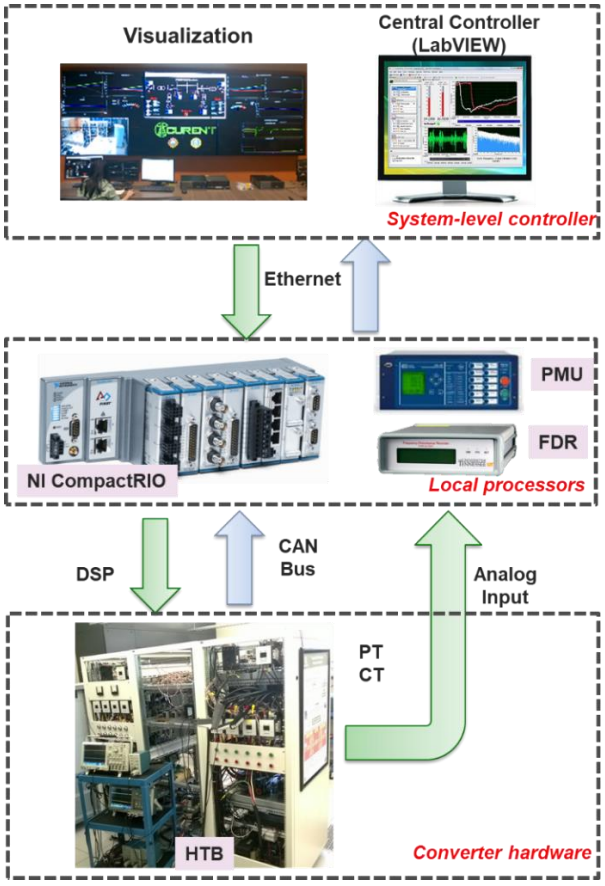


Fig. 2 - 1. HTB architecture [38].

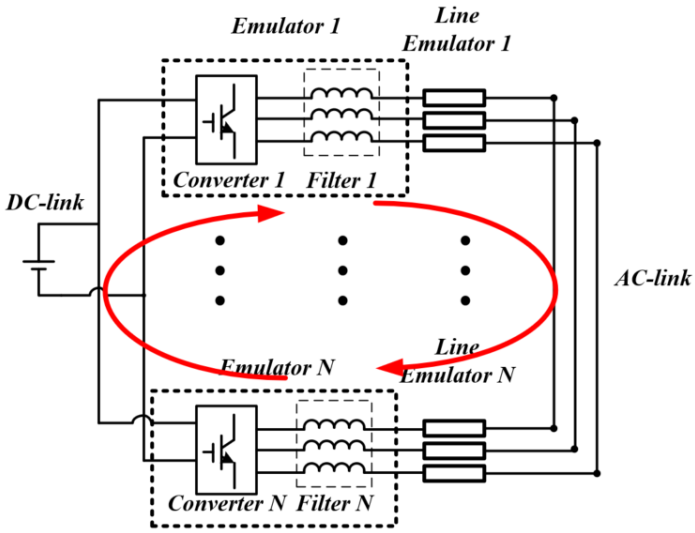


Fig. 2 - 2. Converter connection structure in HTB.

The system-level controller is applied to realize different system operations, which can emulate the control center of utility companies. The system-level controller can get load profiles and start/stop commands from operators. Meanwhile, the sensing feedbacks from local processors are received by the system-level controller for the system-level closed-loop control.

The local processors are applied for certain system areas, which can receive feedback and issue commands to a specific area. The local processors contain CompactRIOs (cRIOs) from National Instruments, phasor measurement units (PMUs) [41], and frequency disturbance recorders (FDRs) [42]. cRIOs are used to communicate between the system-level controller and the power converters [38] to realize the remote converter control; PMUs and FDRs are applied to gather the information from converter output for system-level control. The communication between local processors and system-level controllers is realized through ethernet.

Main circuits in HTB are composed of power converters. As shown in Fig. 2 - 2, the paralleled structure is utilized for HTB. Each grid component is emulated by a two-level dc/ac power converter. All the power converters share the same dc link and ac link to circulate the active power within the circuit, which can improve the power usage efficiency in the lab. The ac link connection is determined by the emulated grid topologies. Therefore, by changing the emulator model and ac-link connections, the HTB has the flexibility to emulate different power grids.

The communication between power converters and CRIOs is realized through CAN bus. The CRIOs issue commands and control references from the system-level controller to DSPs of converters while converters provide CRIOs with analog sensing and control feedback. PMUs and FDRs can get the phase and frequency from the HTB and directly communicate with the central controller in the system-level controller.

2.1.2 Grid Components Emulation

In the HTB, each grid component is usually emulated by a single inverter. As shown in Fig. 2 - 3, grid component models are implemented to generate the ac control references and the ac output voltage and current information are sensed back to realize the control. Therefore, by changing the model, the converter emulator can flexibly emulate different grid components.

The overall grid component emulation is summarized in Fig. 2 - 4. Numerous grid components have been emulated in the HTB, including synchronous generators [43-44], renewable energy resources [45-46], energy storage systems [47], ac transmission lines [48], and electrical loads [49].

The synchronous generator emulator models include the automatic voltage regulator (AVR), excitation control (PSS), governor, and protection. The emulated model evaluates the emulation accuracy and provides guidance on the design of the generator emulation control.

Renewable energy sources include solar photovoltaics (PVs) and wind turbines. The PV emulator models a two-stage PV inverter by considering

maximum power point tracking mode (MPPT) and reserved power control of boost converter [46]. Furthermore, virtual impedance control is proposed in the PV emulator to assist the power compensation and improve the power transfer capability.

The second renewable energy emulator is the wind turbine. In the existing HTB, the behaviors of full-converter wind turbine (FCWT) are emulated by a single inverter and verified under grid cases [50]. Based on the basic wind turbine model, the virtual synchronous generator control and short-term energy storage capability are added to the wind turbine emulator [45]. The enhanced wind turbine emulator can achieve better dynamic response and store the energy to improve the energy usage efficiency. Meanwhile, the wind turbine emulator can both connect with the grid or operate stand-alone to work as a voltage source.

The third type of emulator in the existing HTB is energy storage. Batteries and flywheels are two kinds of energy storage systems that have been emulated. The battery emulator includes both the chemistry behaviors as well as the power electronics interface electrical characteristics when the battery is connected to the grid. For the flywheel emulator, the static and dynamic characteristics of flywheels are modeled and the benefits of applying flywheels in the power systems are evaluated.

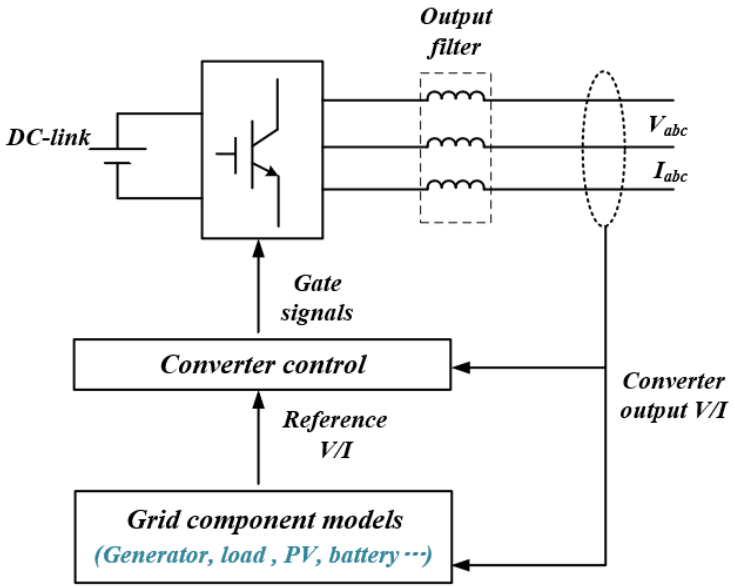


Fig. 2 - 3. HTB converter emulator.

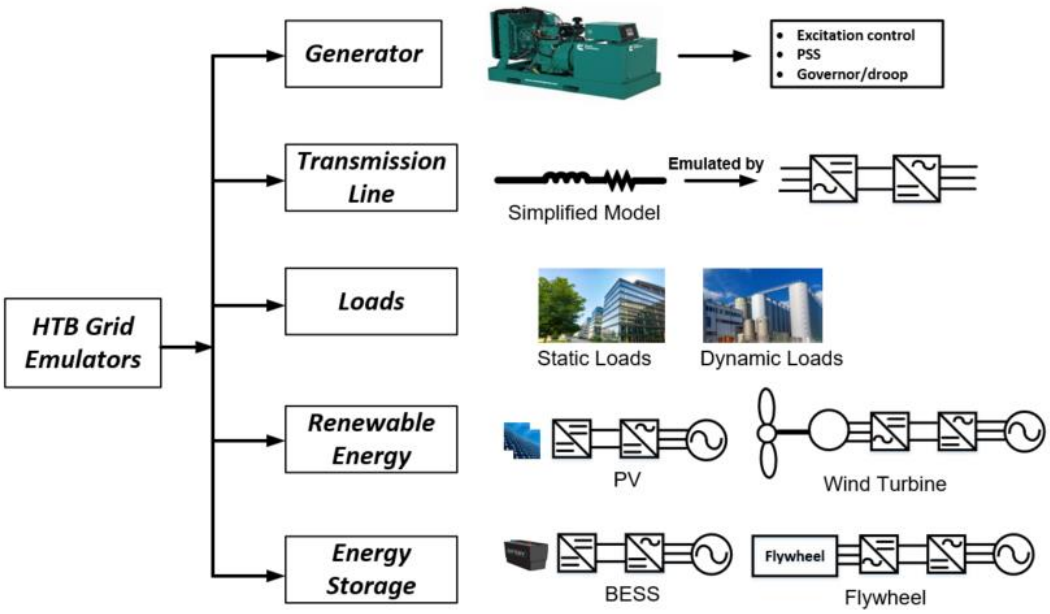


Fig. 2 - 4. Existing HTB grid emulators.

In addition to different types of sources and storage, loads and lines are also significant in transmission systems. In the existing HTB, the static and dynamic loads are also emulated by power converters. For the static loads, the constant-impedance, constant-current and, constant-power (ZIP) model is applied. The HTB emulator can emulate different combinations of ZIP loads by changing the current control references. For dynamic loads, an induction motor load model is utilized because induction motors are the major contributors to load dynamics and make up a large percent of the actual grid load. The HTB load emulator combines both the static and dynamic load models to form a comprehensive load model that can be used for the study of different grid scenarios.

Transmission lines are composed of inductance, resistance, and capacitance to transmit ac power. In the HTB emulator, a back-to-back connected two-level converter is applied as the transmission line emulator. A simplified π model is applied as the transmission line model. Moreover, based on the transmission line emulator, three-phase short circuit fault and switching between fault state and normal state are also emulated [48].

In addition to a three-phase fault on the transmission lines, a shunt-connected converter is applied to emulate different types of faults including single phase-to-ground faults, double phase-to-ground faults, phase-to-phase faults, and three-phase faults. By emulating the power grid fault, the HTB can potentially assist the research on power system protection.

2.1.3 System-Level Study

HTB is a real-time power grid emulating platform which can circulate the actual power, model the measurement noise and communication in a practical way, and has flexibility on the topology changes. Due to these features, the existing HTB has demonstrated its capability on the transmission level system study, which is shown in Fig. 2 - 5. Different operation and control issues in transmission systems are studied, which include power system stability, frequency control, and system separation.

The short circuit critical clearing time (CCT) is an important indicator for the power system transient stability assessment. In the HTB, the fault emulator can be used to identify the CCT of a system. By connecting the fault emulator at the target location and emulating the fault, the CCT can be estimated through the dynamic response of the system [38].

Low-frequency oscillation is a common issue in power systems and has impacts on the power transfer capability, which requires oscillation damping control. Traditional damping control approaches are normally designed and debugged offline, which lack adaptability. Recently, measurement-based online damping control methods are becoming more and more popular. The HTB is a qualified platform for debugging and verification of the measurement-based online damping control since the HTB has actual power flow and real measurement with noises. An adaptive time delay compensator-based online damping control method has been tested and verified on a two-area system emulated in HTB [51].

Voltage stability issue is another frequent stability issue in power systems. Forecasting and estimating the potential voltage stability and responding before the instability occurs is an efficient method of solving this issue. HTB has also played an important role in debugging and testing this approach. A measurement-based voltage stability assessment and control method is tested on the HTB with accuracy and practicality verified [40].

In the future power system, more and more renewable energy sources will be integrated into the grid through interface power converters. The interaction between power converters and passive components in the grid may lead to harmonic stability issues in the power system. The existing HTB is a useful platform for studying this issue because the HTB consists of multiple power converters and can naturally model converter behavior. A *d*-*q* impedance-based harmonic stability analysis approach and design methodology are verified on the HTB [52].

In addition to stability-related issues, frequency control is another key research for transmission systems. The integration of renewable energy sources will cause frequency excursions in power grids. By proposing or integrating frequency support control in renewable emulators such as PV and wind turbines, the HTB has been used to evaluate the performance and system-level impacts of frequency support control [45].

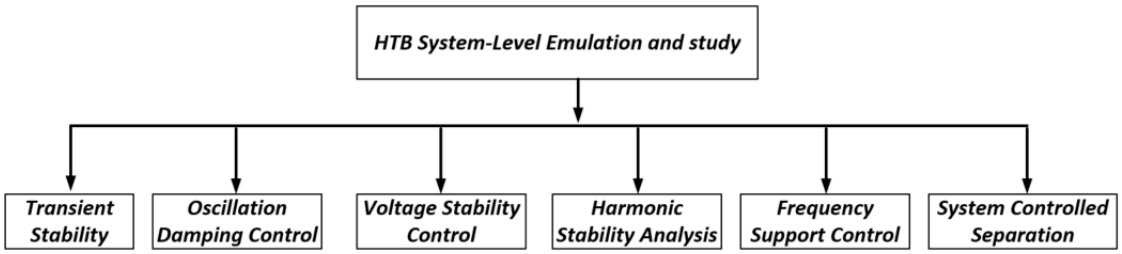


Fig. 2 - 5. System-level emulation and study.

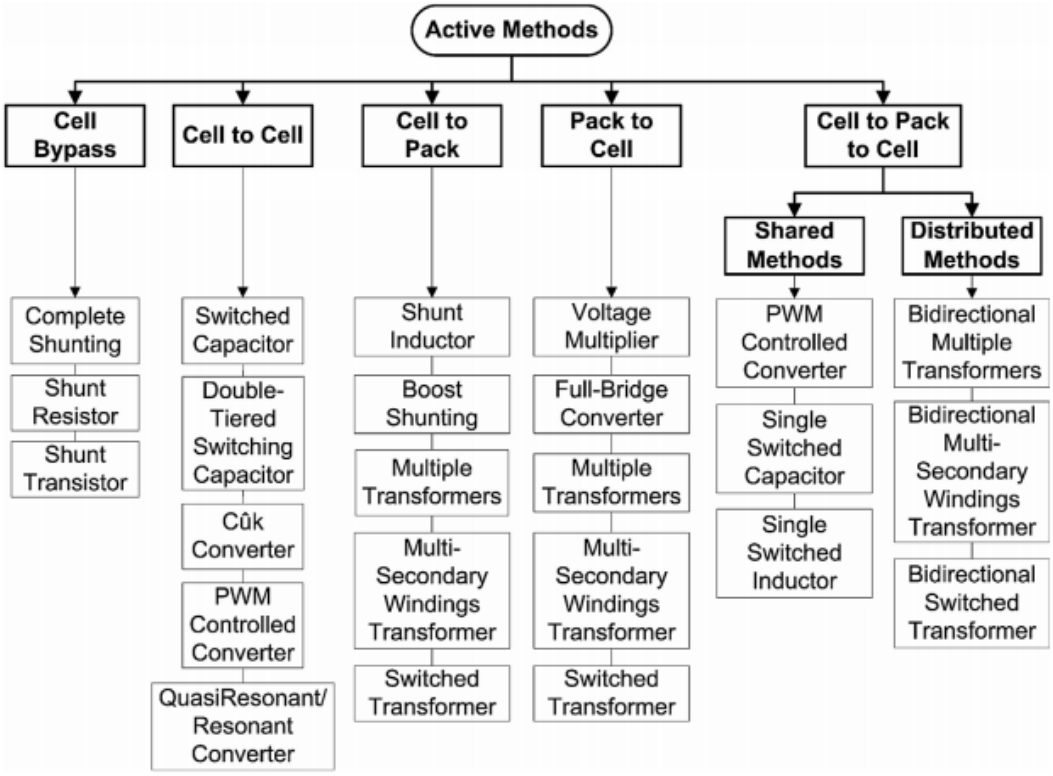


Fig. 2 - 6. Active cell balancing methods for a BESS [54].

The existing HTB has also been applied to assist study the system separation during large disturbances or grid fault conditions. The remedial action scheme is integrated into the system-level controller of HTB, and the controlled system separation is demonstrated on an emulated four-area system.

2.2 BESS Operation (BMS Functions)

BESSs have been widely applied in power grids as they can improve energy usage efficiency and grid resiliency. Plenty of research efforts have been taken on BESSs control and operation, which can be divided into two perspectives. The first type of research focuses on BMS to make the BESS operate normally. The architecture of a BESS is shown in Fig. 1 - 3. In a BESS, the BMS is operating to minimize the system temperature gradients, protect the cell degradation, provide optimal charging patterns, balance the cell voltage, ensure safe operation voltage, and current. Numerous solutions have been proposed to realize better management of BESS operation. Several functions are implemented in a BMS, which includes cell balancing, SOC estimation, battery charging control, where the cell balancing and SOC estimation have attracted attention for the BMS control.

2.2.1 BESS Cell Voltage Balancing

A BESS is usually formed by a series of low voltage battery cells. Cell balancing is necessary for a BESS, especially Lithium-based BESS, as it can protect the battery from overvoltage. There are two types of cell balancing methods which are passive balancing methods and active balancing methods [53]. In the passive balancing methods, shunting resistors are normally applied to dissipate

the unbalanced energy among different cells. The passive balancing approaches are simple to implement. However, the energy is dissipated to be heated, which increases the thermal stress and impacts the BESS lifetime.

An alternative for cell balancing is the active balancing method, which usually introduces external circuits to assist the cell voltage and energy balance. As shown in Fig. 2 - 6, the active methods have been divided into five types which are cell bypass, cell to cell, cell to pack, pack to cell and, cell to pack to cell [54]. In the cell bypass method, the BMS bypasses the cell current at the limited cell voltage. This function can be realized by adding controllable shunting resistors, shunting transistors, or shunting switches (complete shunting) [55].

The cell-to-cell approach is that the BMS transfers the energy among adjacent cells to keep the cell balanced [56]. This method relies on dc/dc power converters to conduct the control, including switching capacitor-based converters, PWM-controlled converters, resonant converters, etc. This method can realize relative accurate power transfer but has the issue for cases where the voltage differences occur on non-adjacent cells. The third approach is to transfer the energy from one highest-voltage cell to the whole pack by applying dc/dc converters. This method can deal with voltage unbalances on non-adjacent cells but cannot guarantee balancing efficiency [57]. The pack-to-cell approach is to transfer the energy from the whole pack to the cell with the lowest voltage by using dc/dc converters [58], which also has transferring efficiency issues. The last approach is to transfer the power from one cell to the pack and then to the other

cell. This method can improve the transferring efficiency and lead to high control complexity.

2.2.2 BESS SOC Estimation

Besides cell balancing, a BMS normally estimates the SOC of the BESS for monitoring real-time remaining capacity. As shown in Fig. 2 - 7, there are four types of basic approaches for the SOC estimation, containing the looking-up table approach, ampere-hour approach, model-based estimation, and data-driven estimation [59]. The SOC is usually related to parameters that include open-circuit voltage, impedances. By measuring these parameters and referring to the table that has the relationship between SOC and these parameters, the SOC can be estimated. However, in real applications, some parameters like open-circuit voltage are not available, therefore, this method is suitable for the SOC calibration rather than real application.

The second approach of SOC estimation is to do the integral of current over time to estimate the energy consumption. However, for this approach, the main challenge is that the initial SOC is usually unknown and the noise in the current measurement also impacts the estimation. The third approach is the model-based estimated approach, which is to get the SOC state equation from the model and apply nonlinear state estimation methods like Kalman filter [60] to estimate the SOC. The battery model becomes the key to this approach. Three commonly used battery models are the electrochemical model [61], equivalent circuit model [62], and the electrochemical impedance model [63].

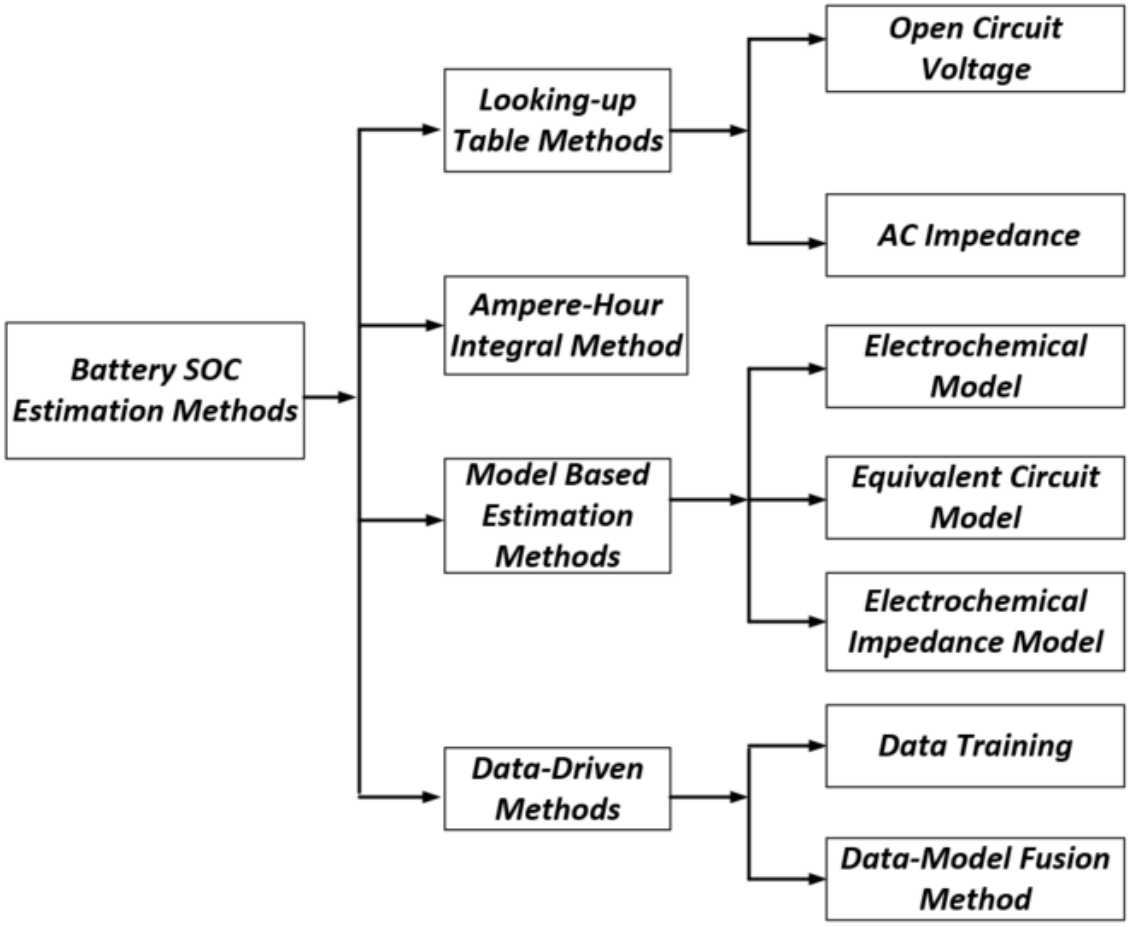


Fig. 2 - 7. Battery SOC estimation methods [59].

The last approach is the data-driven approach, which does not rely on the battery model. This approach relies on artificial intelligence technologies such as neural networks to train the relationship between input data (like terminal voltage) and output data (SOC), and then sequentially, the SOC can be estimated through the trained model. This method does not require an accurate battery model and requires historical data and may have issues like over-fitting when the model is not well selected and tuned.

2.3 BESS Interaction with Power Grids

In grid applications, there are numerous research efforts on studying the interactions between BESS and power grids. As shown in Fig. 1 - 3. BESS structure, a BESS is usually connected to the power grid through a dc/dc, dc/ac converter. The control of the interface converter can determine the BESS performances in the grid. The interactions between BESSs and power grids include the frequency regulation, voltage support, and grid-forming operation for the islanded microgrid.

2.3.1 Grid Frequency Regulation

In power grids, providing stable frequency is critical. Frequency deviations may cause high magnetizing current in motors and transformers as well as impact the electrical equipment that uses frequency for timing. The system frequency is normally determined by the active power balance between generation and loads with droop characteristics, meaning that when the load active power is higher/lower than the generation, the system frequency will drop/increase. The frequency is

regulated through active power control. Different levels of frequency control have been applied in the power grids, which include primary frequency, secondary frequency control, and tertiary frequency control [64].

The primary frequency control has the highest priority and should react within a few seconds. Since the output power of BESSs can have a fast response based on the control requirements, the BESS active power control can assist primary frequency regulation. When the grid generation does not match the load demands instantaneously, BESSs can absorb/deliver power to increase/decrease the grid frequency. Due to the limited storage capacity of BESSs, the primary frequency regulation of BESSs need to coordinate with the SOC of the battery to realize optimal and economic operation. Several control strategies have been proposed to realize the different targets of operation, including setting fixed or adjustable limits for SOC to avoid over-charge/discharge of the BESS, optimizing BESS operations based on certain objectives such as minimizing BESS usage [65], or designing the frequency regulation strategies considering the battery lifetime [66].

All the mentioned operation strategies are based on the BESS active power control, which is realized through the interface inverter control. As shown in Fig. 2 - 8, the active power is transferred from the batter packs through dc/dc and dc/ac inverter to the grid. Therefore, the control of the active power includes the regulation of both dc/dc and dc/ac inverters. The controller controls the output

voltage of the dc/dc converter as well as the output power of the dc/ac inverter [67].

2.3.2 Grid Voltage Support

To realize the stable and reliable operation of power systems, the grid voltage needs to be maintained stable. Stable grid voltage can improve the system's stability as well as protect equipment. The system voltage and reactive power have the droop characteristic. The output voltage can be regulated through reactive power control [32].

There are a few ways of controlling the system voltage, including reactive power sources, line reactance compensators, and regulating transformers. Since the BESS is connected to the power grid through a dc/ac inverter. The interface can provide reactive power to support grid voltage. The reactive support is limited by the interface inverter rating as high reactive power may increase the current stress of the semiconductor devices in the inverter. In the meantime, the reactive support strategies are determined by the system's needs.

Too much reactive power will increase the loss on the line and reduce the transmission efficiency. The reactive power control in the BESS is different from the active power control. As shown in Fig. 2 - 9, the reactive power is mainly provided by the interface inverter. The battery packs and the dc/dc converter will not provide reactive power. Therefore, the reactive support will be controlled by the controller of the dc/ac inverter.

2.3.3 Grid-Forming Operation for Islanded Microgrid

With the development of microgrids, BESSs have also been widely applied in microgrids. In the microgrid applications, besides frequency regulation and voltage support, the BESS inverters are also applied as grid-forming inverters to support the microgrid islanded operation [68].

In the microgrid islanded operation, the BESS inverter is controlled in the grid-forming mode to establish the microgrid voltage and frequency through droop control [68] or virtual synchronous generator control [69]. In the grid-connected mode, different control strategies are applied. The option is to keep the grid-forming operation of the BESS inverter [70], which can avoid efforts on the mode transition control. However, a grid-forming BESS inverter may interact with the main grid and result in potential stability issues.

The other option is that the BESS inverter works in the grid-following mode in the grid-connected mode while works in the grid-forming mode in the islanded mode [71]. However, this control method requires control mode transitions between grid-following mode and grid-forming mode. Different literatures have reported diverse transition control methods, including localized islanding detection-based transition [72], centralized islanding detection-based transition [73].

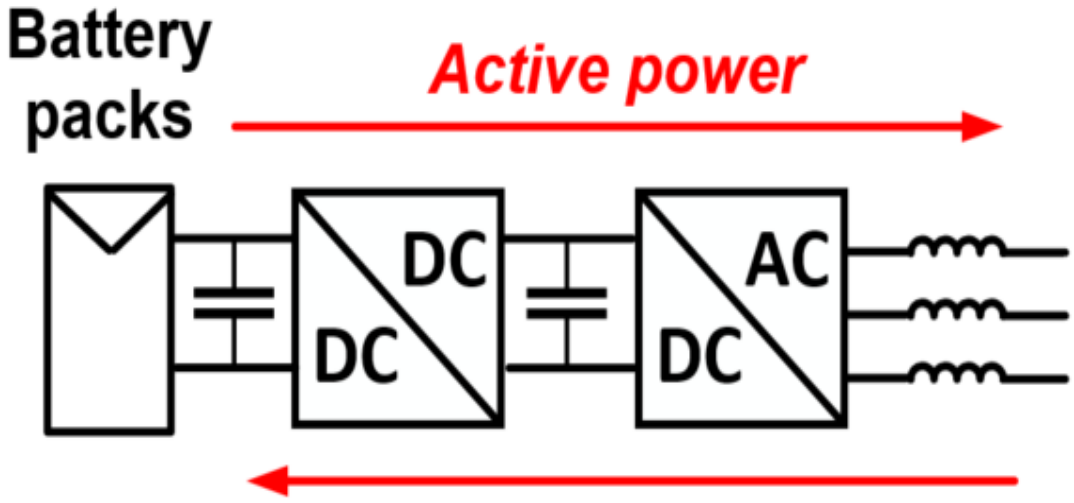


Fig. 2 - 8. BESS active power transferring.

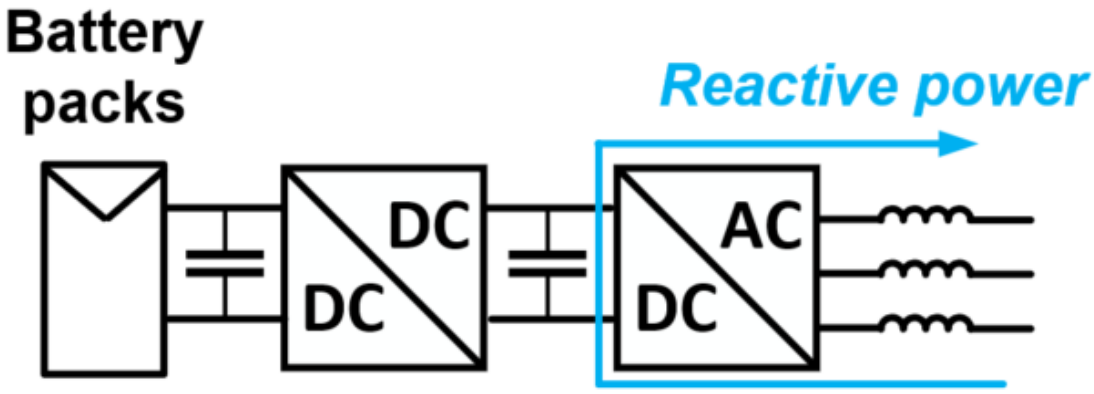


Fig. 2 - 9. BESS reactive power support.

2.4 Summary and Research Objectives

In this chapter, the previous work on the existing converter-based HTB and control strategies of BESSs are reviewed. First, the overall structure, control architecture, and existing emulators are introduced. The HTB applications in transmission-level systems are summarized. Then, the control of BESSs is reviewed from two perspectives, which include the control for the battery management and the interaction between BESSs and power grids.

Based on the review results, there are still many unsolved issues, especially on using HTB for the microgrid controller testing, which are:

- Existing HTB is not capable of emulating distribution systems, especially microgrids.
- Existing HTB has not demonstrated its capability of real-time microgrid controller testing, the control architecture needs to be redesigned.
- There is no comprehensive BESS emulator that is designed for microgrid controller testing, especially for microgrids with complicated control functions.

Therefore, the main tasks of this thesis are corresponding to these unsolved issues:

- Develop a converter-based microgrid emulating platform based on the existing HTB.
- Design the control architecture of HTB to be compatible with HTB control architecture.

- Propose a comprehensive BESS emulator based on the future microgrid controller testing requirements.
- Demonstrate the capability of the developed platform on the microgrid controller function evaluation.

CHAPTER 3. CONVERTER-BASED MICROGRID CONTROLLER TESTING PLATFORM

In this chapter, a converter-based microgrid controller testing platform is designed and developed based on the existing transmission level HTB. The testing platform includes two perspectives which are control architecture and microgrid emulation. The control architecture is designed according to an actual microgrid to improve the emulating accuracy. For the microgrid emulation, features of distribution systems and reconfiguration capability are considered.

3.1 Control Architecture Design

3.1.1 Actual Microgrid Control Architecture

Microgrids are usually built based on existing distribution grids, which requires the architecture of microgrids to be compatible with the control systems of distribution grids. The control architecture of an actual 12.47 kV microgrid is shown in Fig. 3 - 1 [13]. The microgrid central controller is placed in the utility control center and communicates with the Distribution Management System (DMS) or Supervisory Control and Data Acquisition (SCADA) system to monitor microgrid operation status as well as issue high-level control commands to the local controllers and smart switches. Local controllers are applied to control the DERs in the microgrid.

3.1.2 Microgrid HTB Control Architecture Design

Based on the control architecture of the actual microgrid, the control architecture of the microgrid controller testing platform is designed in Fig. 3 - 2. The DMS/SCADA is emulated by the combination of visualization interface and microgrid (MG) control desktop. The visualization interface is designed based on the LabVIEW to indicate the microgrid operation status and get commands from operators. The control desktop is used to control the smart switch emulators in the microgrid and get the voltage and current feedback as well as smart switch status from the sensors locating at the smart switch inputs and outputs.

The smart switches, sensors, and microgrid line emulators are placed in the microgrid topology emulation cabinets. By changing the connection of the topology emulation, the proposed testbed can potentially emulate different microgrids. The microgrid topology emulation cabinet is used to connect different converter-emulated microgrid components to form a microgrid. The converter emulators within the existing HTB cabinets are controlled by the HTB controllers through CAN communication.

Based on the emulated microgrid, the actual microgrid controllers are placed in the loop for function testing. The microgrid local controllers are also placed in the testing loop because different microgrid central controllers may require support from different local controllers. DNP3 protocol, which is used in actual microgrid controllers, is also applied as the communication between central and local controllers in the microgrid HTB to improve the testing accuracy.

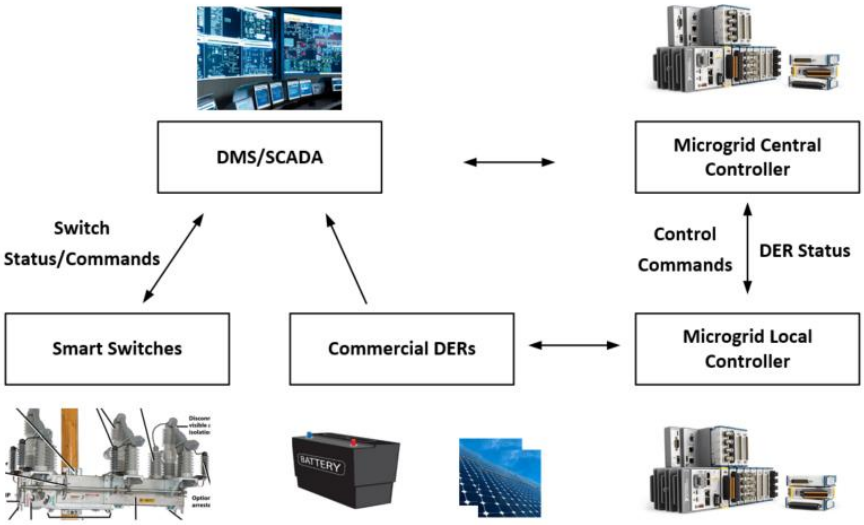


Fig. 3 - 1. Control architecture of an actual microgrid [13].

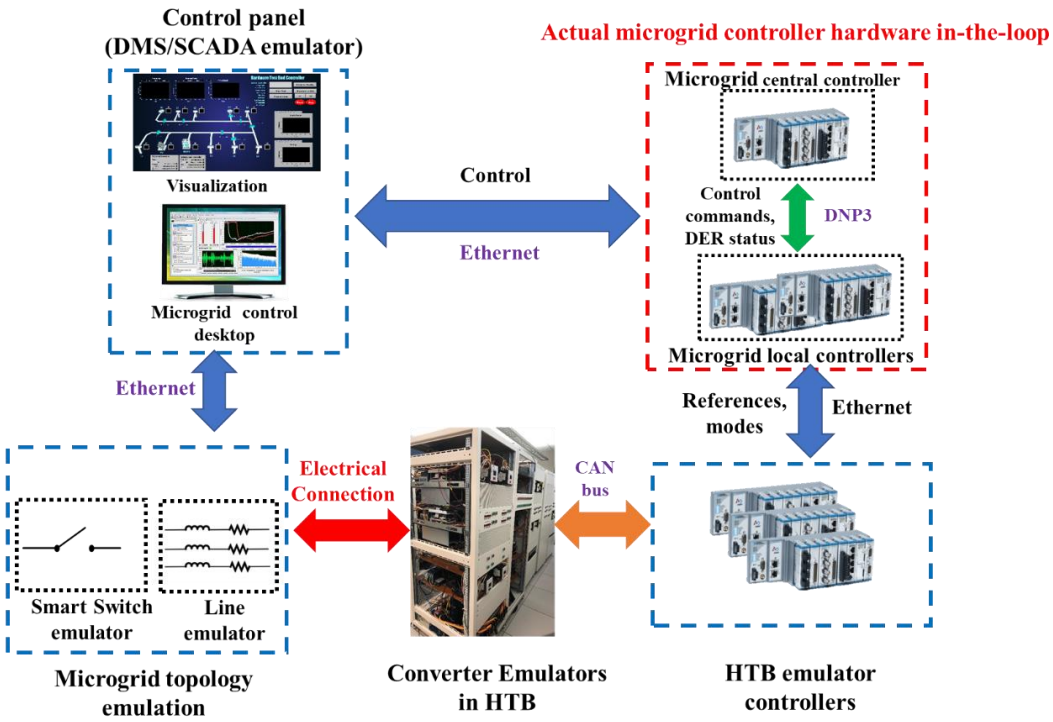


Fig. 3 - 2. Control architecture for microgrid HTB.

The central controller talks to local controllers to issue commands and receive DER status. DER local controllers communicate with the DER emulators in the emulated microgrid platform to determine the DER operation mode, output power. The DMS/SCADA emulator communicates with the microgrid controllers through Ethernet. The microgrid central controller obtains the smart switch information from the DMS/SCADA emulator for the control functions. The central controller and local controllers are connected to the rest of the system through Ethernet, meaning that the developed platform can be reconfigured to test different microgrid controllers easily.

All the microgrid controllers are implemented with cRIOs from National Instrument because they are also commonly applied as controller hardware platforms in actual field implementation. Therefore, the designed platform can be used to not only test the controller algorithms but also verify the hardware performance of microgrid controllers.

3.2 Example Microgrid Topology

3.2.1 Microgrid with Dynamic Boundaries

The first example of microgrid topology comes from an actual 12.47 kV, 2.7 MW microgrid with an airport as the critical load. The simplified topology is shown in

Fig. 3 - 3. In the example microgrid, the BESS and the solar PV work as sources to support the critical load section L8 in the islanded operation. This microgrid has dynamic boundaries, meaning that the microgrid boundary can be changed based

on the output change of the solar PV. The minimum boundary only contains the sources and the critical load section as shown in Fig. 3 - 3(a). This condition may occur at night or when the PV is not available. During this condition, the BESS keeps the critical load operational.

As shown in Fig. 3 - 3 (b), when the output PV output is high, the microgrid controller can expand the microgrid boundary by closing more smart switches to pick up more non-critical loads to improve the solar power usage efficiency and increase the microgrid resilience. Moreover, based on the grid operation status, this microgrid can potentially be connected to different grid interfaces. As shown in Fig. 3 - 3 (c) and (d), there are two potential grid interfaces in the microgrid topology. The microgrid can be either connected to grid interface 1 or grid interface 2, which results in more flexibility for the microgrid operation and more complexity for the microgrid control.

3.2.1 Microgrid with Multiple Sources at Different Locations

In addition to the dynamic boundary, in future microgrids, a microgrid with multiple sources at different locations will be another possible situation. Therefore, the microgrid HTB is also designed to have the capability of emulating this type of microgrid. As shown in Fig. 3 - 4, the second example microgrid contains one grid interface and four energy sources, including one backup generator, one solar PV, and two BESSs. The backup generator, solar PV, and BESS1 are placed at the same location to support one large critical load section L6, and BESS2 is placed at a different location to support a small critical load section L1. Therefore, in a

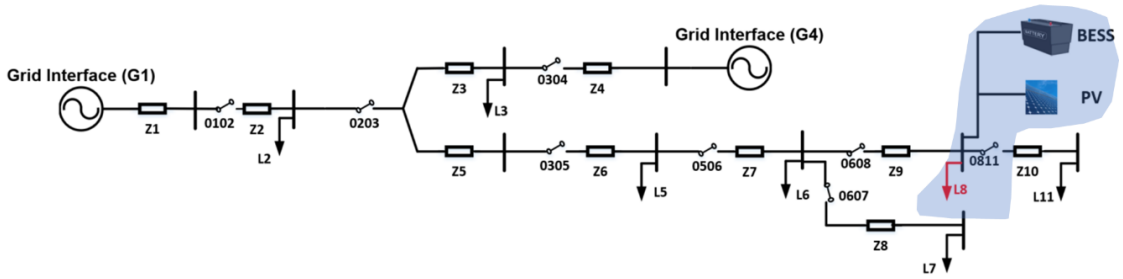
microgrid, multiple sources at different locations can potentially lead to multiple islands.

As shown in Fig. 3 - 4 (a), when the PV output is zero, there are two islands within the microgrid. When the PV output increases, the microgrid central controller gradually closes the smart switches to expand the boundary of island 2. After boundary switch 0203 is closed, island 1 and island 2 are only isolated by 0102. Then the microgrid central controller can do the reconnection control to merge two islands into one large island, which is shown in Fig. 3 - 4 (b).

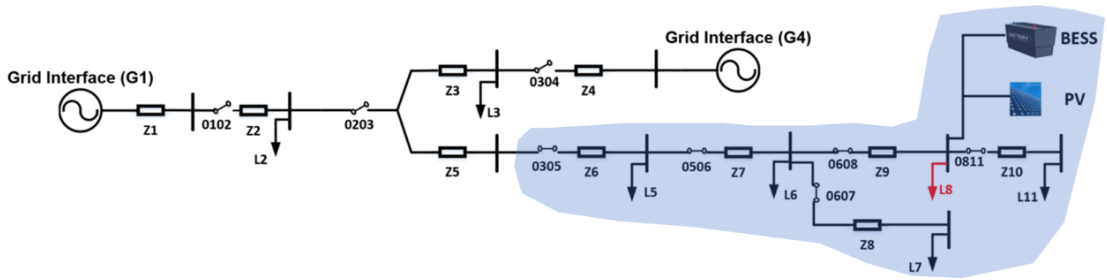
As shown in Fig. 3 - 4 (c), the merged island will eventually connect to the grid interface, and the microgrid will operate in the grid-connected mode. Compared with the first example, besides the dynamic boundary, this topology has more operation modes and has higher requirements on the microgrid central controller, especially on the mode transitions.

3.3 Microgrid HTB Emulation

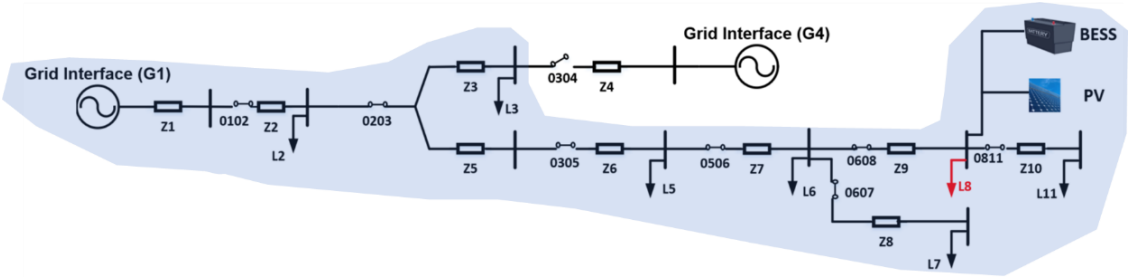
Microgrids are usually part of distribution grids, which feature radial topology, low line impedance, low line inductance (X) and resistance (R) ratio, and high renewable integration. In the meantime, in future microgrids such as microgrids with dynamic boundaries, smart switches are used to sectionalize loads to enable the boundary change capability of the microgrid. Therefore, to develop a microgrid emulating platform, all these characteristics need to be considered.



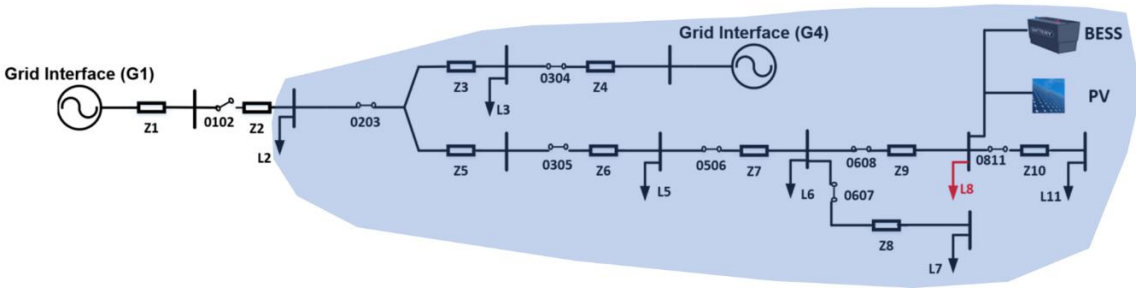
(a) Microgrid with minimum boundary.



(b) Microgrid with expanded boundary.

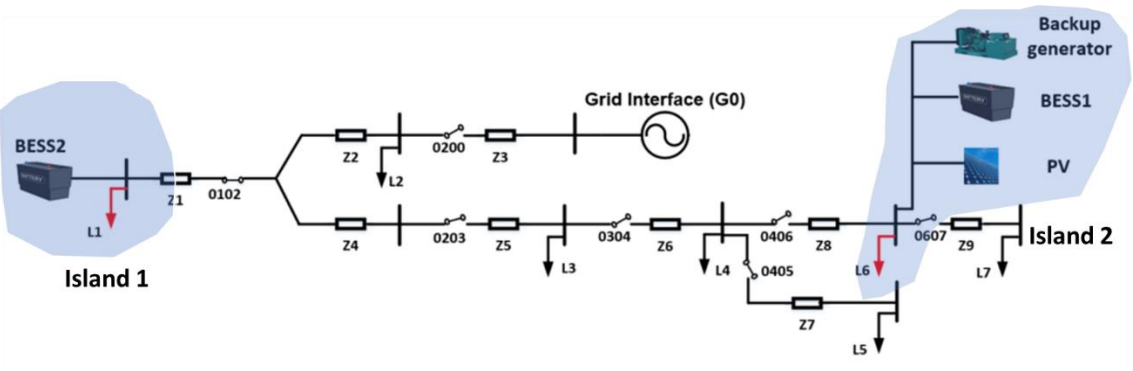


(c) Microgrid connecting to grid interface 1.

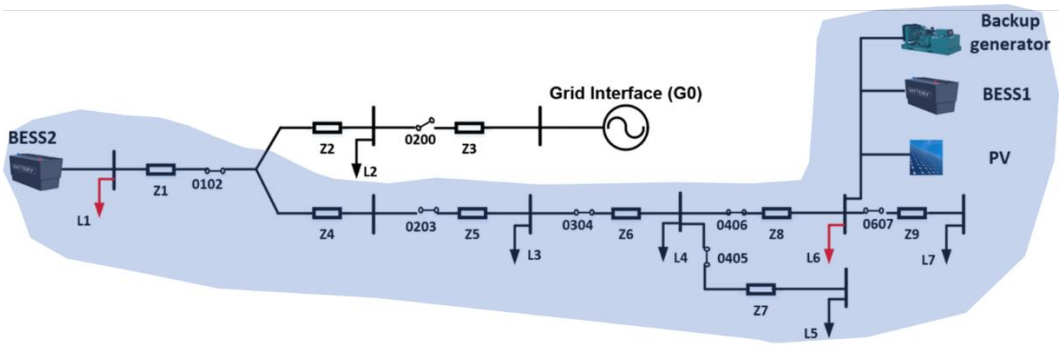


(d) Microgrid connecting to grid interface 2.

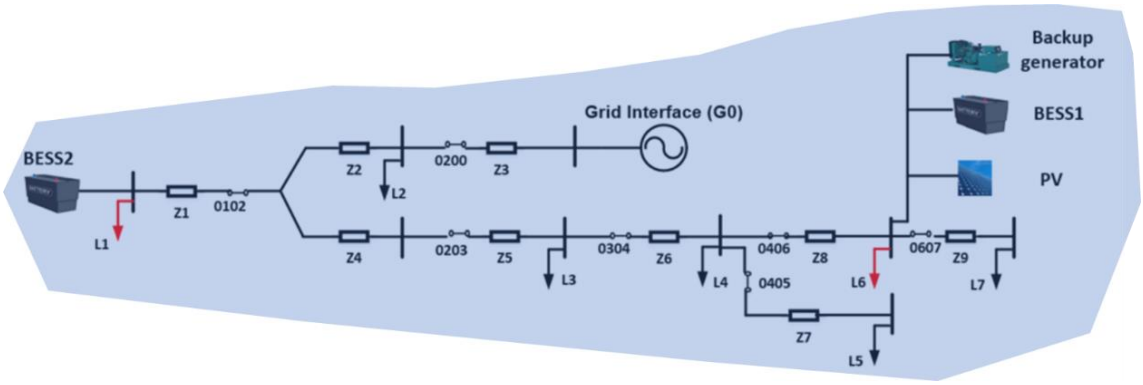
Fig. 3 - 3. Example topology 1: microgrid with dynamic boundaries.



(a) Microgrid with two separate islands.



(b) Microgrid with one merged island.



(c) Microgrid in the grid-connected mode.

Fig. 3 - 4. Example topology 2: microgrid with dynamic boundaries and multiple sources.

3.3.1 Microgrid Line Emulation

The line emulation is based on the actual microgrid lines in example microgrid 1. For the microgrid in the example topology 1, the voltage and power bases are 12.47 kV, 1 MW, respectively, which are difficult to be implemented in the laboratory. For the microgrid HTB, power and voltage bases are downscaled to be 173 V, 3 kW. As shown in Table 3 - 1, the line impedance in microgrid HTB is designed by keeping the same per unit (p.u.) value. For distribution lines, several models have been proposed, including π model [48], sequence impedance-based model [74], series resistance (R), and inductance (L) model. In this emulation platform, a series RL model is applied, which is shown in Fig. 3 - 5.

Based on the series RL model, the actual value, per unit value, downscaled value, and line X/R ratio of the example microgrid topology are summarized in Table 3 - 1. Both the per-unit values and the downscaled values are small. The X/R ratios of line impedance are close to 1, which are lower than the same ratios of transmission lines [37]. Low X/R ratios can potentially impact the power sharing of the sources.

Moreover, the testing platform is designed for microgrid controller testing, meaning that the design of the platform should consider different operation conditions of microgrids. The grid fault condition is one of the most important abnormal conditions that microgrid controllers need to deal with. Therefore, grid faults need to be emulated in the platform, denoting that the line impedance

emulator needs to handle fault current which is usually at least several times the base value (10 A). Therefore, the requirements of line emulators are:

- Low inductance and resistance
- High X/R ratio
- High operation current in the fault condition

Based on these requirements, air-core inductors are applied as line emulators as the inductances of air core inductors do not rely on the current and there is no core saturation issue. In the meantime, the inductance of air core inductance is mainly related to the core size, and resistance is related to the winding length, which provides flexibility for designing the X/R ratio of the inductors. The inductance of air-core inductor can be estimated by (3-1) [75]

$$L_{air} = \frac{N^2 r^2}{22.86r + 254l} \qquad (3-1)$$

where *r* is the radius of the coil; *l* is the coil length and *N* is the number of turns. In the microgrid HTB, coils with a 45 mm radius are applied for the inductor implementation. Based on the scaled line parameter in Table 3 - 1, three inductance values are selected for the line emulation, which are 10 uH, 25 uH and, 40 uH. Based on (3-1), the number of turns is 10, 18, and 26, respectively. As shown in Fig. 3 - 6, three inductors are designed in the ANSYS to obtain accurate inductance and resistance values. The designed inductances and resistances are 10.5 uH (5.1 mΩ), 24.8 uH (9.2 mΩ), and 39.6 uH (13.2 mΩ), respectively.

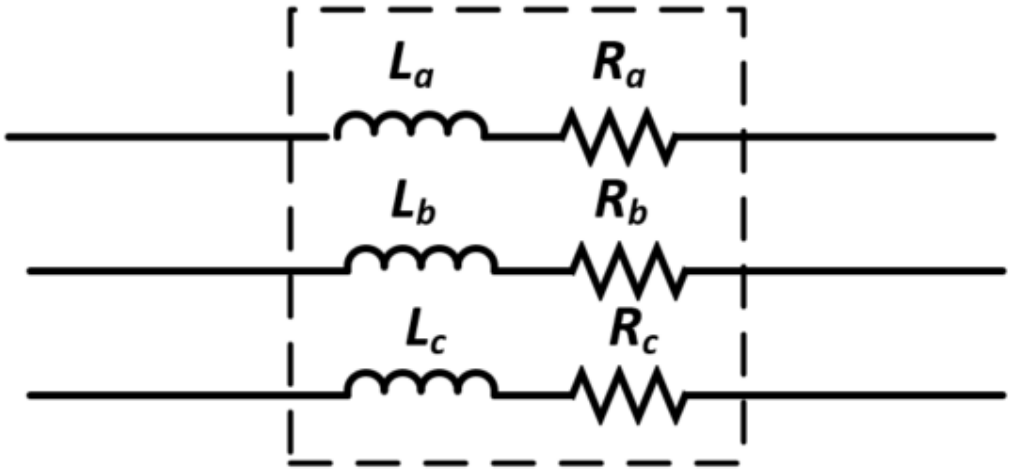


Fig. 3 - 5. Series RL model for microgrid lines.

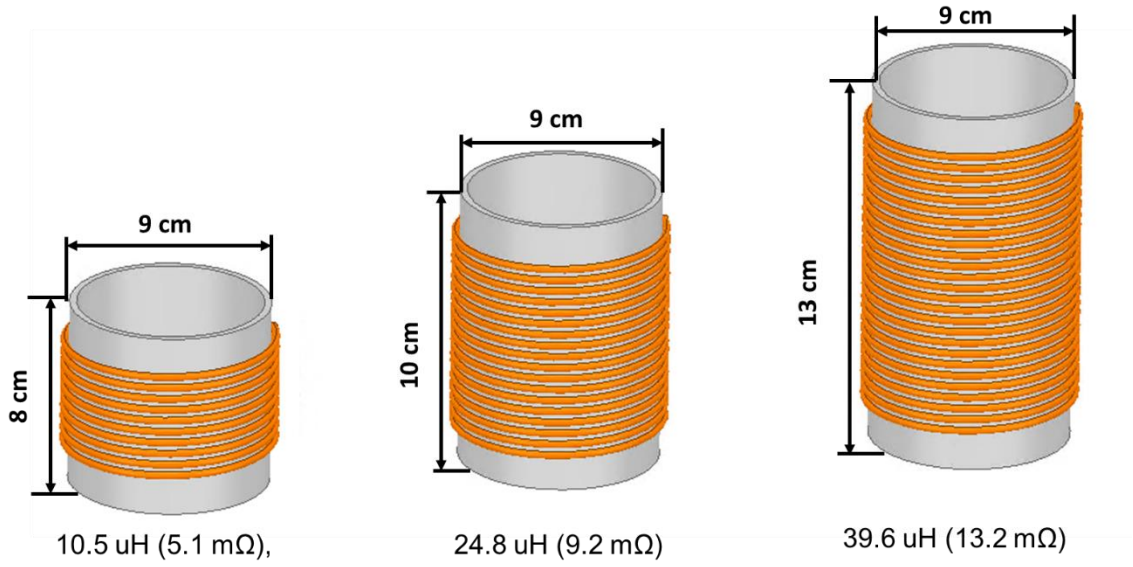


Fig. 3 - 6. Line emulator design.

Table 3 - 1 Line impedance in the microgrid HTB.

Name		Actual value	Per unit value (p.u.)	Downscaled value	X/R
Z1	R1	0.0322 (Ω)	0.0002	2.0 (mΩ)	3.7113
(N/A)	L1	0.3170 (mH)	0.00197	19.7 (μH)	
Z2	R2	0.1407 (Ω)	0.00087	8.7 (mΩ)	3.6931
(Z1)	L2	1.3783 (mH)	0.00854	85.4 (μH)	
Z3	R3	0.0207 (Ω)	0.00013	1.3 (mΩ)	2.7440
(Z2)	L3	0.1507 (mH)	0.00093	9.3 (μH)	
Z4	R4	0.0916 (Ω)	0.00057	5.7 (mΩ)	2.4881
(Z3)	L4	0.6045 (mH)	0.00375	37.5 (μH)	
Z5	R5	0.0356 (Ω)	0.00022	2.2 (mΩ)	2.4973
(Z4)	L5	0.2358 (mH)	0.00146	14.6 (μH)	
Z6	R6	0.0368 (Ω)	0.00023	2.3 (mΩ)	1.7011
(Z5)	L6	0.1661 (mH)	0.00103	10.3 (μH)	
Z7	R7	0.1413 (Ω)	0.00088	8.8 (mΩ)	1.6285
(Z6)	L7	0.6104 (mH)	0.00379	37.9 (μH)	
Z8	R8	0.009 (Ω)	0.00006	0.6 (mΩ)	1.5778
(Z7)	L8	0.0377 (mH)	0.00023	2.3 (μH)	
Z9	R9	0.1109 (Ω)	0.000688	6.88 (mΩ)	0.6094
(Z8)	L9	0.1793 (mH)	0.0011	11.1 (μH)	
Z10	R10	0.8897 (Ω)	0.00552	55.2 (mΩ)	0.3795
(Z9)	L10	0.8955 (mH)	0.00555	55.5(μH)	
Note: the impedance names in topology 2 are in brackets					

3.3.2 Microgrid Smart Switch Emulation

In the actual microgrids, smart switches are applied to monitor voltage and power information for certain load sections and protect the microgrid when the fault occurs. Smart switches are the basis of microgrids with dynamic boundaries. In the microgrid HTB, the smart switches are emulated by a combination of contactors, sensors, and boundary controllers. The emulator and control structure is shown in Fig. 3 - 7. The smart switch emulator is controlled by the microgrid boundary controller. Two voltage sensors are applied to sense the input and output voltage of the contactor so that the boundary controller can have the voltage information of both sides of the contactor. The current sensor is used to get the current measurement.

Moreover, in the actual microgrid, the opening and closing speeds of the smart switches are usually several cycles. The delay caused by switching actions will impact the controller's performance. However, the switching delay is usually ignored in the digital simulation so that its impact on the microgrid controller may not be well evaluated in the simulation and cause inaccuracy of the controller testing results. Therefore, the switching action also needs to be emulated by the microgrid HTB. Fortunately, the contactor is one of the mechanical switches, which have the switching action by nature. The switching behaviors are obtained from the testing, which is shown in Fig. 3 - 8. The opening and closing times are around three cycles (47 ms for opening, 46 ms for closing), which are close to the switching actions of smart switches in the actual microgrid.

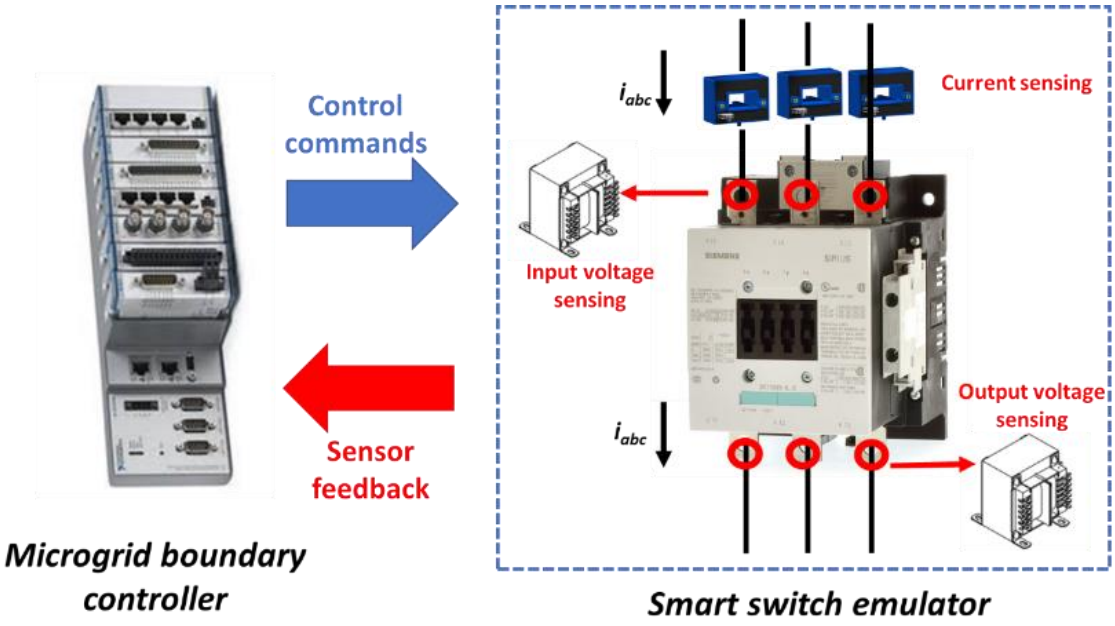
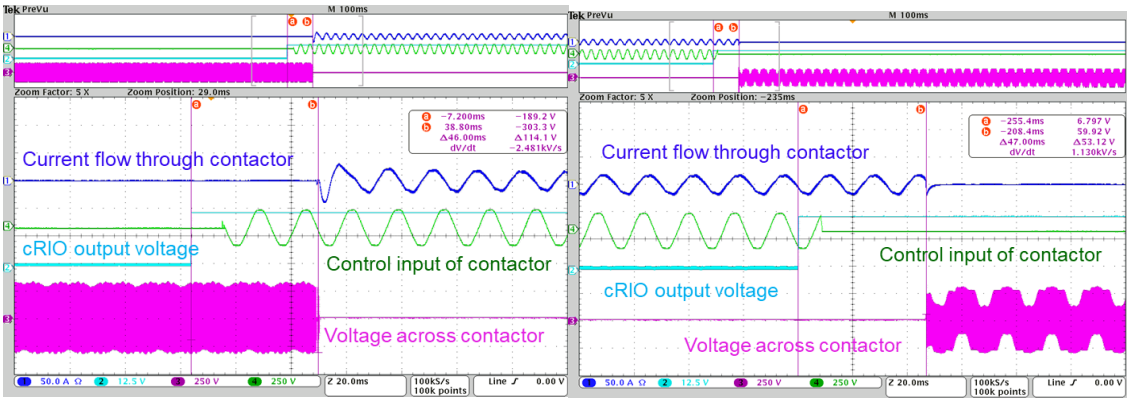


Fig. 3 - 7. Smart switch emulator and control structure.



(a) closing transient (b) opening transient

Fig. 3 - 8. Testing results of smart switch emulators.

Table 3 - 2. Microgrid HTB parameters.

Type	Parameters	Value
Operation condition	DC voltage (V_{dc})	200 V
	AC voltage base (V_{acb})	100 V
	Power base (P_b)	1732 W
	Line frequency (f_l)	60 Hz
	Grid line impedance emulator (L_{Line})	0.575 mH
Inverter emulator information	Inverter filter inductance (L_f)	0.575 mH
	Inverter filter resistance (R_f)	0.2 Ω
	Switching frequency (f_s)	10 kHz

Table 3 - 3. Grid components' rating in HTB testing.

Type	Original Rating	Scaled Rating
BESS 1	560 kW in microgrid 1 280 kW in microgrid 2	967 W in microgrid 1 (3.p.u over-current capability) 484 W in microgrid 2 (3.p.u over-current capability)
	250 kWh in microgrid 1 125 kWh in microgrid 2	0.214 kWh in microgrid 1 0.107 kWh in microgrid 2
BESS 2	280 kW in microgrid 2	484 W in microgrid 2 (3.p.u over-current capability)
	250 kWh in microgrid 2	0.107 kWh in microgrid 2
Generator	560 kW	967 W in microgrid 1
PV	2.1 MW	3637 W
Critical load in microgrid	560 kW in microgrid 1 840 kW in total in microgrid 2	967 W in microgrid 1 1452 W in total in microgrid 2

3.3.3 Microgrid Component Emulators

According to example topology 1 and 2, the microgrid components include grid interface, backup generator, load, PV, and BESS. Moreover, in order to evaluate the controller in the fault conditions, the grid fault is also emulated. Besides BESS which will be discussed in the next chapter, emulations of the rest of the components are discussed in this chapter. The converter operation parameters are summarized in Table 3 - 2, and grid component ratings are summarized in Table 3 – 3.

1) Grid interface

The main distribution grid can be modeled as a voltage source plus equivalent line impedance. In the microgrid HTB, as shown in Fig. 3 - 9, the distribution grid is emulated by a voltage source converter with open-loop control. In this case, the filter impedance of the inverter works as the grid impedance emulator. The grid interface emulator provides stable voltage and frequency to support all the loads and DERs in the grid-connected mode.

2) Backup generator

In the microgrid HTB, the synchronous generator is emulated to work as the source in the islanded mode. As shown in Fig. 3 - 10, the generator is composed of the excitation model, electrical model, and mechanical model [44]. In the excitation model, the field winding voltage (e_{tf}) is determined by the terminal voltage reference. K_A and T_e are the gain and time constant in the excitation system. The mechanical model includes the governor model, turbine model, and

droop characteristic and generates frequency as well as frequency for the control. In the mechanical model, *M* is the inertia constant, and *D* is the mechanical friction damping factor.

The electrical model describes the generator stator winding model, which is summarized in (3-2) -(3-5):

$$V_d^{ref} = E'_d + X'_q I_q - R_a I_d \quad (3-2)$$

$$V_q^{ref} = E'_q - X'_d I_d - R_a I_q \quad (3-3)$$

$$T'_{qo}\dot{E}'_d = -E'_d - \left(X_q - X'_q\right) I_q \quad (3-4)$$

$$T'_{do}\dot{E}'_q = e_{tf} - E'_q + (X_d - X'_d) I_d \quad (3-5)$$

where E_d', E_q' are the transient back electromotive forces; X_d', X_q' are the transient reactance; T_{do}' *and* T_{qo}' are the transient open-circuit time constants and R_a is the winding resistance.

3) Load

In the microgrid HTB, the ZIP load model is applied for the power load emulation. The control diagram of the load model is shown in Fig. 3 - 11. The load emulator senses the voltage and current from sensors. The load emulator is controlled as a current source in the *dq* coordinates. The current references are generated by the ZIP load model in [49], which is shown in (3-6) and (3-7)

$$I_d^{ref} = \frac{V_d P_{ref} + V_q Q_{ref}}{V_d^2 + V_q^2} \quad (3-6)$$

$$I_q^{ref} = \frac{V_q P_{ref} - V_d Q_{ref}}{V_d^2 + V_q^2} \quad (3-7)$$

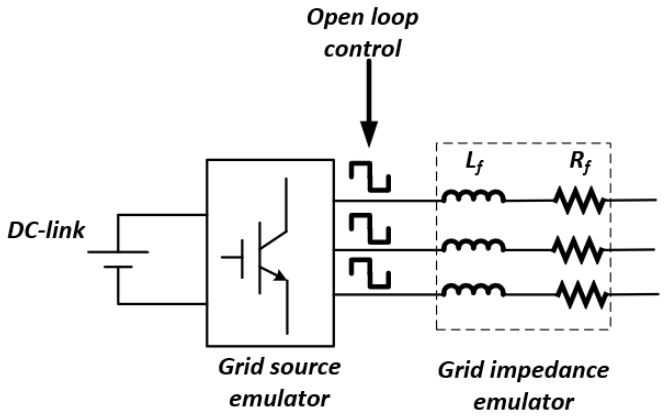


Fig. 3 - 9. Main distribution grid emulator.

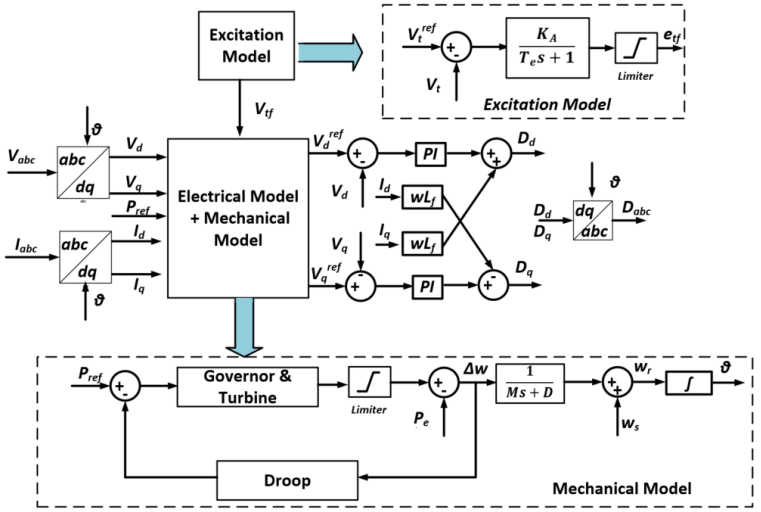


Fig. 3 - 10. Control of the generator emulator.

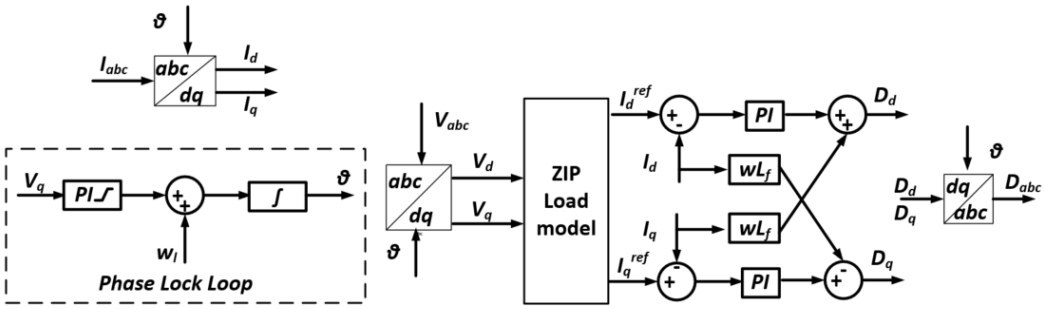


Fig. 3 - 11. Control diagram of the load emulator.

where all the values in (3-6) and (3-7) are p.u. values. The references of active and reactive power are described in (3-8) and (3-9)

$$P_{ref} = P_0(p_1(V_t)^2 + p_2(V_t) + p_3)\left(1 + k_p\Delta f\right) \quad (3-8)$$

$$Q_{ref} = Q_0(q_1(V_t)^2 + q_2(V_t) + q_3)\left(1 + k_q\Delta f\right) \quad (3-9)$$

where p_1 and q_1 are the coefficients for constant impedance load; p_2 and q_2 are the coefficients for constant current load; p_1 and q_1 are the coefficients for constant power load. The k_p and k_q are the coefficients to model the frequency impacts on the active and reactive power. All the values in (3-8) and (3-9) are also p.u. values.

4) PV

The PV emulator models a two-stage PV converter which contains a dc/dc boost converter and a dc/ac converter. The control model is shown in Fig. 3 - 12. The boost converter controls the inductor current. The inductor current reference is generated from the incremental conductance (INC) MPPT control [46].

The dc/ac stage is applied to work as a rectifier to regulate the dc voltage and transfer active power. In the meantime, the reactive power of the dc/ac stage can also be controlled to support grid voltage. In the PV emulator, the PV model is integrated to generate active and reactive current references. The PV emulator is connected to the grid through the phase lock loop (PLL).

5) Grid fault

To support the microgrid protection testing, the grid fault is emulated. In the microgrid HTB, as shown in Fig. 3 - 13, grid fault is emulated by applying a low impedance load to generate fault current and reduce grid voltage.

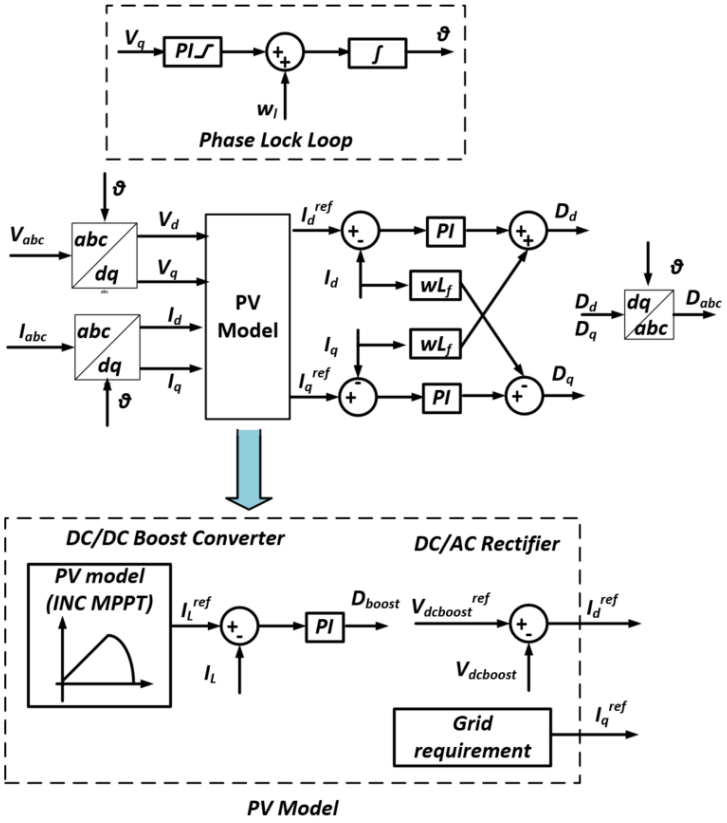


Fig. 3 - 12. Control of the PV emulator.

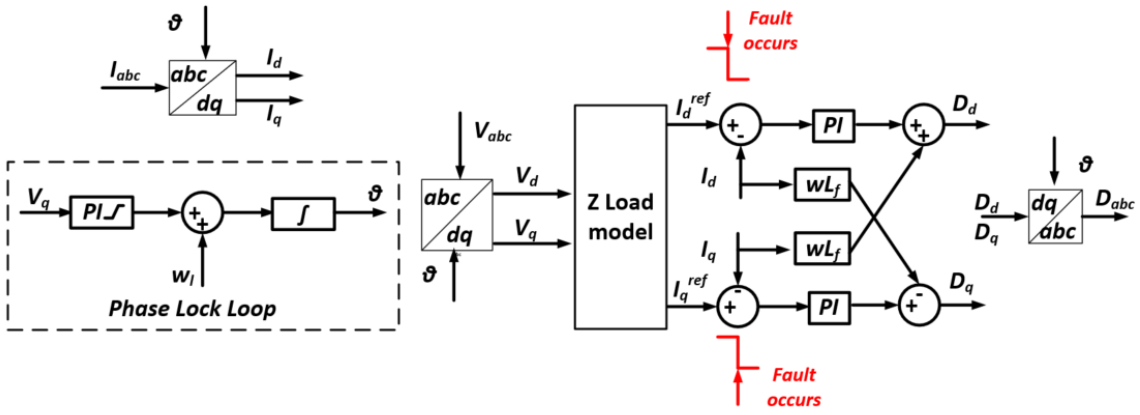


Fig. 3 - 13. Control of the fault emulator.

Therefore, for the fault condition, the fault emulator is a constant impedance load. The stepping down of impedance reference is applied when the fault occurs. Since the impedance of the line emulator is small, the fault emulation can be viewed as a high impedance fault.

3.3.4 Experimental Results of Emulators

The testing results of all the emulators are provided based on the topology in Fig. 3 - 4, all the smart switches are closed and only the emulators under test are enabled. The parameters are summarized in Table 3 - 1, Table 3 - 2, and Table 3 - 3.

1) Grid and Load Emulators

The testing waveforms of grid and load emulators are shown in Fig. 3 – 14, where one grid emulator and two load emulators (L4 and L5) are applied. The grid emulator establishes stable voltage and frequency. The load emulator controls the output impedance to be a constant. The load L4 and load L5 increase power at t_1 and t_2, respectively. The grid current increases accordingly while the load emulators do not impact each other.

2) Generator Emulator

The testing waveforms of the generator emulator are shown in Fig. 3 – 15. The generator starts up to connect to the grid, which includes three steps. Step 1 is phase synchronization, where the generator utilizes PLL to obtain the grid frequency and phase information to change the initial output phase angle to synchronize with the grid. By doing the synchronization, the startup transient is

limited. Step 2 is open-loop control, where the generator output voltage is established but there can be static errors. Step 3 is the closed-loop control, where the output voltage is regulated to the reference.

3) PV Emulator

The testing waveforms of the PV emulator are shown in Fig. 3 – 16, where one grid emulator, one PV emulator, and two load emulators (L4 and L5) are applied. The PV output power increases at t_1 to support loads and the grid current drops. The PV output power decreases at t_2 and the grid emulator increases to meet the load demands.

4) Grid Fault Emulation

The testing waveforms of the fault emulator are shown in Fig. 3 – 17, where one grid emulator and one fault emulator are applied at L5. The fault is applied at t_1 by decreasing the output resistance of the fault emulator and the fault is cleared at t_2. When the fault is applied, the fault emulator current increases and the fault location voltage drops.

However, the line impedance is relatively small and the fault emulator current capability is limited, resulting in a small voltage drop of the fault location. Therefore, the emulated fault in microgrid HTB is a high impedance fault. When the fault is cleared, the fault emulator current is regulated to be normal, and the fault location voltage recovers as well.

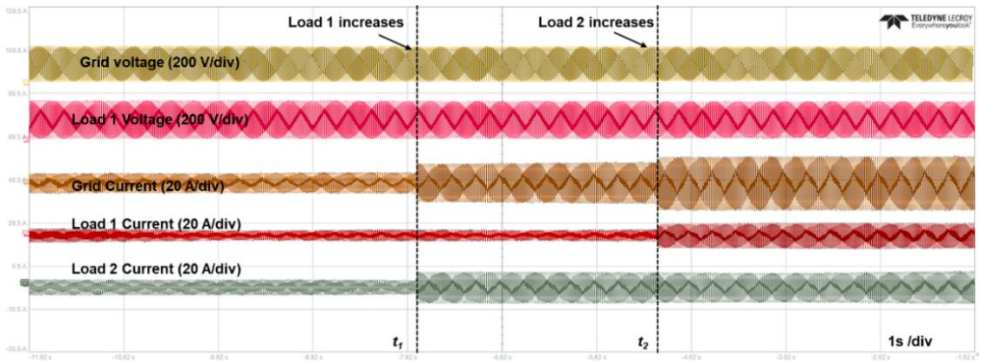


Fig. 3 - 14. Test waveforms of grid and load emulators.

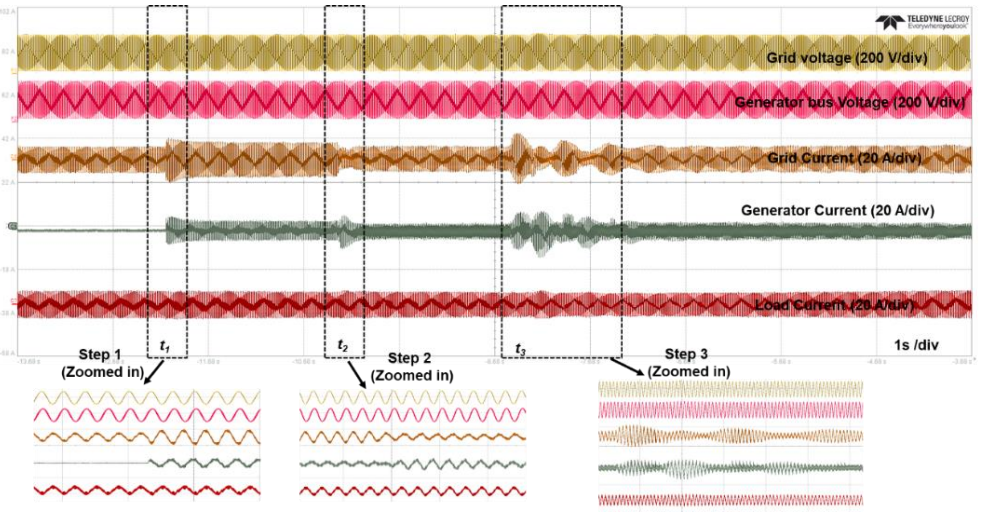


Fig. 3 - 15. Test waveforms of the generator emulator.

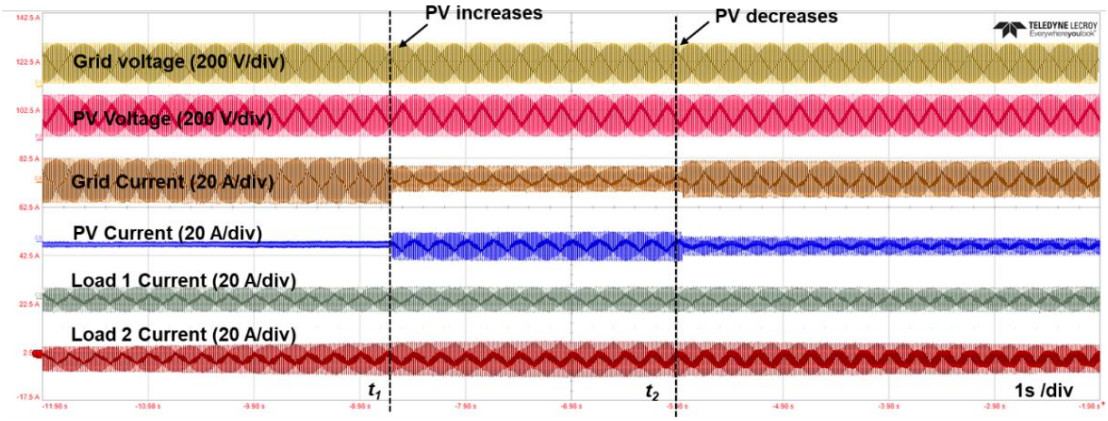


Fig. 3 - 16. Test waveforms of the PV emulator.

3.3.5 HTB Reconfiguration Design

In order to support flexible grid emulation, the proposed microgrid HTB is required to have the reconfiguration capability, which contains two perspectives: first, the microgrid HTB needs to support different microgrid topologies; second, the microgrid HTB should be compatible with the transmission-level HTB.

According to these two requirements, the reconfiguration capability is designed. As shown in Fig. 3 - 18, isolation switches are added to help realize the system reconfiguration. Each converter emulator has two isolation switches so that it can support either the transmission system HTB or microgrid HTB. The isolation switches are implemented by contactors.

3.3.6 Hardware Implementation

The hardware of microgrid HTB includes converter emulators, line emulators, isolation switches, smart switch emulators. Except for converter emulators, other components are implemented in the microgrid emulating cabinet. As shown in Fig. 3 – 19, there are five shelves in the cabinet.

The microgrid controllers and the network switch are placed on the top shelf to decouple with the main power circuit to reduce the electromagnetic noise impact on the controller operation. The controllers are connected to the ethernet through the network switch. The main power circuit is realized in shelf 2 to shelf 5, which contains smart switch emulators, relays for contactor control, line emulators, isolation switches, and dc power supplies for microgrid controllers.

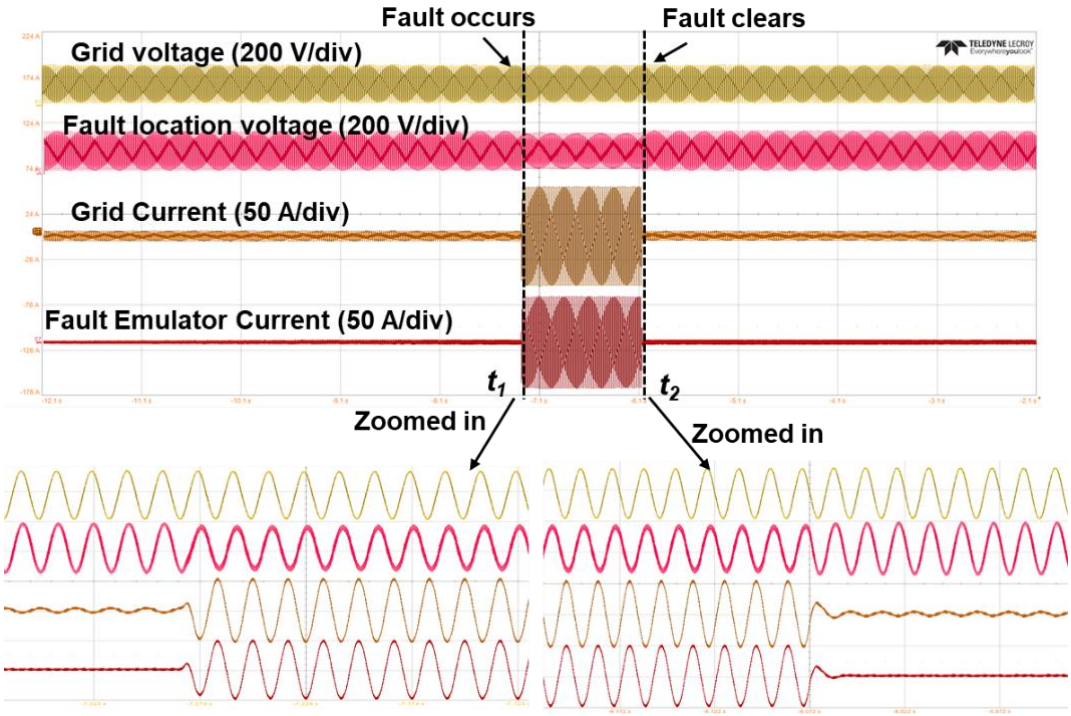


Fig. 3 - 17. Test waveforms of the fault emulator.

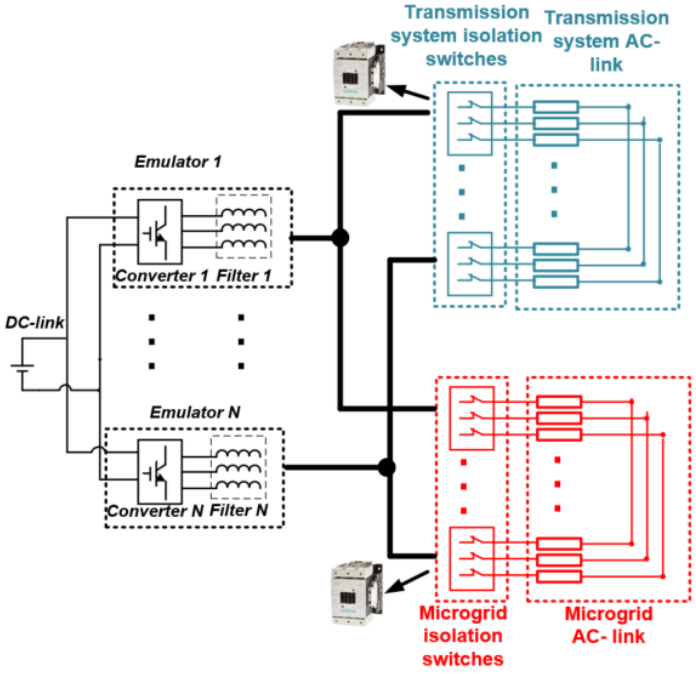


Fig. 3 - 18. HTB reconfiguration design.

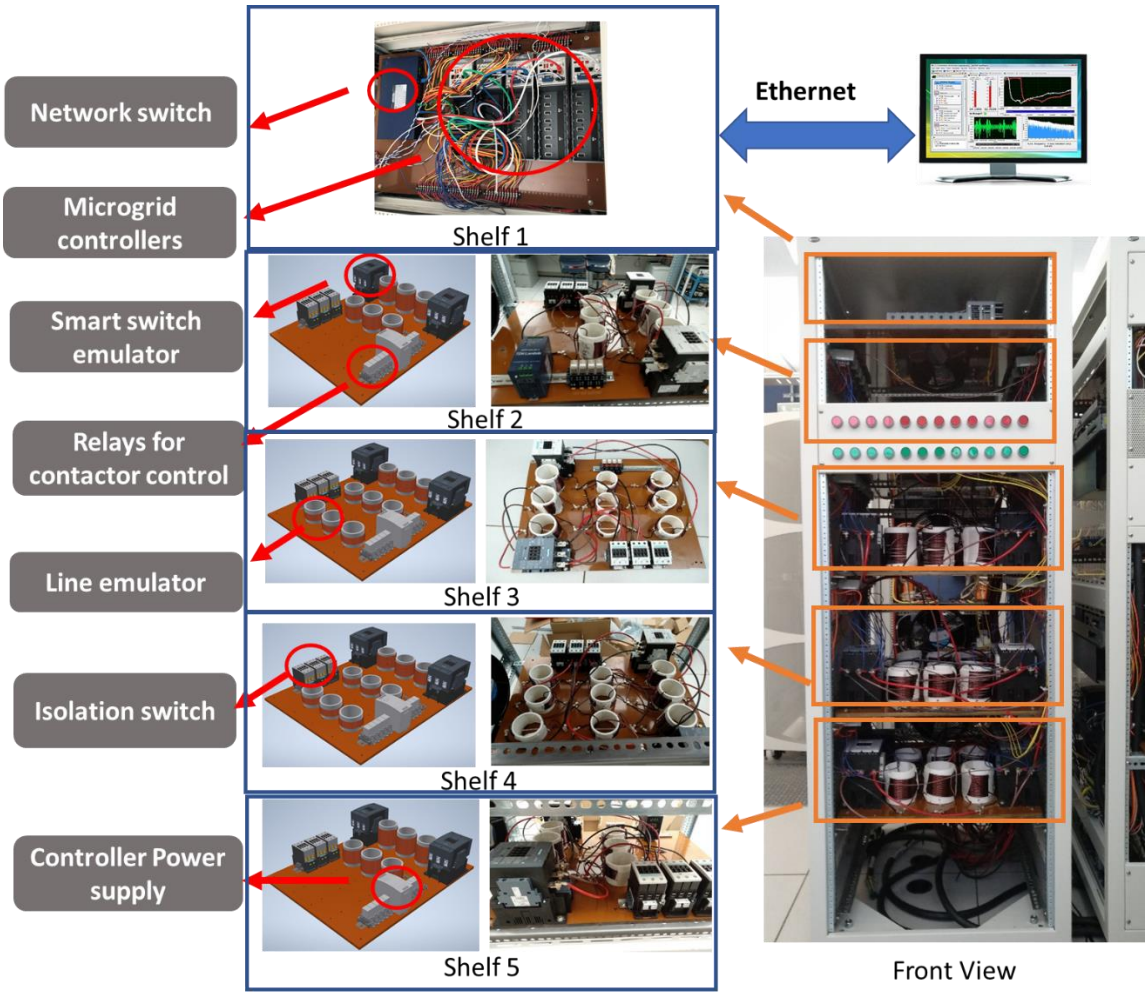


Fig. 3 – 19. Emulating cabinet of microgrid HTB.

The emulating cabinets contain the microgrid topology as well as the controller hardware. The isolation switches are applied as the interfaces of converter emulators, meaning that by changing the connection of line emulators and switches emulators, different microgrids can be emulated. Therefore, the developed microgrid test platform can realize flexible topology changes to test different microgrid controllers.

3.4 Summary

A converter-based microgrid controller testing platform is designed and implemented, including the control architecture design, microgrid topology selection, and emulation component implementation. The control architecture is designed based on the real utility microgrid and the example microgrid topology is simplified from an actual microgrid, which can provide a practical testing condition to evaluate the microgrid controller performances.

The grid interface, DERs, and loads in the microgrid are emulated by power converters, which can realize flexible component changing by reprogramming the model of the converters. Experimental results of microgrid component emulators are provided to demonstrate that the converter emulators are capable of supporting the microgrid controller testing.

The microgrid topology connections are emulated by the topology cabinet, which contains the line emulators and smart switch emulators. Air-core inductors are applied as the line emulators to realize low impedance, high X/R ratio, and high operation current without saturation. The contactors, boundary controller, and

sensors are coordinated to emulate the smart switches in the microgrid, which can emulate actual switching actions and potentially be used for protection implementation.

Moreover, the designed microgrid HTB also considers the reconfiguration capability. By adding one isolation switch to each converter emulator, the microgrid HTB can emulate different microgrid topologies and can also be reconfigured back the transmission level system emulation.

CHAPTER 4. MICROGRID CONTROLLER HTB TESTING REQUIRED BESS FUNCTIONS

In this section, a BESS emulator for microgrid controller HTB testing is proposed. The proposed emulator models the BESS functions for the microgrid central controller testing. The microgrid central controller functions are described first. Then related BESS emulators functions are discussed, and the function coordination, as well as transitions are also provided.

4.1 Microgrid Controller Functions

The controller for a microgrid with dynamic boundaries is applied as the controller under testing, of which the required functions are summarized in Table 4 – 1 [76]. The central controller functions can be divided into four types, which are functions for microgrid information input, functions for recording, functions for long-time operation, and functions for real-time operation.

4.1.1 Functions for Microgrid Information Input

Under different microgrid conditions, the topology and power flow of a microgrid with dynamic boundaries can be different. The microgrid information input function includes four main functions, which are model management, topology identification, state estimation, and communication.

The model management function is to load certain microgrid-related data and convert data to the format that the microgrid controller can deal with. The topology identification function is to transfer the microgrid topology to a topology

matrix [13], which includes the smart switch locations, grid interface conditions, and microgrid boundary information.

The state estimation function is to estimate the node voltage and angle to reduce the measurement error and assist the power flow calculation. The communication is set up to communicate with the local controllers and smart switches so that the central controller can obtain the real-time information of the whole system.

4.1.2 Functions for Recording

Recording functions are applied for the data analysis and recording abnormal events during the microgrid operation. The recording-related functions include data logging and event recorder. Both data and events will be recorded into real-time local files so that the operators can analyze the data or deal with the events in time.

4.1.3 Functions for Long-Time Microgrid Operation

For long-time microgrid operation, an optimal operation goal is usually needed, which requires the energy management function. In existing microgrids, day-ahead economic power dispatch is a common objective for energy management. In order to determine the power dispatch for the day ahead, the energy management function needs the future load and DER information, which requires load forecasting and PV forecasting functions. Based on the day-ahead

forecasting results and microgrid system constraints, the energy management function will determine the economic power dispatch through optimization.

4.1.4 Functions for Real-Time Microgrid Operation

To keep the microgrid operational, the central controller needs to keep the real-time power balance and determine the microgrid operation modes according to the grid condition. The microgrid real-time operation is related to five functions, including PQ balance function, finite state machine function, reconnection function, black start function, and the protection coordination function.

1) PQ balance function

The PQ balance function mainly operates in the microgrid islanded mode to keep the active and reactive power balancing between DERs and loads. The PQ balance function keeps the power balanced by regulating the DER output power, voltage, frequency, as well as smart switches based on the load demands. When the DER (such as PV) can generate more/less power than the load demand, the PQ balance function can control the smart switches and DER outputs to expand/shrink the microgrid boundary to pick up/shed loads, which can improve the usage efficiency of DER power and promote the microgrid resilience. In the grid-connected mode, the microgrid power is supported by the main distribution grid. The PQ balance function is disabled.

2) State Machine-Related Functions

Table 4 – 1. Summary of microgrid central controller functions

Function type	Function block	Description
Microgrid information input	Model management	Load system information
	Topology identification	Obtain the real-time topology and smart switch information
	Communication	Link central controller, local controllers, and other components
	State Estimation	Estimate the voltage and angle information for nodes in the microgrid
Recording	Data logging	Record real-time data
	Event recorder	Record events
Long-time microgrid operation	Energy management	Realize system optimal (economic, etc.) operation by controlling DERs and/or loads
	PV/load forecasting	Forecast long-time PV/load power for energy management
Real-time microgrid operation	Active & reactive power (PQ) balancing	Realize real-time power balancing among sources and loads
	Finite state machine	Determine states and transitions
	Resynchronization control	Reconnect the islands to the main grid or merge multiple islands into one island
	Black start	Start the microgrid from a shutdown condition
	Protection coordination	Monitor the DER and smart switch status and response accordingly when the fault is detected by the relay/smart switches

The finite state machine function determines the operation modes of the microgrid. The state machine is summarized in Fig. 4 – 1. There are two main modes, which are grid-connected mode and islanded mode. In order to define the transitions clearly, the islanded mode is divided into merged island mode and separate islanded mode for microgrids with multiple islands. There are six types of transitions among these modes. The detailed descriptions of each mode and transitions are summarized in Table 4 - 2. For the transitions, the islanding and island separating transitions are realized by cooperating with the DER local controllers and controlling the smart switches.

Two other central controller functions are related to the state machine function, including resynchronization control and black start. Compared with the islanding and island separating transitions, the reconnection and island merging transitions are more complicated. A specific control function called resynchronization control is usually applied for the reconnection and islands merging transition, which needs to coordinate with the topology identification function to determine the boundary switch and regulate the voltage and phase angle differences of the two sides of the boundary switch to reduce the transient of the transition. Another finite state machine-related function in the central controller is the black start function, which is to start up the whole microgrid from the shutdown condition to the steady-state islanded mode operation.

3) Protection Coordination Function

The protection coordination function is to update the protection curves of smart switches under different operation modes and coordinate with other functions (state machine, PQ balance) to keep the microgrid operational under fault conditions. In the grid-connected mode, since the fault current is provided by the grid, current-related protection strategies are applied as fault current can be distinguished with the load current in an easy manner. In the islanded mode, since DERs are the sources to provide fault current, the fault current is limited by the current ratings of the DER inverters. The voltage-based protection strategies are applied as the fault current may be hard to be detected. All the protection strategies are integrated into the smart switches as protection curves. Since the protection strategies in grid-connected and islanded mode may be different, the protection coordination function will update the protection curves of the smart switches when the microgrid operation mode changes.

4.2 BESS Emulator Functions

A BESS usually works as a power source to support the flexible microgrid operation in the grid-connected mode and can serve as a grid-forming source in the islanded mode to support the voltage and frequency of the microgrid. The testing of microgrid central controller functions needs the support of BESS emulators. Different central controller functions have different requirements for BESS functions. The corresponding relationships between BESS emulator functions and microgrid central controller functions are shown in Fig. 4 - 2.

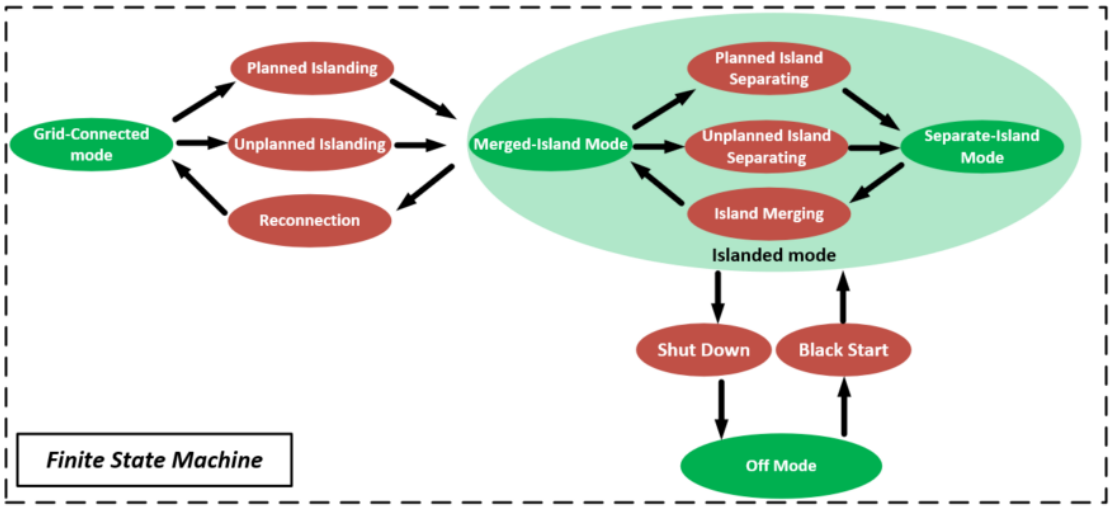


Fig. 4 – 1. Finite state machine.

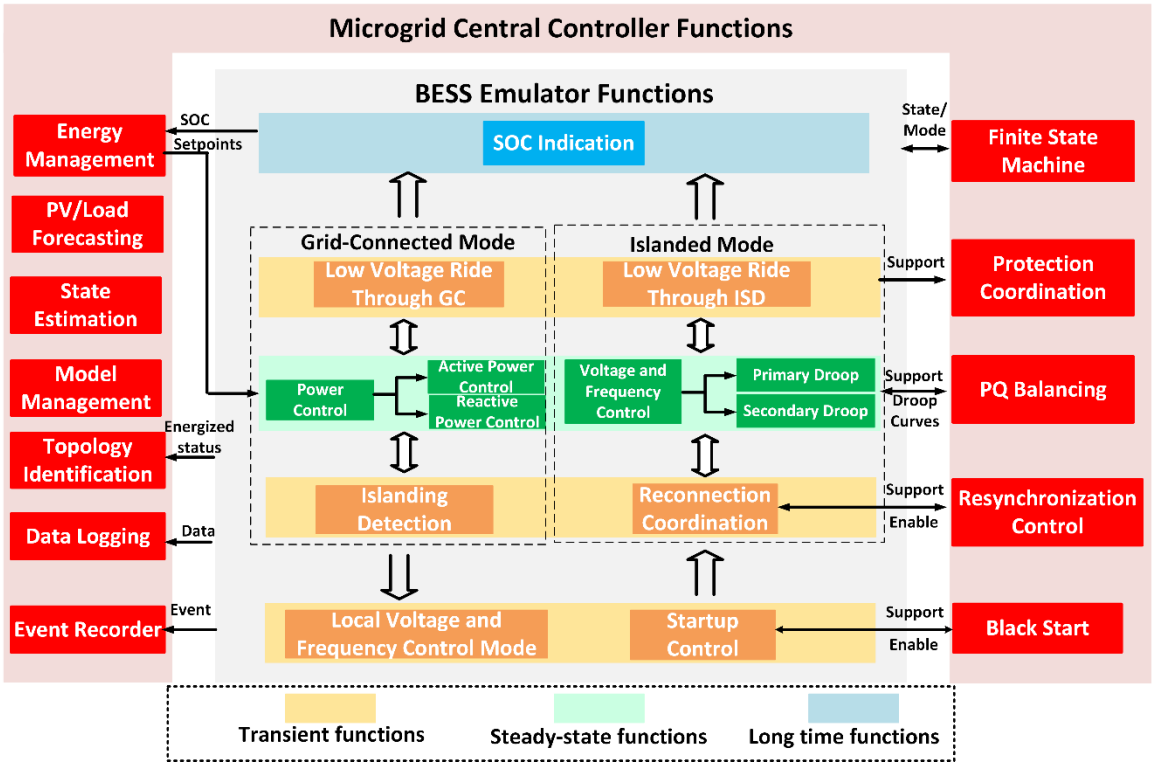


Fig. 4 - 2. BESS emulator functions for microgrid central controller testing.

Table 4 - 2. Microgrid central controller modes and transitions.

Types	Items	Descriptions
Steady-state modes	Grid-connected mode	The microgrid is connected to the main grid
	Merged-island mode	The microgrid is in islanded mode; multiple sources operate together to support a merged island
	Separate-island mode	The microgrid is in islanded mode; multiple sources operate separately to support multiple islands
Transitions	Black start	The microgrid starts up to the steady-state islanded mode
	Planned islanding	The operation mode is changed from grid-connected to islanded as scheduled
	Unplanned islanding	The operation mode is changed from grid-connected to islanded in abnormal conditions
	Reconnection	The operation mode is changed from islanded to grid-connected
	Planned island separating	The islanded microgrid is changed from a merged island to separate islands as scheduled
	Unplanned island separating	The islanded microgrid is changed from a merged island to separate islands in abnormal conditions
	Island merging	Separate islands merged into one island

For the longtime operation functions, the BESS emulator needs to provide real-time SOC indication so that the energy management can have available BESS power information for the optimization. In the meantime, the BESS emulator needs to realize the power setpoints from the energy management, which requires the power control functions in the BESS. For the real-time operation functions, the BESS emulator needs to support the microgrid operation under steady-state operation, mode transitions, and fault conditions.

Therefore, the BESS emulator functions are defined based on the requirements of real-time operation functions. The detailed algorithm and implementation of these functions are discussed in this section.

4.2.1 SOC Indication

As discussed in chapter 2, the SOC is estimated in the BMS system. However, in the HTB testing, the central controller testing focuses on the system operation and coordination. The BESS emulator is to support the central controller testing, which only requires the SOC information for central controller function validation. Therefore, in the HTB BESS emulator, the BMS system is simplified to be a SOC indication function to provide the central controller with real-time SOC information. The SOC indication function is shown in Fig. 4 - 3. The real-time voltage and current of the BESS emulator are sensed and transformed from *abc* coordinates to *dq* coordinates to calculate the real-time BESS power based on (4-1):

$$P_{BESS}(t) = V_d(t)I_d(t) + V_q(t)I_q(t) \qquad (4-1)$$

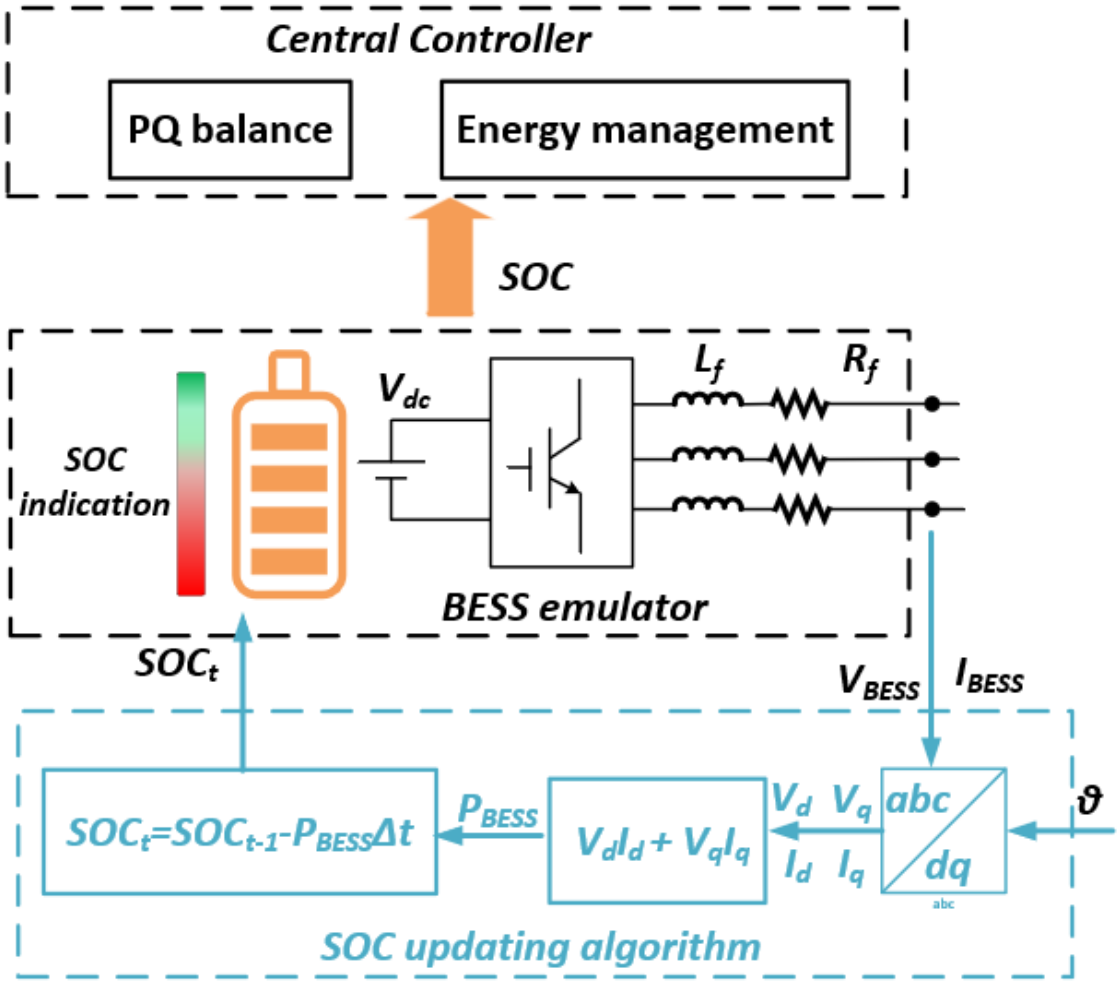


Fig. 4 - 3. BESS SOC indication function.

The real-time SOC is calculated as:

$$SOC(t) = SOC(t-1) + P_{BESS}(t)\Delta t \qquad (4-2)$$

where *SOC(t)* is the SOC for time *t, Δt* is the scaled unit time length for SOC updating, P_{BESS} is the active power of the BESS in p.u. value. The BESS emulator sends the SOC to the central controller through communication. At each time, the SOC range is defined as:

$$0 \leq SOC(t) \leq 1 \qquad (4-3)$$

Two central controller functions require the SOC information, including the energy management and the PQ balance function. The energy management function needs the SOC information to ensure that the power dispatch strategy will not cause over-charge or over-discharge of the BESS. The PQ balance function requires real-time SOC information to balance the source and load. In the BESS emulator, the initial SOC of the BESS is viewed as known since the central controller testing only requires SOC indication. The SOC estimation is not the focus of this testing so it is not modeled in the BESS emulator.

4.2.2 BESS Functions in Grid-Connected Mode

1) Power Control

In the grid-connected mode, the BESS emulator is controlled as a power source to generate the output power required by the energy management function of the central controller. The power control diagram is shown in Fig. 4 - 4, where the BESS emulator reads the grid voltage and frequency information through PLL. The output power current references are generated based on the voltage and

power commands. The power control is a dual loop control structure. The outer loop determines the output current references as equations summarized in (3-6) and (3-7) in chapter 3. The inner loop regulates the output current to realize the current output.

2) Fault Ride Through

The protection coordination is one key function in the central controller, which needs to be verified on the microgrid HTB. Therefore, the fault conditions need to be considered in both grid-connected and islanded modes. Based on IEEE standard 1547 [77], the grid-connected inverters are required to ride through the grid fault condition.

During the fault condition in the grid-connected mode, the BESS emulator outputs power to support the grid. The ride-through strategy is to provide power support when the grid voltage drops considering the maximum output current capability of the emulated BESS. When the BESS emulator detects the voltage drop, the output current will increase based on equations (3-6) and (3-7). When the total current is greater than the maximum output current capability, the BESS will reassign the output current references to keep the maximum output. The scaled-down strategy of d axis and q axis current is described in (4-4) and (4-5)

$$I_d^{ref} = \frac{I_{BESS}^{max}}{\sqrt{\left(I_{dgf}^{ref}\right)^2 + \left(I_{qgf}^{ref}\right)^2}} I_{dgf}^{ref} \qquad (4-4)$$

$$I_q^{ref} = \frac{I_{BESS}^{max}}{\sqrt{\left(I_{dgf}^{ref}\right)^2 + \left(I_{qgf}^{ref}\right)^2}} I_{qgf}^{ref} \qquad (4-5)$$

where I_d^{ref}, I_q^{ref} are the current references when the BESS emulator current hits the limit; I_{dgf}^{ref} and I_{qgf}^{ref} are the current references calculated based on the power commands and voltage condition; I_{BESS}^{max} is the maximum current capability of the emulated BESS.

3) Islanding Detection

Islanding is the transition from grid-connected to islanded mode, which includes planned islanding and unplanned islanding. The transition control functions are implemented in the central controller state machine function. During planned islanding, the microgrid controller regulates the output power of the sources in the microgrid to minimize the power flow through planned islanding. For the unplanned islanding triggered by fault or other abnormal conditions, the protection coordination function needs to coordinate the central controller and local controllers to realize the transition.

In order to detect the islanding status under abnormal conditions, the islanding detection function is usually applied during the unplanned islanding transition. For the microgrid with dynamic boundaries, the boundary of the microgrid is not fixed, meaning that the islanding can happen at multiple locations. In the microgrid central controller, the islanding is detected by obtaining all the smart switch statuses. However, the communication in the actual microgrid can be seconds level, meaning that the central controller may not be able to detect the islanding in time.

Since the BESS works as the grid-forming source in the islanded mode, the localized islanding detection function is needed for the BESS emulator to assist the testing of the transition function. The localized islanding detection function is summarized in Fig. 4 - 4. The islanding condition is detected by the voltage and frequency of the BESS emulator, once the abnormal voltage or frequency is detected by the PLL of the BESS emulator, the BESS will start to ride through first. If the voltage or frequency is abnormal and the BESS cannot ride through, then the BESS emulator will report abnormal voltage or frequency to the central controller. Once the BESS emulator cannot ride through both the abnormal voltage or frequency at the same time, meaning that the BESS emulator has lost the main grid, then the islanding condition is detected, and the BESS emulator changes to the islanded mode control.

4.2.3 BESS Functions in Islanded Mode

1) Voltage Control and Fault Ride Through

In the islanded mode, as shown in Fig. 4 - 5, the BESS emulator works as the grid-forming source to provide microgrid voltage and frequency. A dual-loop control is applied, where the outer loop regulates the output voltage to generate current references and the inner loop controls the output current. The fault ride through is realized by limiting the current references by the outer loop. When the required current is greater than the capability of the BESS emulator, the output loop saturates to limit current references and the inner loop continues to regulate the output current. Reference limiting is the same as equations (4-4) and (4-5).

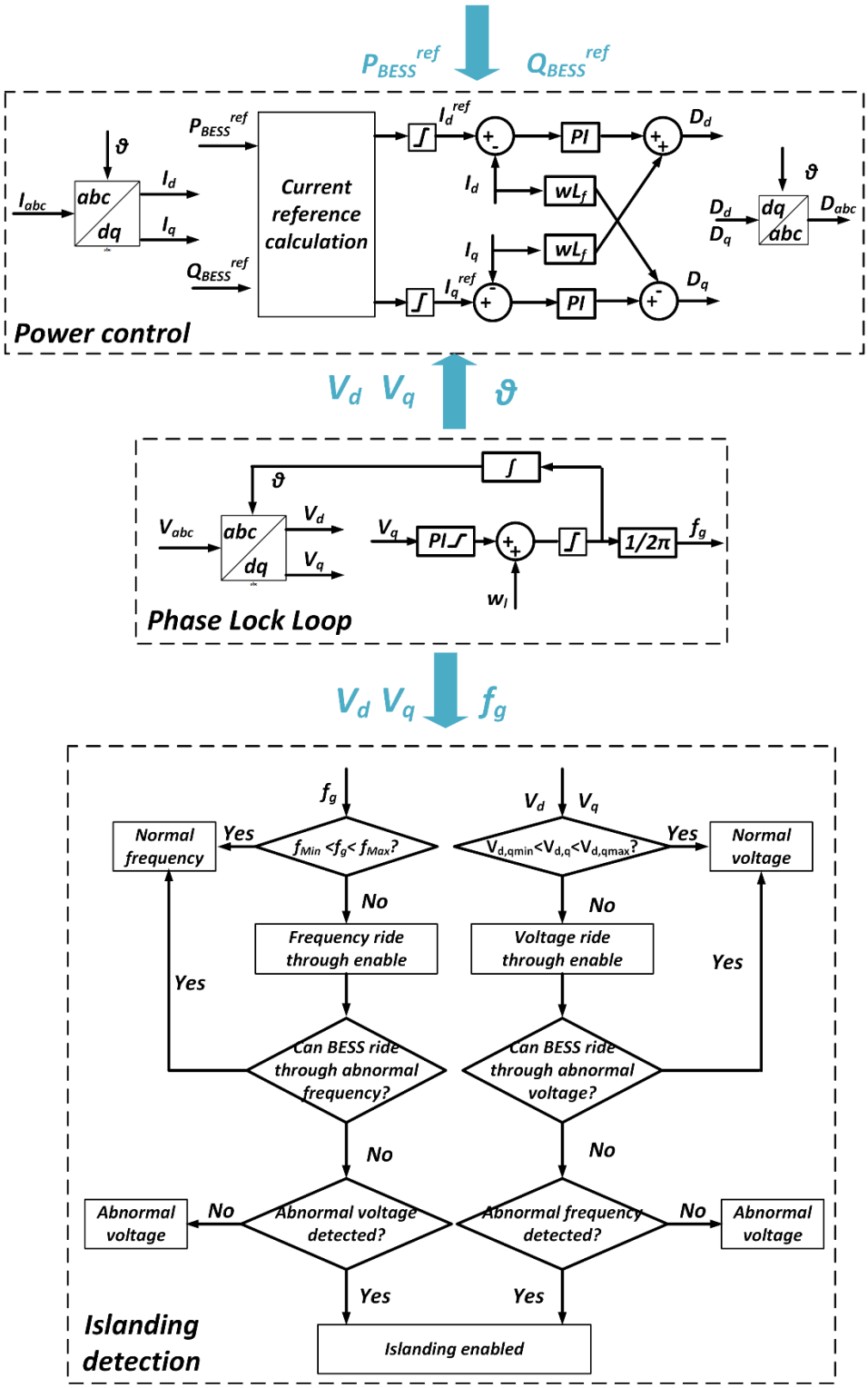


Fig. 4 - 4. BESS emulator control algorithms in grid-connected mode.

2) Primary and Secondary Droop Control with Virtual Impedance

Droop control is applied for grid-forming BESS emulators to provide frequency regulation capability and realize paralleling of multiple inverters. Two paralleled grid-forming BESS emulators are used as an example to discuss the droop control algorithm, which is shown in Fig. 4 - 6. The output voltages V_1 and V_2 are controlled by the BESS emulators. The angle of V_1 is assumed to be δ while the angle of V_2 is assumed to be 0. Therefore, the output apparent power of BESS emulator 2 is described as:

$$S_2 = V_2 I_2^* = V_2 \left(\frac{V_1 \angle \delta - V_2}{R_{Line} + j\omega_{Line} L_{Line}} \right)^* \quad (4-6)$$

where R_{Line} and L_{Line} are the line resistance and inductance. When the line impedance is dominated by the inductance as in (4-7)

$$\omega_{Line} L_{Line} \gg R_{Line} \quad (4-7)$$

the active and reactive power of BESS emulator 2 can be expressed as:

$$P_2 = \frac{V_1 V_2}{\omega_{Line} L_{Line}} sin\delta \quad (4-8)$$

$$Q_2 = \frac{V_1 V_2 cos\delta - V_2^2}{\omega_{Line} L_{Line}} \quad (4-9)$$

When δ is small, $sin\delta \approx \delta$, $cos\delta \approx 1$, then the voltage and angle differences can be expressed as

$$\delta = \frac{V_1 V_2}{P_2 \omega_{line} L_{Line}} \quad (4-10)$$

$$\Delta V = \frac{V_2}{Q_2 \omega_{Line} L_{Line}} \quad (4-11)$$

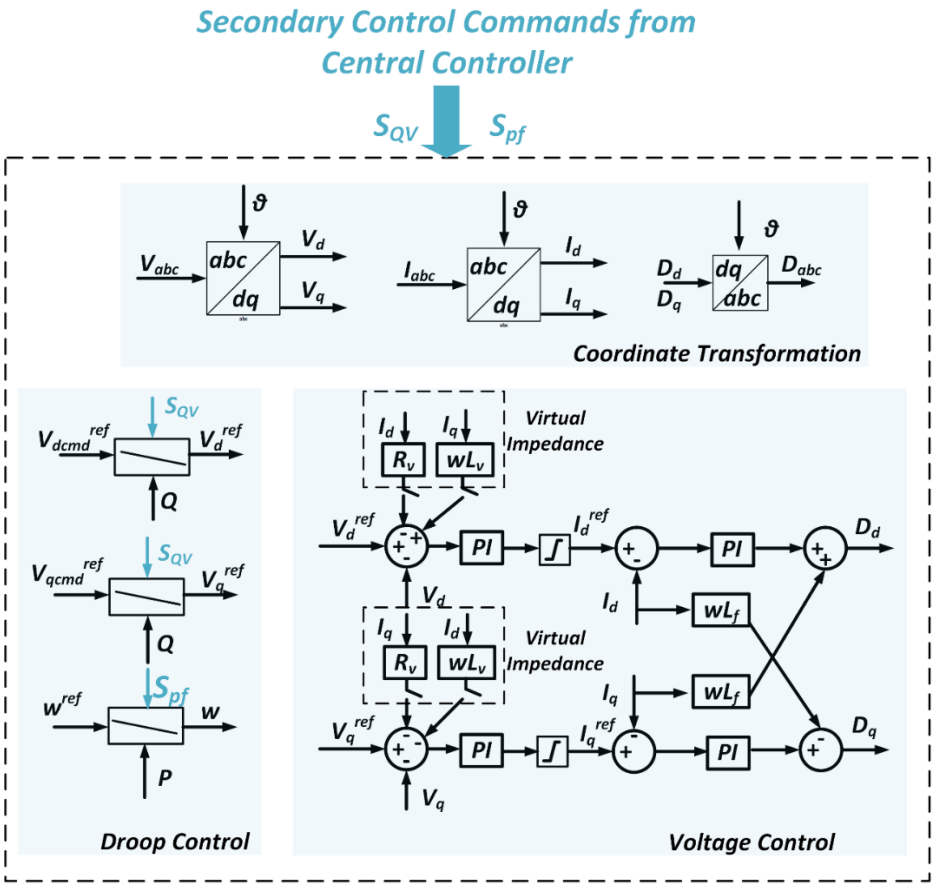


Fig. 4 - 5. BESS emulator control algorithms in islanded mode.

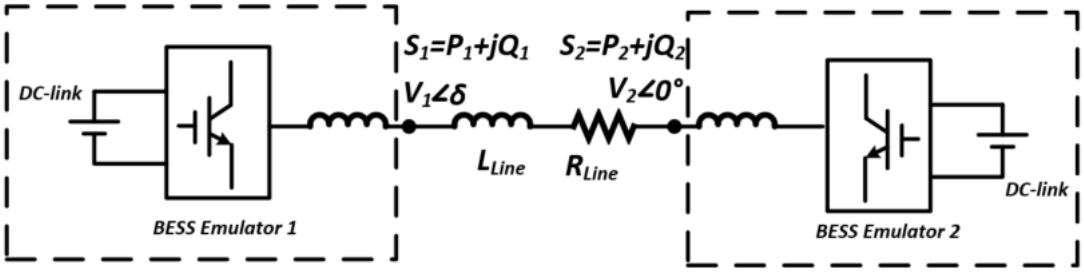


Fig. 4 - 6. Power transferring for two grid-forming BESS emulators.

Therefore, the angle differences are coupled with the active power, and the voltage differences are coupled with the reactive power, which results in the active power-frequency droop (P-f) and reactive power voltage droop (Q-V) characteristics. The droop characteristics are represented by as:

$$\omega_t = \omega_0 - k_{Pf}(P_t - P_0) + S_{PF} \quad (4-12)$$

$$V_t = V_0 - k_{QV}(Q_t - Q_0) + S_{QV} \quad (4-13)$$

where subscript *t* represents the real-time value; subscript *0* is for initial offset; k_{Pf} and k_{QV} are droop constants. S_{PF} and S_{QV} are the secondary control commands from the central controller.

The primary and secondary droop control functions are explained in Fig. 4 - 7. In the primary control, the frequency and voltage amplitudes change with the active and reactive power following the defined droop curves, respectively. However, due to the primary droop regulation, the frequency or voltage may deviate from the targeted value. The secondary will be applied to regulate the voltage and frequency to the targeted value by moving the droop curves.

Taking the *P-f* droop as an example, as shown in Fig. 4 - 7, when the active power of the inverter is P_t, the frequency will be regulated to ω_t. Assume ω_0 is the targeted frequency for the microgrid. The inverter needs to rely on the secondary control to move the droop curve to regulate the output frequency from ω_t to ω_0. Moreover, for paralleling multiple BESS emulators, the secondary control can control the power sharing among different emulators.

However, in microgrids, especially those small in scale, the line impedance may not meet (4-7). This may lead to inaccurate *P-f* and *Q-V* droop characteristics. Moreover, according to [78], smaller line impedances are more likely to induce instability issues in microgrids with multiple droop-controlled inverters. Therefore, to solve the issues caused by the line impedance, the virtual impedances can be added to the output impedances of BESS emulators [79-80].

As shown in Fig. 4 - 5, by adding the virtual impedances, so that they can meet (4-14):

$$\begin{cases} R_v \gg R_{Line} \\ L_v \gg L_{line} \end{cases} \quad (4-14)$$

Then the output impedances emulators are dominated by the virtual impedances. At this condition, when the added virtual impedance meets (4-7), the P-f and Q-V droop characteristics can be valid for control implementation.

Furthermore, besides voltage regulation, frequency regulation, and power sharing among different emulators, the applied droop control can also assist reconnection. During the reconnection transition, the central controller regulates the BESS emulator frequency to resynchronize with the main grid. Due to the communication delay, the mode transition commands may not arrive at BESS emulators before a boundary switch is closed by the reconnection function. During this short period, the BESS emulator with droop control can connect to the grid in the grid-forming mode first and then change to the grid-following mode once the commands arrive.

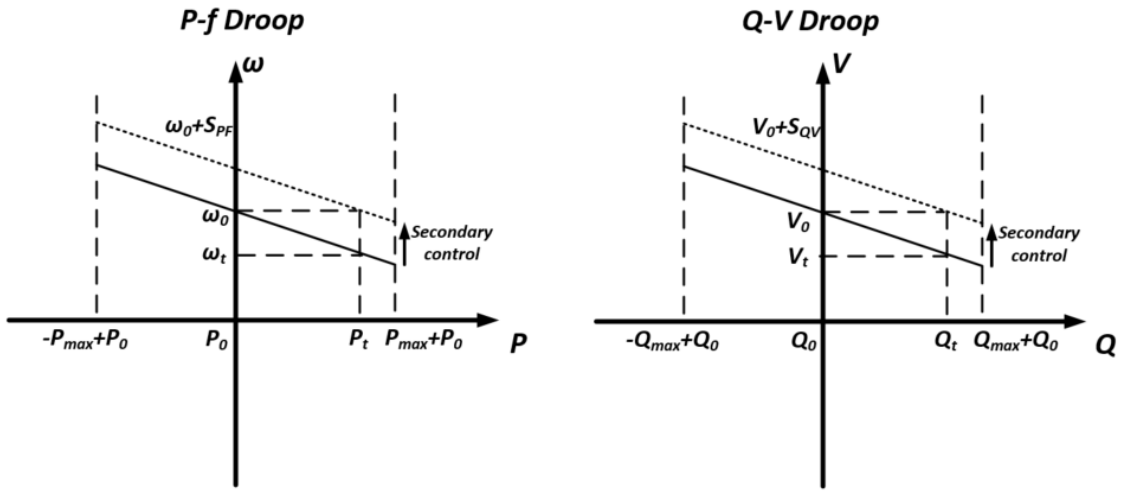


Fig. 4 - 7. Primary and secondary droop control.

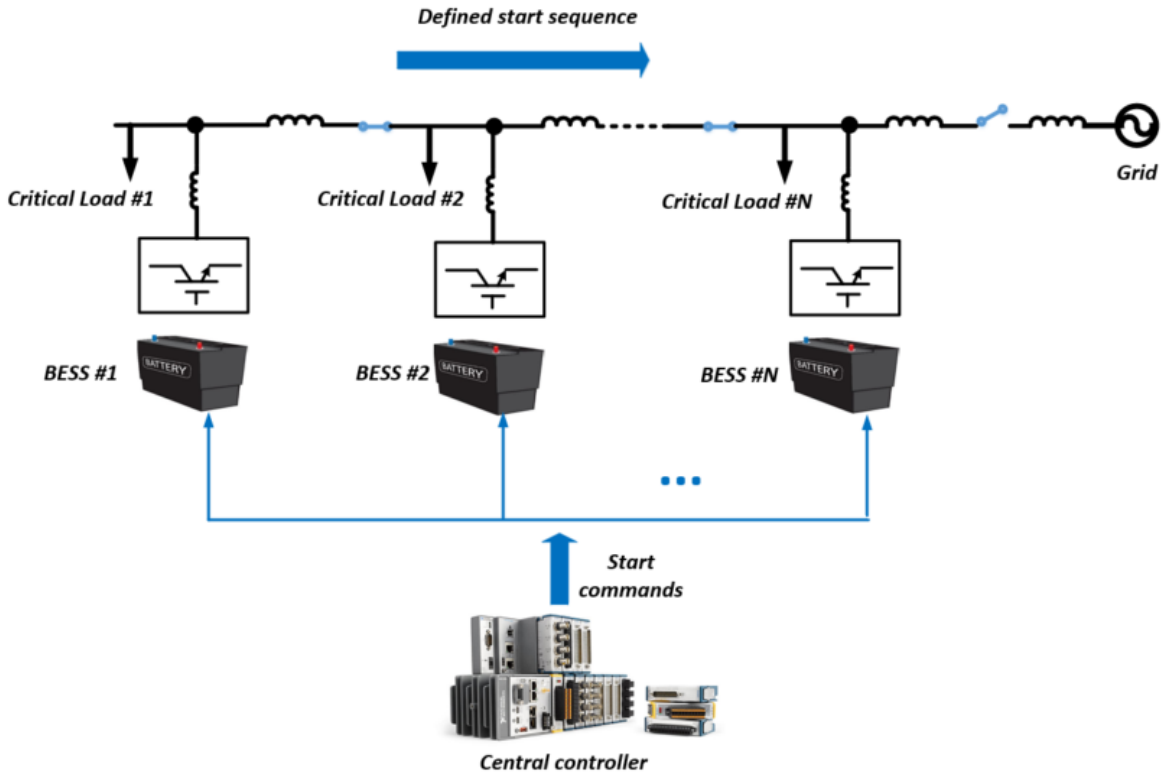


Fig. 4 - 8. Merged island black start control.

4.2.4 BESS Functions in Transitions

1) Black Start

Black start is the startup transition that the microgrid is enabled from the shutdown condition to the steady-state islanded mode. In a microgrid with dynamic boundaries and multiple sources, the black start function can potentially enable the microgrid to a merged island or separate islands.

The BESS regulates the output voltage and frequency with droop control in the islanded mode. For the cases that the microgrid starts to a merged island, the initial frequency and phase angles of multiple BESSs may be different, and droop control cannot respond fast enough to regulate the frequency and phase angle, which can result in a large inrush current among different BESSs.

Therefore, the BESSs need to coordinate with the central controller to reduce the inrush current. As shown in Fig. 4 - 8, the central controller will define the starting sequences of multiple BESSs so that the first enabled BESS can establish the voltage and frequency to the whole microgrid. After the voltage and frequency are established, the rest of the BESSs will obtain the voltage, frequency, and phase information locally and starts the islanded operation.

Therefore, in the HTB testing of microgrids with multiple sources, the BESS emulator is required to have the local startup detection function of voltage, frequency, and phase angle of the microgrid. As shown in Fig. 4 - 9, the startup detection is realized through PLL. Before the BESS executes the islanded mode control, the PLL will keep operating to get the voltage, frequency, and phase

information. Once the PLL reaches the steady-state, the BESS emulator can enable the control in the islanded mode by using the detected voltage, frequency, and phase as the initial point for the control.

2) Local Grid-Forming Mode in Islanding transition

During the unplanned islanding transition, due to the communication delay, the mode transition commands from the central controller cannot arrive in time to change BESS operation mode. The local islanding detection function detects the islanded condition and issues mode change. However, the state machine of the central controller still requires the grid-connected operation, which results in an operation mode conflict of the BESS emulator.

To solve this issue, as shown in Fig. 4 - 10, a local grid-forming mode is defined for the islanding transition. When the islanding detection issues the islanded operation command, the BESS will switch to the local grid-forming mode and the grid-connected operation commands will not be executed in this mode. The BESS will change to the normal grid-forming mode when the islanded operation commands from the central controller arrive.

During the local grid-forming mode, the secondary droop control is not available because the central controller commands are not available. The local grid-forming mode only contains primary droop control, voltage control, and virtual impedance control for power sharing.

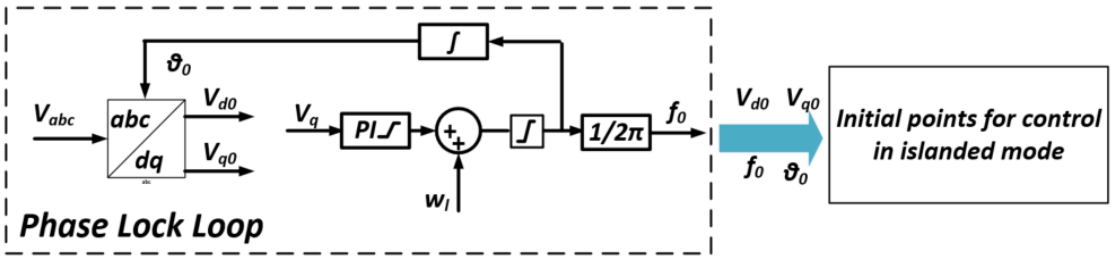


Fig. 4 - 9. PLL-based startup control method.

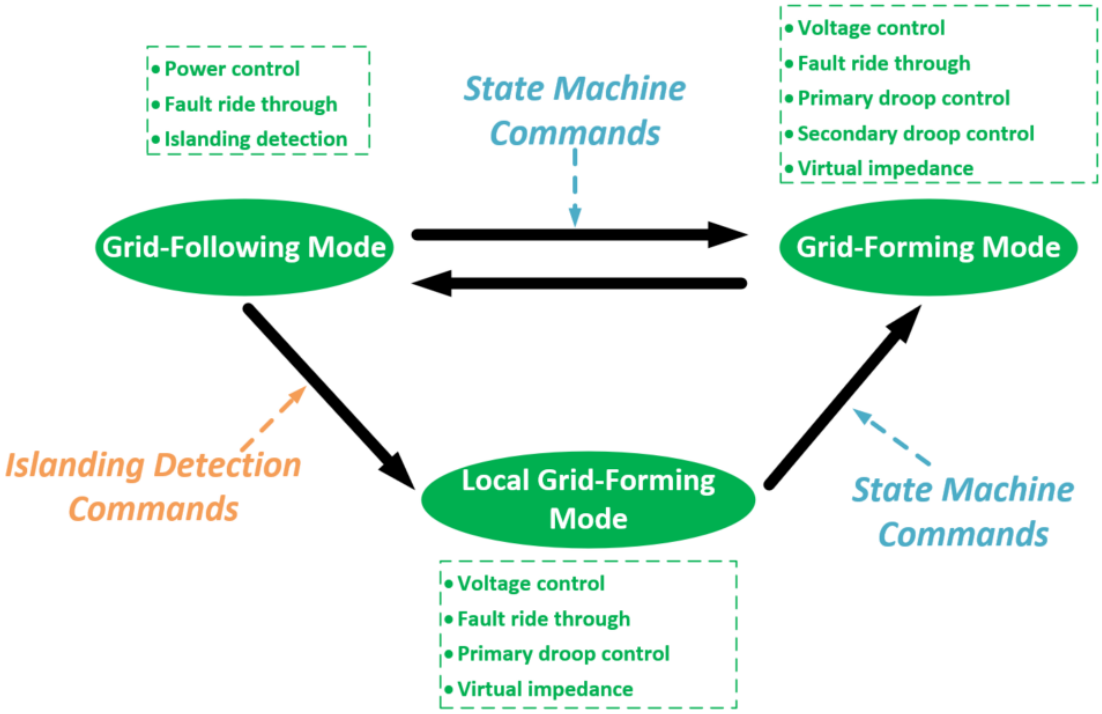


Fig. 4 - 10. Control mode transition of BESS emulator.

4.3 Experimental results

In this section, the proposed BESS emulator is verified independently on the developed HTB. The testing conditions in this section are summarized in Table 3 - 1, Table 3 - 2, and Table 3 - 3. Five testing cases are designed to verify all the proposed BESS functions, which are BESS in grid-connected mode with grid suddenly unavailable, BESS in grid-connected mode with fault occurred, BESS startup and steady-state islanded operation, BESS in islanded mode with fault occurred, BESS in islanded mode with secondary control.

4.3.1 BESS in Grid-Connected Mode with Grid Suddenly Unavailable

In the grid-connected mode, using the topology in Fig. 3 - 4, all the smart switches are closed, grid interface G0, load L3 and BESS 2 are enabled for the testing. As shown in Fig. 4 - 11, before time t_1, the BESS controls the output power. At t_1, the grid becomes unavailable, the grid current changes to zero and the voltage starts to drop. Once the islanding condition is detected at t_2, the BESS emulator switches the operation mode to local grid-forming mode to establish voltage and frequency and the load can be supported.

4.3.2 BESS in Grid-Connected Mode with Fault Occurred

In the grid-connected mode, to demonstrate the fault ride through and transition capability, using the topology in Fig. 3 - 4, all the smart switches are closed, grid interface G0, load L3, and BESS2 are enabled for the testing. As shown in Fig. 4 - 12, the fault of L3 occurs at t_1, and the grid is disconnected manually at t_2 to emulate the protection response.

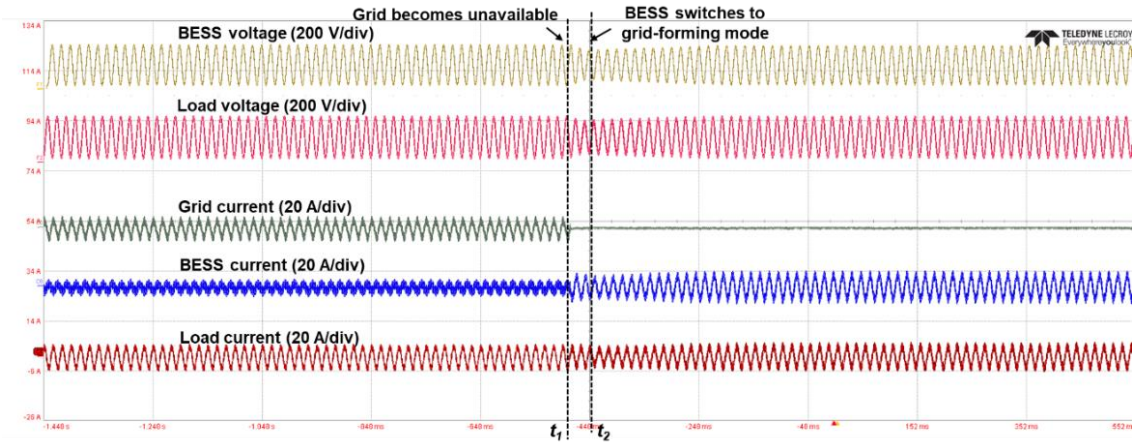


Fig. 4 - 11. Experimental waveforms when grid suddenly becomes unavailable in grid-connected mode.

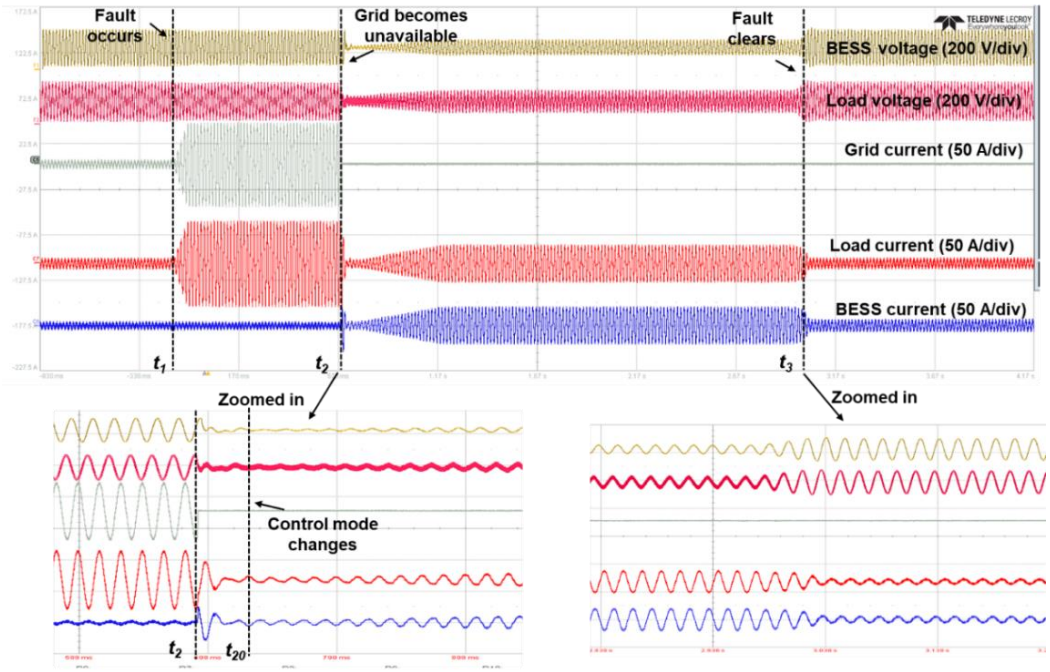


Fig. 4 - 12. Experimental waveforms when the grid is unavailable, and fault still occurs.

The fault is cleared at t_3 to emulate a temporary fault. During this process, the BESS ride though, islanding detection and mode transition functions can be verified. At t_1, the grid provides fault current, and the BESS keep its output as it is a power-controlled source; at t_2, the grid becomes unavailable while the fault still occurs, the islanding is detected by the BESS at t_{20} and the BESS control mode transition changes to the grid-forming mode. Since the fault still exists, the grid-forming controlled BESS starts to ride through to limit the output current. When the fault clears at t_3, the BESS regulates the voltage to the normal condition.

4.3.3 BESS Startup and Steady-State Islanded Operation

Using the topology in Fig. 3 - 4, all the smart switches are closed. BESS1, BESS2, and Load L3 are enabled for testing. The experimental results of BESS startup and steady-state islanded operation are shown in Fig. 4 - 13. Two BESS are applied to demonstrate the startup transition and power sharing. BESS1 and BESS2 start at t_1 and t_2, respectively. When the voltage is established by BESS1, BESS2 locks the frequency and phase angle of BESS1 and enables voltage control. The transient current of startup transition is small.

Since the ratings of the two BESS emulators are the same, the initial droop curves of the two BESS emulators are the same. The load increases at t_3 and the currents of two BESS emulators increase accordingly to support the load, showing that two voltage-controlled BESS emulators can realize the load sharing. BESS1 is shut down at t_4 and BESS2 can continue to support the load, demonstrating that BESS2 is in the grid-forming mode.

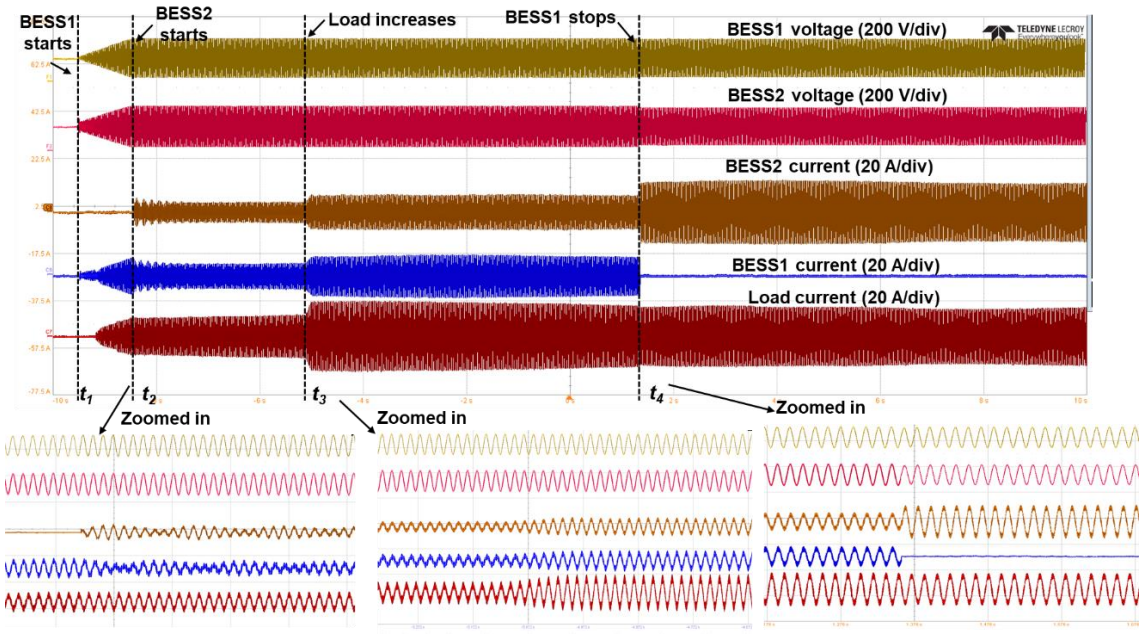


Fig. 4 - 13. Experimental waveforms of BESS emulator's startup and operation in islanded mode.

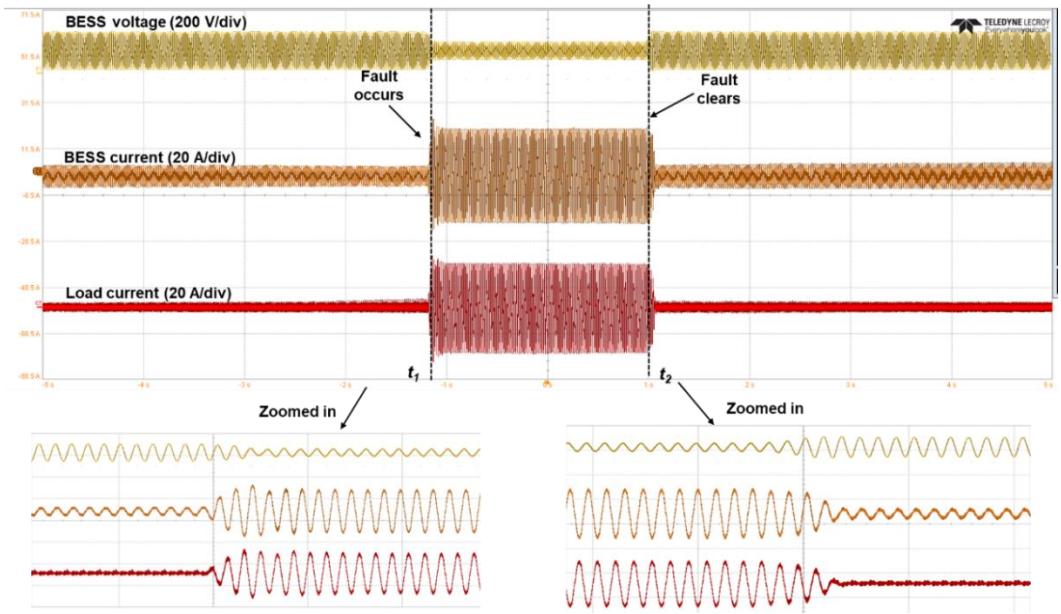


Fig. 4 - 14. Experimental waveforms of BESS fault ride through in the islanded mode.

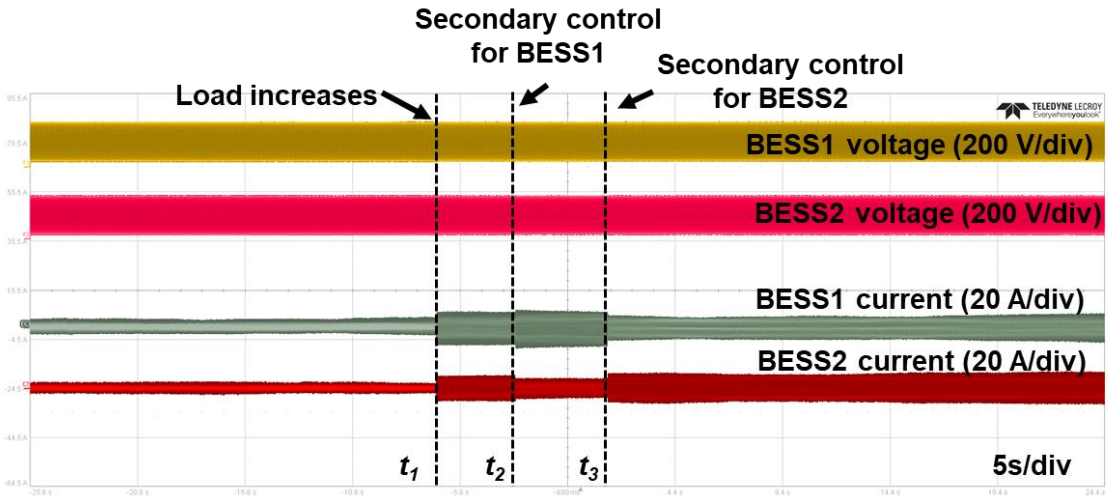
4.3.4 BESS in Islanded Mode with Fault Occurred

Using the topology in Fig. 3 - 4, all the smart switches are closed. BESS2 and Load L3 are enabled for the testing. As shown in Fig. 4 - 14, by decreasing the resistance of the load emulator L3, the fault is emulated at t_1. Since in the islanded mode, the microgrid voltage is provided by the BESS emulator, when the load required current is greater than the current capability, the BESS limits its output according to (4-4) and (4-5), which results in voltage drop. The voltage drops at t_1 and the output current is limited to the maximum value. When the fault clears at t_2, the microgrid voltage recovers to the normal condition.

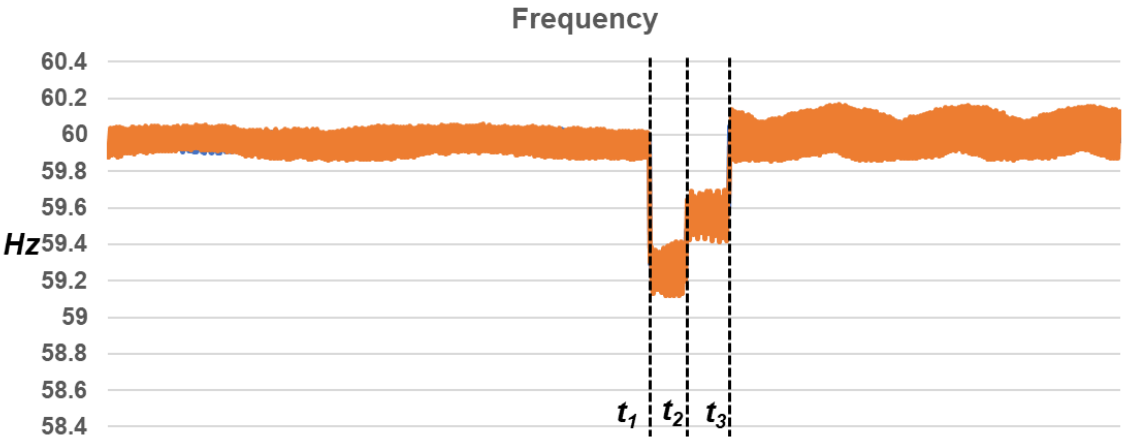
4.3.5 BESS in Islanded Mode with Secondary Control

Using the topology in Fig. 3 - 4, all the smart switches are closed. BESS1, BESS2, and Load L3 are enabled for testing. As shown in Fig. 4 - 15, the secondary droop control is verified with two BESS emulators with the same droop curve for primary control and one load.

The load increases at t_1 and two BESS emulators increase the power to support the load, which results in frequency drop. The secondary control is emulated by manually moving the droop curves of the BESS1 and BESS2 to regulate the frequency back to 60 Hz. During the changing process, the power sharing among two BESSs changes with the droop curve moving.



(a) Waveforms of BESS voltages and currents from the oscilloscope.



(b) Microgrid frequency from controller data logging.

Fig. 4 - 15. Experimental waveforms BESS emulator operation in islanded mode.

4.4 Summary

Different microgrid central controller functions require different support from BESSs. By summarizing the central controller functions, the required functions of BESS emulators are determined, including SOC indication, functions in grid-connected and islanded modes, and functions in transitions. The algorithm of each function is stated and coordination among different functions is also discussed. During different microgrid operation modes, the BESS emulator can work in either grid-following mode with islanding detection or grid-forming mode with primary and secondary droop regulation. Moreover, specific control functions are proposed in the mode transitions to improve the transient performances.

Experimental results demonstrate that the proposed BESS emulator can realize the targeted operation in both grid-connected mode, islanded mode, and mode transitions. The proposed BESS emulator can be applied for the microgrid central controller testing.

CHAPTER 5. DEMONSTRATION OF MICROGRID CONTROLLER HTB TESTING

In this chapter, the developed microgrid testing platform is applied for the actual microgrid central controller testing. Two different microgrid controllers are tested. The first controller is for the microgrid with dynamic boundaries and the second controller is the microgrid for dynamic boundaries and multiple sources at different locations. The testing focuses on the real-time operation of the microgrid to evaluate the controller performances [81].

5.1 Controller for Microgrid with Dynamic Boundaries

The controller for the microgrid mentioned in chapter 3.2.1 (shown in Fig. 3 - 3) is tested on the developed microgrid HTB with the proposed BESS emulator. The testing condition is summarized in Table 3 - 1, Table 3 - 2, and Table 3 - 3. In this microgrid, load section L8 is the critical load while other loads are non-critical. For this controller, since all the DER sources are placed at one location, meaning that there is only one island with dynamic boundaries in this microgrid. Six testing scenarios are designed for the controller debugging, which are summarized in Table 5 - 1. In this chapter, the testing demonstrating sequence is the black start, steady-state islanded operation, reconnection, unplanned islanding, steady-state grid-connected operation, and protection coordination.

5.1.1 Black Start Test

The black start is the process that the microgrid starts from the shutdown condition to the steady-state islanded operation in a safe and smooth manner. The

testing results are shown in Fig. 5 - 1, where the data comes from the central controller data logging function. The BESS startup command is issued at t_1, and the BESS emulator starts at t_2 by increasing the output power.

The PV emulator starts after the BESS emulator establishes the voltage and frequency of the microgrid at t_3 and power starts to change at t_4. During this process, the microgrid central controller regulates the PV output to avoid over-charge of the BESS. After the PV emulator reaches steady-state, the microgrid is in the steady-state islanded operation.

5.1.2 Steady-State Islanded Operation Test

In the steady-state islanded operation, the controller regulates the maximum boundary based on the available DER power outputs. The testing results of the steady-state islanded operation are shown in Fig. 5 - 2 and Fig. 5 - 3, where Fig. 5 - 2 is obtained from the oscilloscope and Fig. 5 - 3 is based on the recorded data in the microgrid controller.

The oscilloscope waveforms include the real-time voltage waveforms of BESS, load L2, and load L3 as well as current waveforms of the PV and BESS emulators. The recorded data contains the power information of BESS and PV emulators as well as statuses of all the smart switches. The testing starts after the black start finishes when the PV emulator output is zero and the critical load L8 is supported by the BESS emulator. The output of the PV emulator starts to change at t_1, and the controller starts to pick up loads when the PV output increases.

Table 5 - 1. Testing cases for the controller of microgrid with dynamic boundaries

Type	Test case name
Steady-state cases	Steady-state islanded operation
	Steady-state grid-connected operation
Dynamic cases	Black start
	Islanding
	Reconnection
	Protection coordination

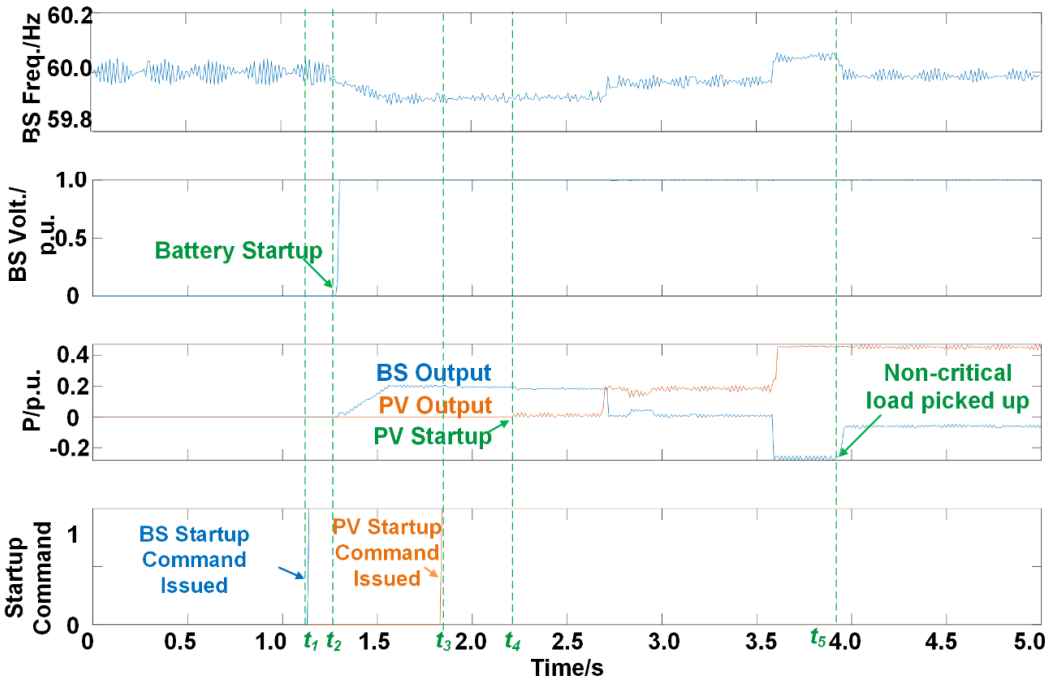


Fig. 5 - 1. Testing results of steady-state islanded operation.

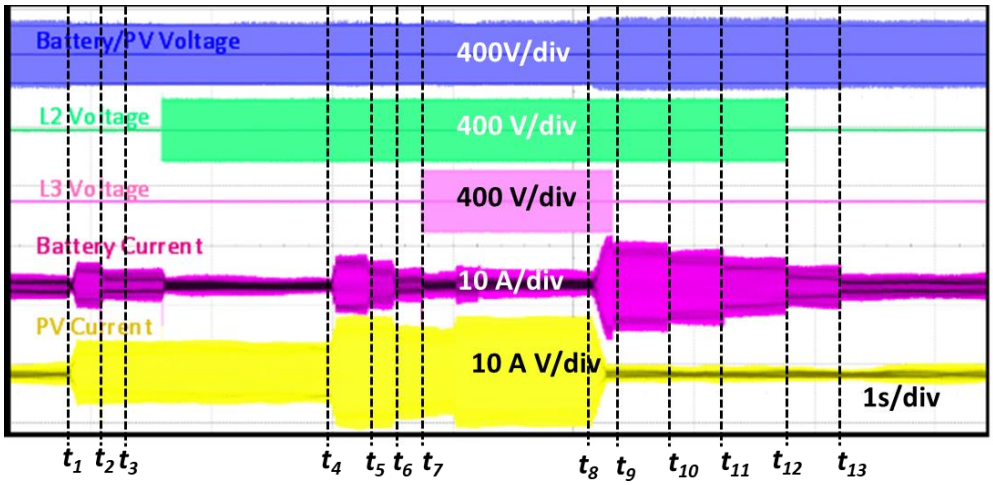


Fig. 5 - 2. Testing results of steady-state islanded operation.

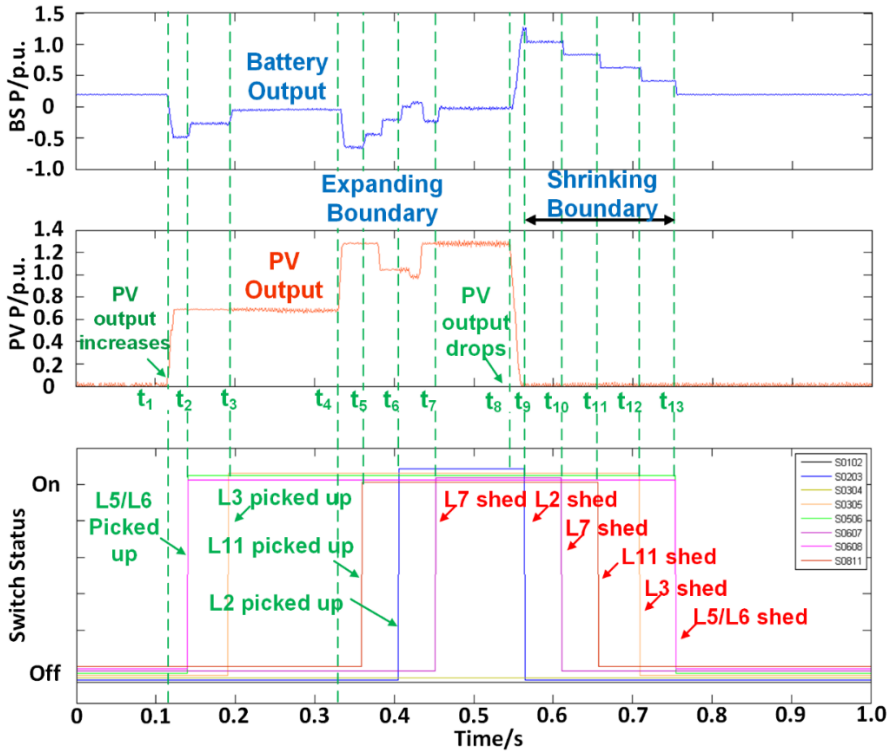


Fig. 5 - 3. Detailed information of steady-state islanded operation.

All the loads are picked up at t_7 while the extra PV output is stored in the BESS emulator. Starting from t_8, the PV emulator output power starts to decrease, and the controller starts to shrink the boundary by shedding loads. All the non-critical loads are shed at t_{13} when the PV output changes back to zero. This testing demonstrates the dynamic boundary control in the islanded mode.

During this testing, the HTB testing can evaluate the controller performance under measurement noise since the power calculation needs the actual power information. The controller is expected to operate normally when there is measurement noise. To reduce the impact of measurement noise, digital filters are added to central controller functions. Due to actual power flow and inverter switching actions, the controller is placed in the environment with electromagnetic noise to further evaluate the controller noise immunity performance. Meanwhile, during this testing, the proposed BESS emulator works as the grid-forming source to provide stable voltage and frequency to the microgrid. When the load changes, the BESS emulator can respond to the load change, showing that the proposed BESS emulator can support microgrid controller testing in the islanded mode.

5.1.3 Reconnection Test

The islanded microgrid can reconnect to the main grid through reconnection transition. For the microgrid with dynamic boundaries, since the boundary is not fixed, the microgrid can reconnect to the grid at multiple locations. In this chapter, the reconnection at the smart switch “0608” is applied to demonstrate the testing. The testing results are shown in Fig. 5 - 4, Fig. 5 - 5, and Fig. 5 - 6.

During the reconnection transition, the central controller will regulate the voltage, frequency, and phase angle difference between the two sides of switch “0608” to reduce the transients. During the reconnection, the microgrid starts from the minimum boundary. At t_1, grid voltage becomes available, and the reconnection starts. The grid gradually picks up loads from t_2 to t_5 where switch 0608 is identified as the boundary at t_4.

Then the central controller starts to regulate the voltage and phase differences between the two sides of switch 0608 by coordinating with the BESS and PV emulator. Once the voltage and phase differences are reduced to be less than the predefined thresholds, the switch 0608 closes and the BESS emulator changes from the grid-forming mode to grid-following mode at t_7. The last non-critical load L11 is picked up at t_8 and reconnection transition is completed. The microgrid is in the grid-connected operation.

During the reconnection transition testing on HTB, the measurement noise of the smart switches challenge the controller threshold design. Due to the noise impact, a small threshold may never be triggered as the measurement error may be larger than the threshold. However, a large threshold will increase the transient current. Communication delay (between t_6 and t_7) observed in the testing also results in challenges of the central controller. The local controller functions such as transition functions in BESSs may be applied to reduce the transient during the delay, requiring coordination among central and local controllers.

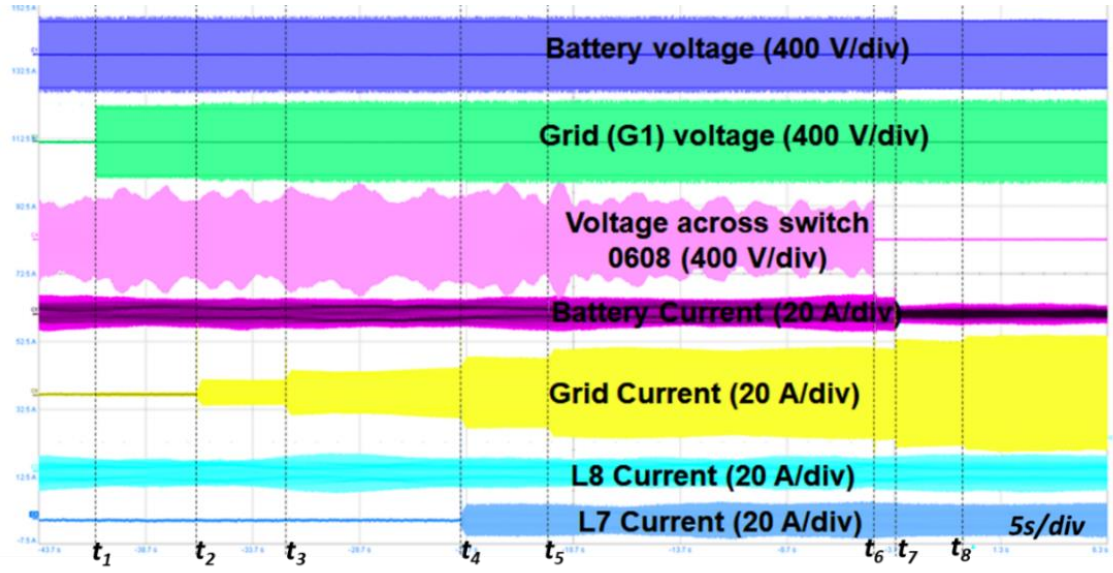


Fig. 5 - 4. Oscilloscope waveforms of the reconnection transition.

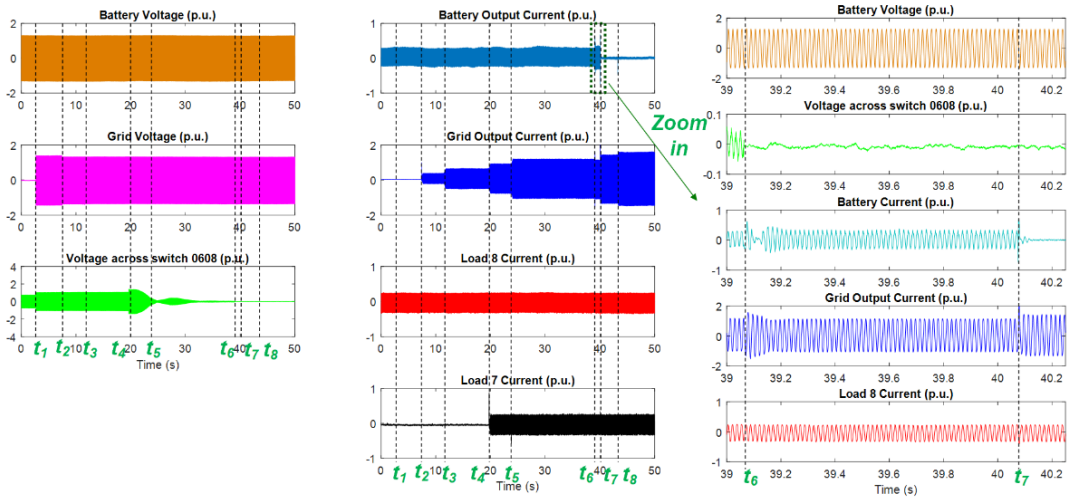


Fig. 5 - 5. Detailed information of reconnection transition.

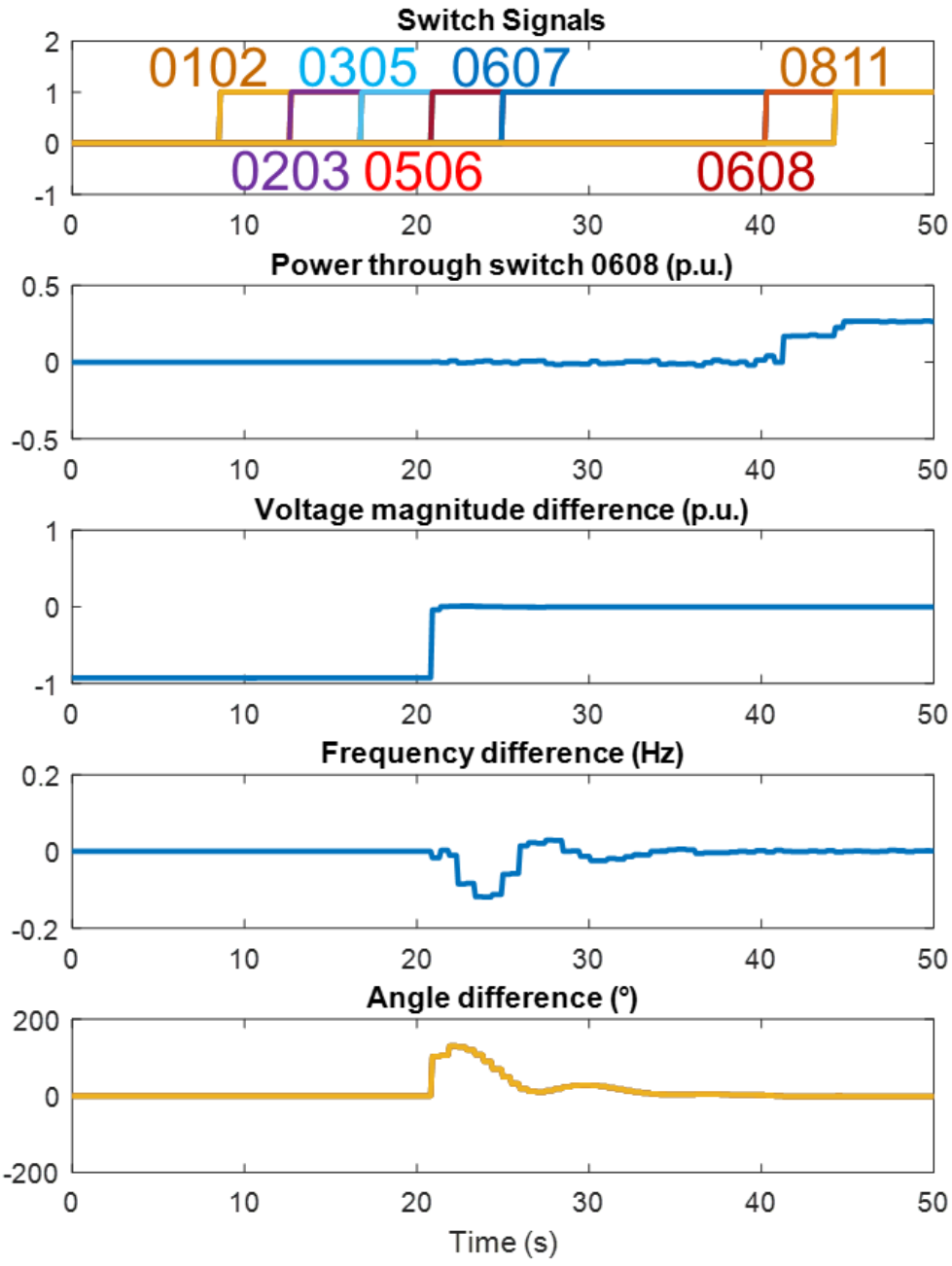


Fig. 5 - 6. Experimental results of reconnection process through switch 0608 acquired from controller data logging function.

5.1.4 Islanding Test

The unplanned islanding is tested to demonstrate the microgrid HTB capability for islanding transition. The testing results are summarized in Fig. 5 - 7 and Fig. 5 - 8. The oscilloscope waveforms are shown in Fig. 5 - 7, where the grid emulator becomes unavailable at t_1 and the BESS emulator switches to grid-forming mode to support the microgrid voltage. The PQ balance function starts to operate to control the load condition through smart switches at t_{PQ} when the load L_2 and L_3 are shed and BESS current drops.

The zoomed-in results are shown in Fig. 5 - 8. When the grid becomes unavailable, the BESS emulator loses the voltage and frequency information, and the local islanding detection function detects the islanding condition at t_{10} and starts to regulate the voltage and frequency. The central controller mode transition commands arrive at t_2 and the BESS changes to the normal islanded operation.

5.1.5 Steady-State Grid-Connected Operation Test

In the testing microgrid topology, there are two potential grid interfaces for the microgrid. The testing of the grid-connected operation is to change the grid interface of the microgrid based on the sequence shown in Fig. 5 - 9: steady-state grid-connected operation with grid interface G1, the microgrid does the islanding from G1 at t_1 and then reconnects to G4 at t_2. This testing demonstrates coordination among different central controller functions.

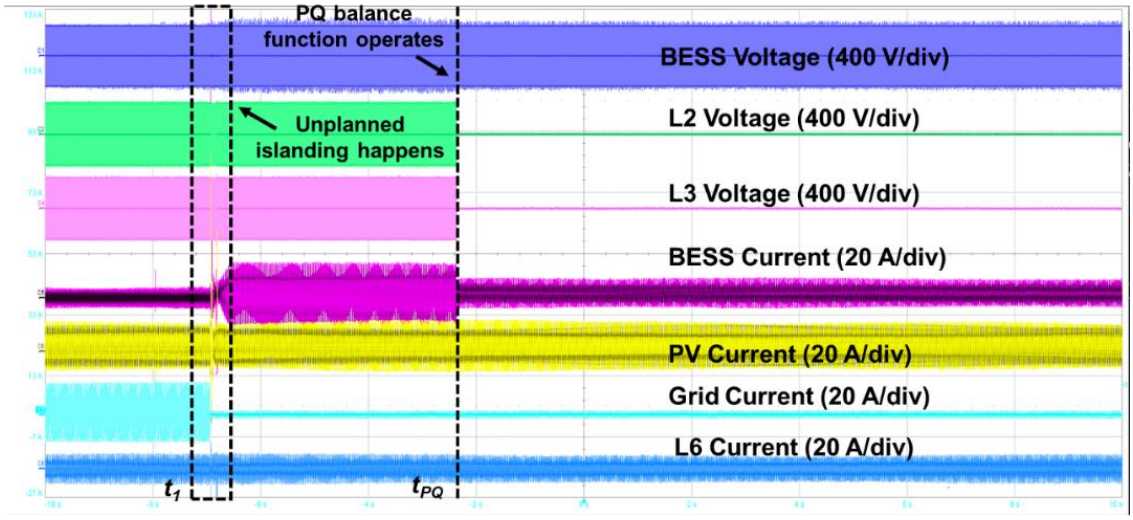


Fig. 5 - 7. Oscilloscope waveforms of the unplanned islanding transition.

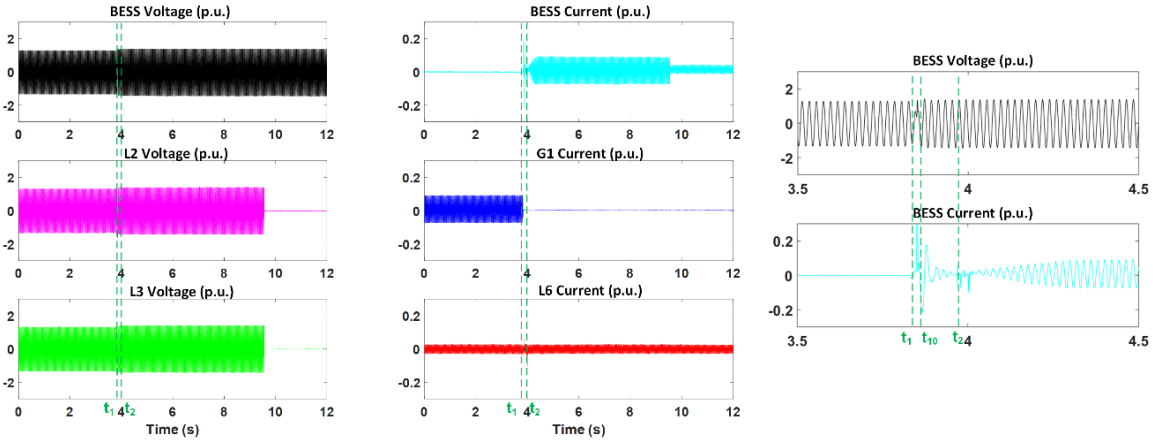


Fig. 5 - 8. Detailed information of the unplanned islanding transition.

.

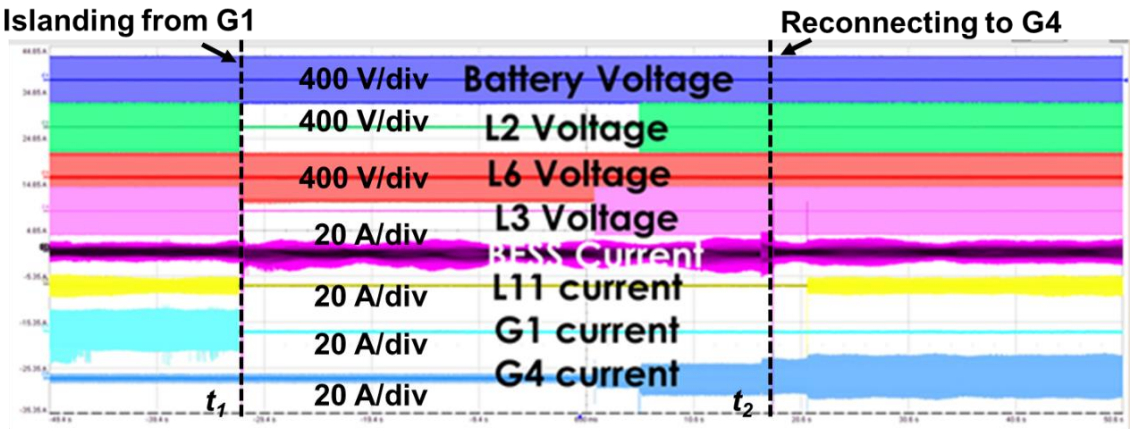


Fig. 5 - 9. Waveforms of grid-connected mode with dynamic boundary operation

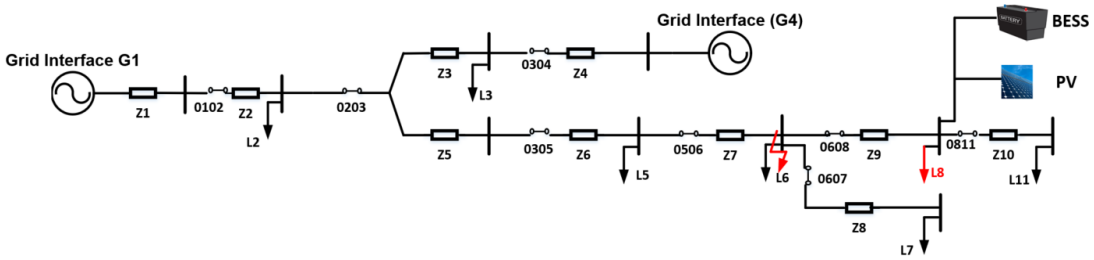


Fig. 5 - 10. Fault applied at load L6 in the grid-connected mode.

5.1.6 Protection Coordination Test

In the grid-connected operation, the microgrid is formed by the main distribution grid which provides a large current during the fault condition. Therefore, the current based protection strategy is usually applied. In the islanded mode, since the microgrid is usually formed by local DERs which have limited fault current capability, the voltage-current coordinated protection strategies are potential selections. Therefore, the protection testing includes two cases: 1) fault in grid-connected mode and 2) fault in islanded mode.

1) Fault in Grid-Connected Mode

As discussed in chapter 3, since inverter emulators in HTB have limited capability to only emulate high impedance fault, high impedance fault will be tested. As shown in Fig. 5 - 10, the fault is applied at load L6. The testing results are shown in Fig. 5 - 11. The permanent fault occurs at t_1, and fault current flows through switch 0506 to the main grid. The protection responds at t_2 by opening switch 0506 and sending a transfer tripping signal to switch 0608. The BESS changes to the grid-forming mode. Since the fault at L6 has not been cleared, and transfer trip signals have not arrived at switch 0608 because of communication delay, the BESS limits the output current to rides through the fault. Once the transfer trip signal arrives at switch 0608 at t_3, the fault is isolated, and the BESS voltage recovers to the normal condition. After the fault is cleared, the smart switch 0506 tries to reclose three times at time t_4 – t_6. However, since the permanent fault is

applied, the reclosing cannot be successful, and the switch 0506 is locked after reclosing attempts.

2) Fault in Islanded Mode

In the islanded mode, the protection curves of all the smart switches are updated to voltage-based protection curves. The protection coordination is also tested by applying fault at load L6. The testing results are shown in **Error! R eference source not found.**. The permanent fault occurs at $t_{1,}$ and the BESS starts to ride through. The smart switch 0608 detects and isolates the fault at t_2. After the fault isolation, three reclosing are conducted by the smart switch at t_3, t_5, and t_7. After the reclosing, the smart switch 0608 is locked at t_8.

5.2 Controller for Microgrids with Dynamic Boundaries and Multiple Sources at Different Locations

The controller for the microgrid mentioned in chapter 3.2.1 (shown in Fig. 3 - 4) is also tested on the developed microgrid HTB with the proposed BESS emulator. In this microgrid, there are two critical load sections (L1 and L6) with three grid-forming sources at different locations, meaning that two islands can be formed in the islanded mode. To test the controller of this microgrid, five testing scenarios are designed for the controller debugging, which are summarized in Table 5 - 2. The testing design focuses on the coordination of multiple sources both in steady-state operation and mode transitions. The testing demonstrating sequence is the black start, steady-state islanded operation, reconnection, islanding, and steady-state grid-connected operation.

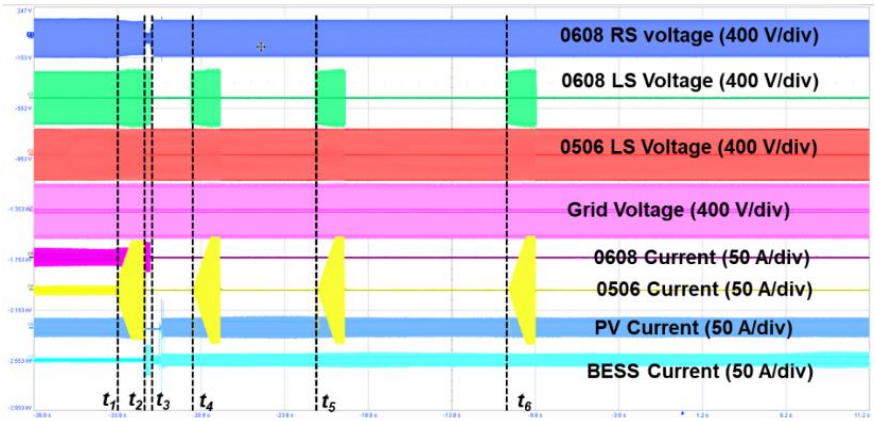


Fig. 5 - 11. Protection coordination testing results in grid-connected mode.

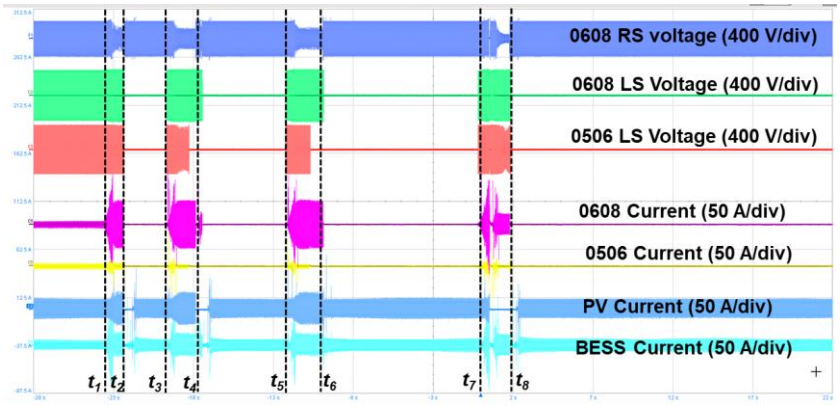


Fig. 5 - 12. Protection coordination testing results in islanded mode.

Table 5 - 2. Testing cases for the controller of microgrid with dynamic boundaries and multiple sources.

Type	Test case name
Steady-state cases	Steady-state islanded operation
	Steady-state grid-connected operation
Dynamic cases	Black start
	Islanding
	Reconnection

5.2.1 Black Start Test

In this microgrid, after the black start command is issued by the central controller, two BESSs start first at t_1 to pick the critical loads within each island. As shown in Fig. 5 - 13, in the island with BESS1 in Fig. 3 - 4, the PV and the backup generator also start at t_2 and t_3, respectively. After all the sources start to pick up critical loads, black start finishes, and steady-state islanded mode is reached.

5.2.2 Steady-State Islanded Operation Test

The microgrid topology is shown in Fig. 3 - 4, where two islands can be formed in the islanded mode. Testing results of the islanded operation are shown in Fig. 5 - 14, the boundary of the island with BESS 1 can be expanded and shrunk based on PV power. When the PV output increases, the boundary is expanded from t_2 to t_7, and load section L2 is picked up at t_8.to realize the maximum boundary of that island. The boundary switch between two islands is switch 0102.

5.2.3 Reconnection Test

1) Two Separate Islands Reconnected to the Main Grid Independently

From Fig. 5 - 15, the main grid gradually picks up loads by closing 0200, 0203, 0304, and 0405. Island 2 on the left is reconnected to the main grid first by closing switch 0102 through resynchronization, then island 1 on the right side resynchronizes to the main grid through switch 0406. Fig. 5 - 16 shows the voltage and current measurements during this process. ‘0102 Voltage’ and ‘0406 Voltage’ indicate the voltage differences between the two sides of each switch, respectively.

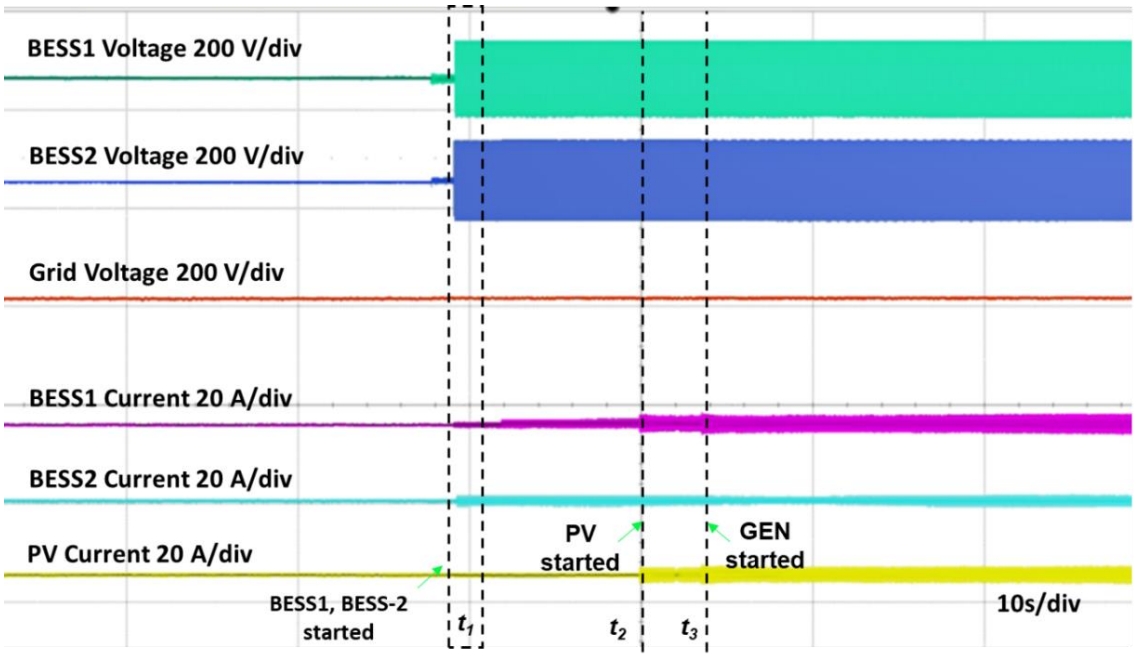


Fig. 5 - 13. Black start for a microgrid with multiple sources at different locations.

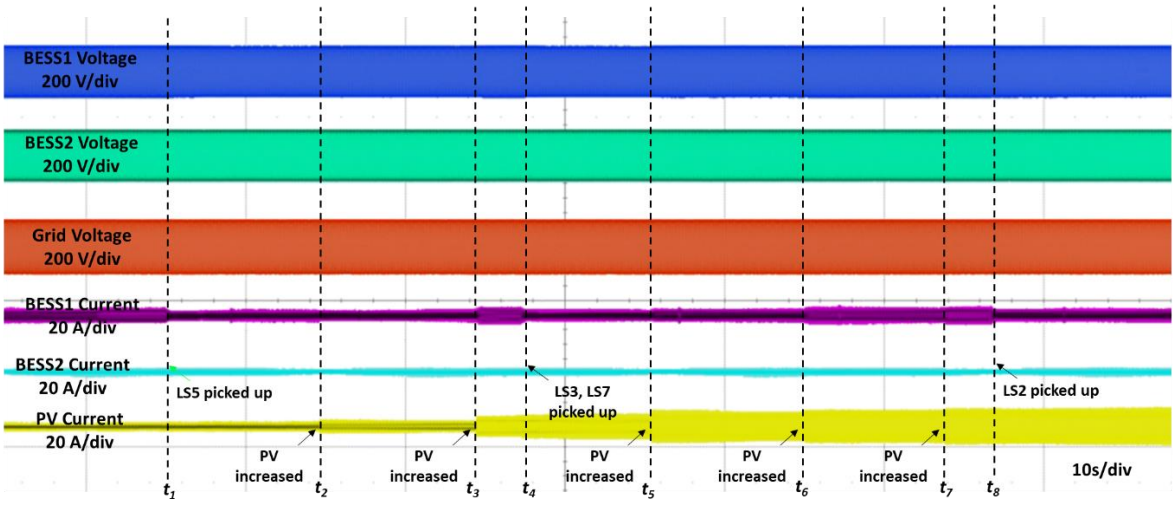


Fig. 5 - 14. Testing results for the islanded operation of two separate islands.

2) Two Separate Islands Merged to one island and Reconnected to the Grid

The second test case is to merge two islands and then reconnect to the main grid. As given in Fig. 5 - 17, before this reconnection, island 2 on the left was serving L1, while island 1 on the right was serving all other loads. These two islands are merged into a larger islanded microgrid first by closing switch 0102 through resynchronization and then reconnected to the main grid by closing switch 0200 through resynchronization. The voltage and current measurements during this process are shown in Fig. 5 - 18.

5.2.4 Islanding Test

1) Islanding from One Merged Island to Multiple Separate Islands

In one merged island, the PV output drops, and the BESSs outputs start to increase to support the load. Two BESSs both work in the grid-forming mode. As shown in Fig. 5 - 19, at time t_4, the PQ balance function is triggered by the decrease of PV output, which causes loads L5 and L7 to be dropped. The boundary of the island is shrunk.

When the generation in a merged island becomes insufficient to support the loads on the critical path that connects the source locations, the PQ balance function issues a command to trigger the planned island separating function at t_8. After t_8, the two islands are separate.

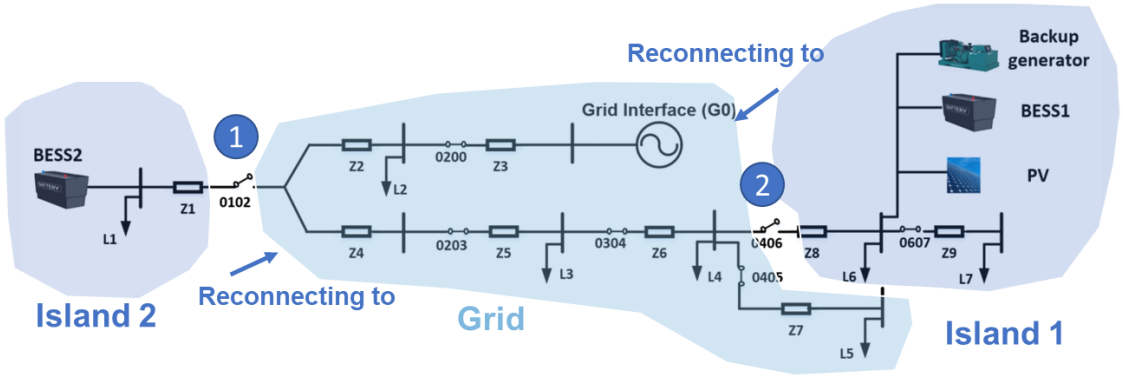


Fig. 5 - 15. Process of two separate islands reconnected to the main grid.

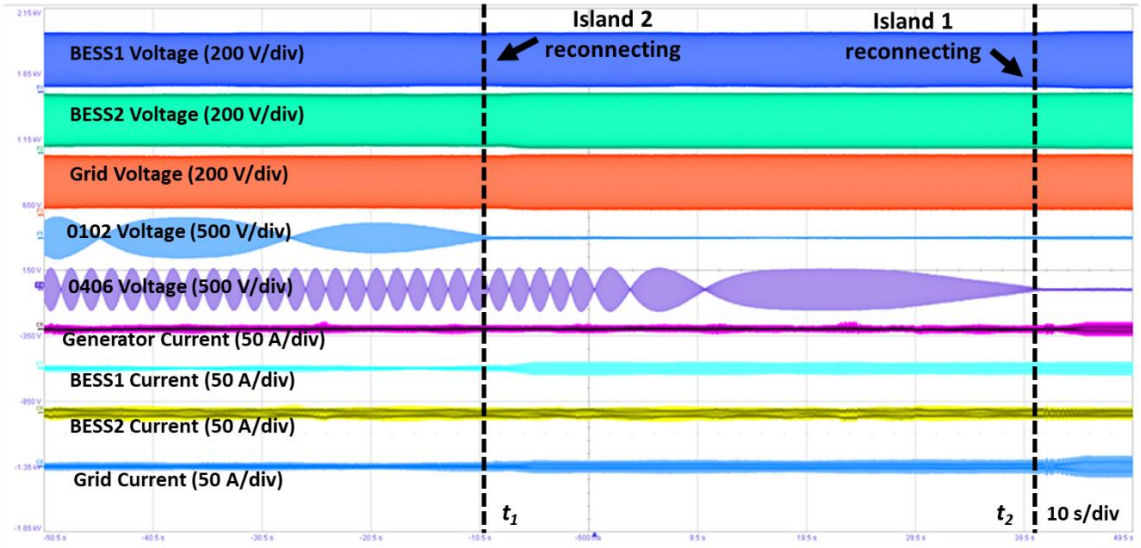


Fig. 5 - 16. Testing waveforms of two separate islands reconnecting to the main grid.

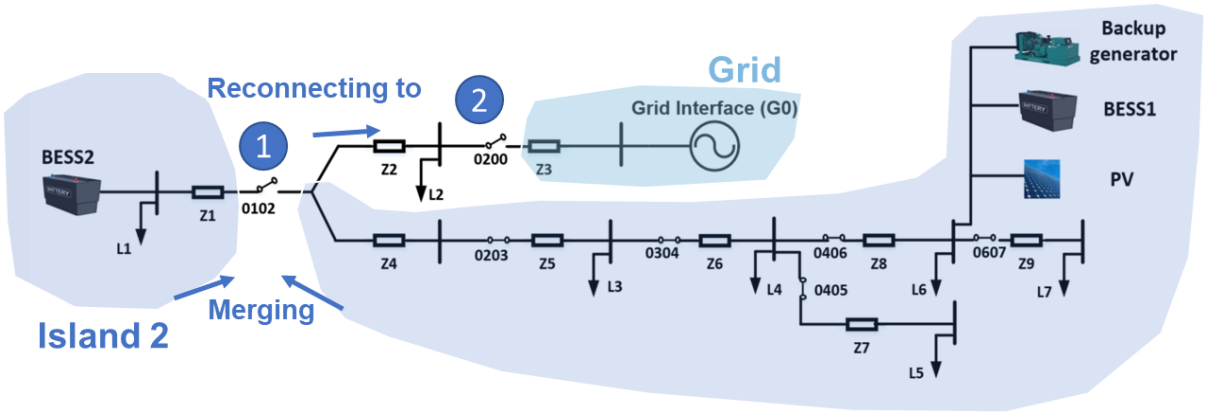


Fig. 5 - 17. Process of two separate islands merging to a large microgrid and reconnected to the grid.

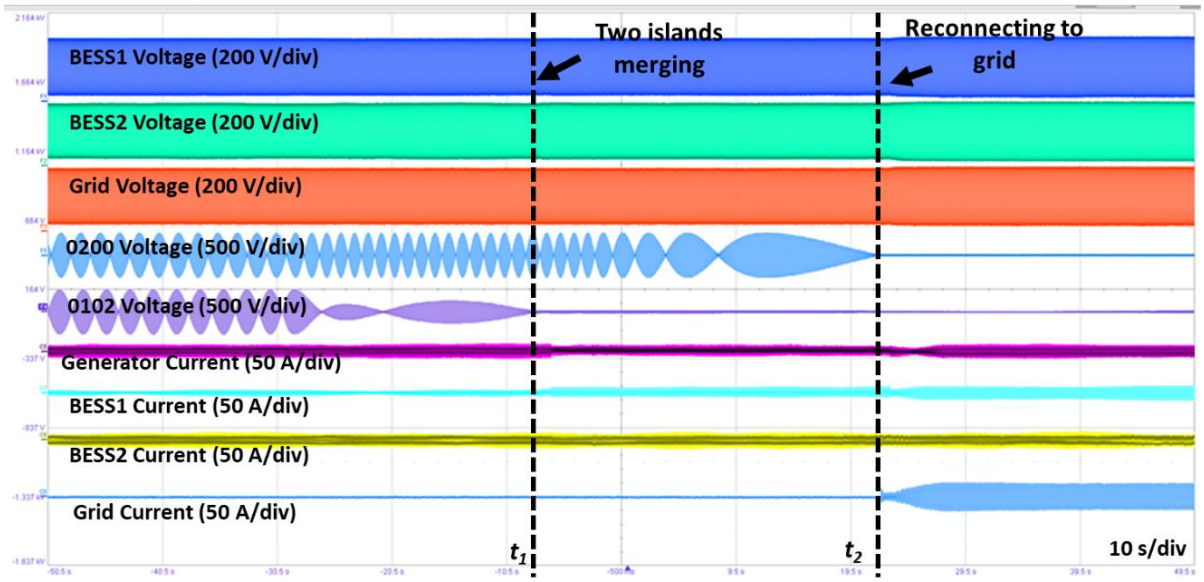


Fig. 5 - 18. Testing waveforms of two separate islands merging to a large microgrid and reconnecting to the grid.

2) Islanding from Grid-Connected Mode to One Merged Island

In the grid-connected mode, BESS emulators and the PV emulator are controlled as power sources. As shown in Fig. 5 - 20, when the load is picked up from t_1 to t_3, the load current is provided by the grid emulator. The planned islanding command is issued at t_4. During the planned islanding, the central controller minimizes the power flow, therefore, the BESS output power is decreased at t_4 and the planned islanding of switch 0200 happens at t_5. After the planned islanding, the grid is disconnected, and two BESS switch control modes to grid-forming mode to support the load in one merged island.

5.2.5 Steady-State Grid-Connected Operation Test

In the grid-connected mode, the energy management function is to minimize the overall cost of the microgrid by dispatching sources in an economic way. The load and PV forecasting data are applied as the input of the energy management. In the HTB testing, the load and PV forecasting algorithms are verified offline to generate profiles for the controller and the energy management function utilizes profiles to generate setpoints for sources. The generated setpoints are realized by the converter emulators in real-time. As shown in Fig. 5 - 21, the energy management function realization is demonstrated on the HTB. Based on the different load and PV output conditions, the outputs of two BESSs, the curtailment of PV, and microgrid boundaries are regulated by the energy management function. During this testing process, the grid voltage is stable, and sources can realize the commands required by the central controller.

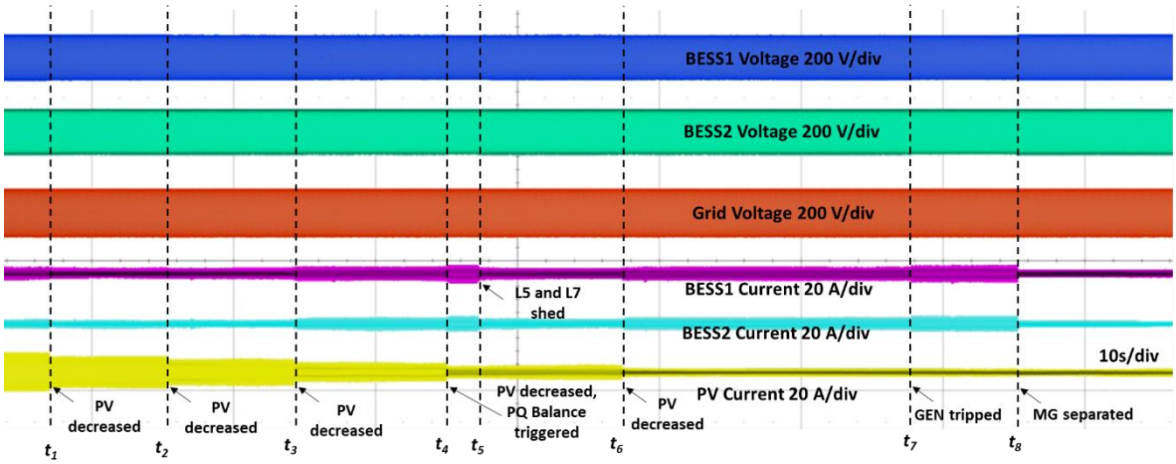


Fig. 5 - 19. Testing waveforms of planned island separating from one merged island to multiple separate islands.

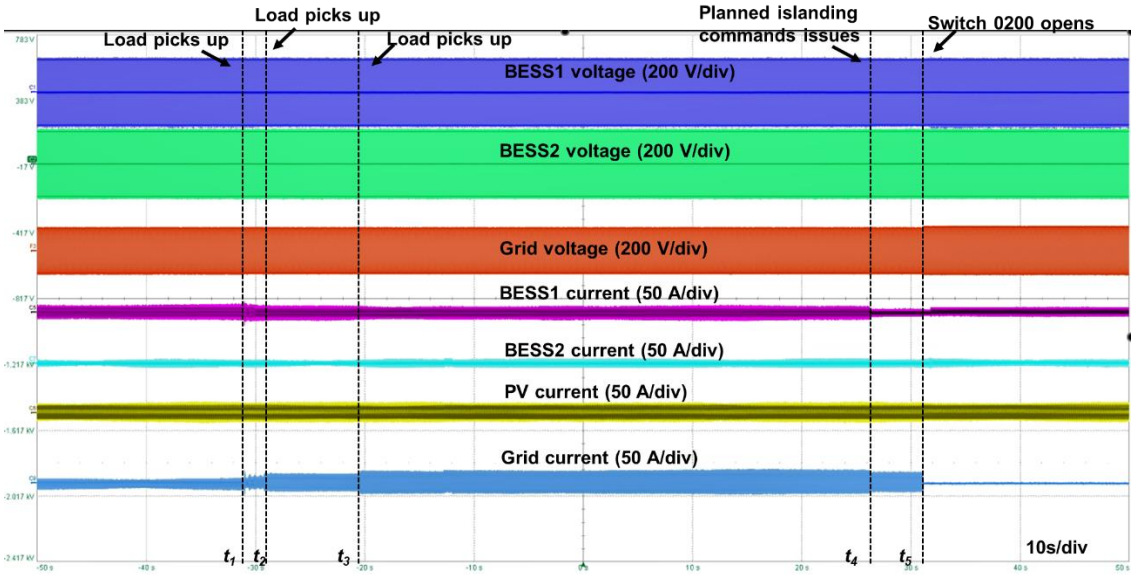


Fig. 5 - 20. Testing waveforms of planned islanding grid-connected mode to one merged island.

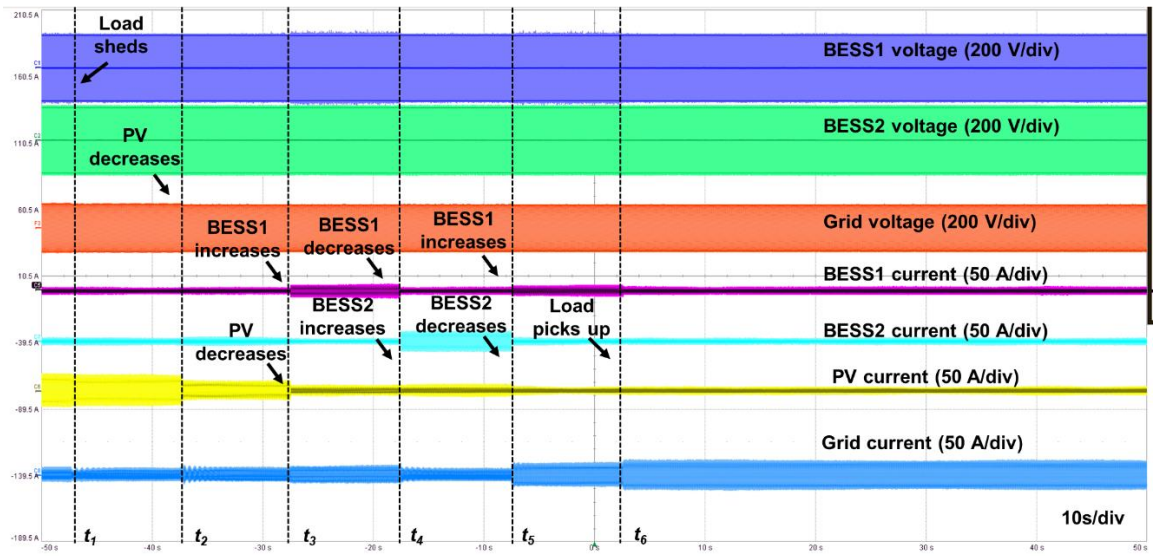


Fig. 5 - 21. Testing waveforms of energy management in the grid-connected mode.

5.3 Summary

The developed testing platform and the proposed BESS emulator are applied for testing two microgrid controllers, which are one microgrid with dynamic boundaries and one microgrid with dynamic boundaries and multiple sources at different locations, respectively. For each controller, different testing scenarios are considered and tested, including steady-state operation, transitions, and fault conditions.

Besides controller algorithm validation, the testing on HTB can provide more practical evaluations to the controller under testing. The testing on HTB evaluates the controller capability under actual power flow and measurement noise. Measurement noise requires digital filters in the microgrid controllers. Meanwhile, measurement noise impacts the threshold design of resynchronization control functions as thresholds may never be triggered due to the noise impacts.

Moreover, since the actual communication delay and switching actions can be modeled by nature in the HTB testing, the central controller functions, and coordination between central and local controller during transitions are verified through the HTB testing. Due to the communication delay and switch actions, the islanding transition commands from the central controller cannot arrive in time, which requires the coordination of the controller of BESSs.

CHAPTER 6. CONCLUSIONS AND FUTURE WORK

6.1 Conclusions

Microgrid controllers perform an indispensable role in existing and future microgrids. Before the actual field implementation, the testing and evaluation of controller performances are critical. To realize flexible testing without numerical oscillations, a converter-based microgrid HTB is developed for the microgrid controller testing.

The microgrid HTB is designed based on the real microgrids, where the microgrid components are emulated by power converters. The microgrid lines are emulated by air-core inductors, and the smart switches are emulated by a combination of contactors, sensors, and the boundary controller. The BESS is one of the essential components in the microgrid, which can increase the microgrid resilience in the grid-connected mode and form the microgrid voltage and frequency in the islanded mode.

Therefore, to realize the microgrid controller HTB testing, a BESS emulator is developed considering the requirements of different microgrid controller functions under different microgrid modes and conditions. The functions of the BESS emulator include:

- SOC indication for long-term operation.
- Flexible power control in steady-state grid-connected mode.
- Voltage and frequency forming capability in steady-state islanded mode. Primary and secondary regulations are also implemented.

- The ride-through capability of fault conditions in both grid-connected and islanded modes.
- Mode transition functions, including black start, islanding, and reconnection.

The developed microgrid HTB with proposed BESS emulators is applied for the evaluation of two microgrid controllers. Besides the basic function validation, through the HTB testing, the microgrid controller is evaluated from the following perspectives:

- The microgrid controller is operating under conditions with noise, including measurement noise from sensors and data transferring as well as electromagnetic noise from actual power flow. To reduce the impacts of measurement noise, digital filters are applied for controller data processing. Furthermore, during the reconnection transition, the switch closing-related thresholds are redesigned considering the noise impact.
- The microgrid controller is operating with actual communication delays and coordination with actual local controllers. Local support functions (local islanding detection, etc.) are needed to support the microgrid operation and the central controller needs to coordinate with the local support functions.
- The microgrid controller is operating with real power flow and mechanical switching actions of smart switches. The local controller needs to coordinate with the central controller to deal with the impact of mechanical switching actions. Meanwhile, during transitions or other transients in the microgrid, the protection of converter emulators may be triggered to disable the

microgrid operation, which requires solutions from controllers. However, in the digital simulation, short transients may be ignored as no actual protection is modeled in microgrid components such as PVs and BESSs.

6.2 Future Work

In terms of the microgrid HTB emulation, the developed HTB can only emulate balanced load and fault conditions. As one important feature of distribution grids, load unbalance can also potentially have requirements on microgrid controllers. Moreover, the unbalanced fault condition is also common in microgrids. To emulate the unbalance in the microgrid, both the models of converter emulators and the topology cabinet need to be updated.

Due to the limitations of line impedance values and converter hardware ratings, existing microgrid HTB can only emulate high impedance fault. However, low impedance faults are widely observed in microgrids, which challenges the protection coordination function of microgrid controllers. The microgrid HTB should be improved to emulate low impedance to further support the microgrid protection-related testing.

In this work, BESS emulators only consider the support of microgrid controller testing under balanced microgrid conditions. When the load or fault is unbalanced, the BESS emulators also need to update the control to support the unbalance, especially in islanded operation. Furthermore, virtual impedance is applied to the BESS emulators to improve the power sharing among different

inverters, which may destabilize the microgrid in some conditions. Therefore, the virtual impedance impacts need to be further investigated in the future.

REFERENCES

[1] N. Pogaku, M. Prodanovic and T. C. Green, "Modeling, Analysis and Testing of Autonomous Operation of an Inverter-Based Microgrid," *IEEE Transactions on Power Electronics*, vol. 22, no. 2, pp. 613-625, March 2007.

[2] Y. Zhang, N. Gatsis and G. B. Giannakis, "Robust Energy Management for Microgrids With High-Penetration Renewables," *IEEE Transactions on Sustainable Energy*, vol. 4, no. 4, pp. 944-953, Oct. 2013.

[3] H. Mahmood, D. Michaelson, and J. Jiang, "Accurate Reactive Power Sharing in an Islanded Microgrid Using Adaptive Virtual Impedances," *IEEE Transactions on Power Electronics*, vol. 30, no. 3, pp. 1605-1617, March 2015.

[4] R. H. Lasseter and P. Paigi, "Microgrid: a conceptual solution," in *Proc*. *IEEE 35th Annual Power Electronics Specialists Conference (IEEE Cat. No.04CH37551)*, Germany, 2004, pp. 4285-4290.

[5] S. F. Zarei, H. Mokhtari, and M. A. Ghasemi, "Enhanced control of grid forming VSCs in a micro-grid system under unbalanced conditions," in *Proc*. *9th Annual Power Electronics, Drives Systems and Technologies Conference (PEDSTC)*, Tehran, Iran, 2018, pp. 380-385.

[6] "IEEE Standard for the Specification of Microgrid Controllers," *IEEE Std 2030.7-2017*, vol., no., pp.1-43, 23 April 2018.

[7] S. F. Zarei, H. Mokhtari and F. Blaabjerg, "Fault Detection and Protection Strategy for Islanded Inverter-Based Microgrids," *IEEE Journal of Emerging and Selected Topics in Power Electronics*, vol. 9, no. 1, pp. 472-484, Feb. 2021.

[8] D. Shi *et al*., "A Distributed Cooperative Control Framework for Synchronized Reconnection of a Multi-Bus Microgrid," *IEEE Transactions on Smart Grid*, vol. 9, no. 6, pp. 6646-6655, Nov. 2018.

[9] M. E. Nassar, M. M. A. Salama, "Adaptive self-adequate microgrids using dynamic boundaries", *IEEE Transactions on Smart Grid*, vol. 7, no. 1, pp. 105-113, Jan. 2016.

[10] F. Wang, Y. Liu, L. Tolbert, X. Shi, L. Zhu, Y. Ma, “MICROGRIDS WITH DYNAMICALLY CONFIGURABLE BOUNDARIES INCLUDING MULTIPLE MAIN GRID FEEDER COUPLING LOCATIONS AND METHODS OF OPERATING THE SAME” US Patent Application Serial No. 15/809,329, Filed: November 10, 2017.

[11] X. Hu, *et al*., "Real-time power management technique for microgrid with flexible boundaries." *IET Generation, Transmission & Distribution*, vol. 14, no. 2, pp. 3161-3170, May 2020.

[12] A. Hooshyar and R. Iravani, "Microgrid Protection," *Proceedings of the IEEE*, vol. 105, no. 7, pp. 1332-1353, July 2017.

[13] Y. Ma *et al*., "Real-Time Control and Operation for a Flexible Microgrid with Dynamic Boundary," in *Proc*. *IEEE Energy Conversion Congress and Exposition (ECCE)*, USA, 2018, pp. 5158-5163.

[14] "IEEE Standard for the Testing of Microgrid Controllers," *IEEE Std 2030.8-2018*, vol., no., pp.1-42, 24 Aug. 2018.

[15] K. Yu, Q. Ai, S. Wang, J. Ni, and T. Lv, "Analysis and Optimization of Droop Controller for Microgrid System Based on Small-Signal Dynamic Model," *IEEE Transactions on Smart Grid*, vol. 7, no. 2, pp. 695-705, March 2016.

[16] K. Prabakar, A. Pratt, D. Krishnamurthy, and A. Maitra, "Hardware-in-the-Loop Test Bed and Test Methodology for Microgrid Controller Evaluation," in *Proc*. *IEEE/PES Transmission and Distribution Conference and Exposition (T&D)*, USA, 2018, pp. 1-9.

[17] T. Funabashi, G. Fujita, K. Koyanagi, and R. Yokoyama, "Field Tests of a Microgrid Control System," in *Proc*. *Proceedings of the 41st International Universities Power Engineering Conference*, UK, 2006, pp. 232-236.

[18] Jin-Hong Jeon, Jong-Yul Kim, Seul-Ki Kim, Ong-Bo Ahn, and J. Park, "Development of HILS(Hardware In-Loop Simulation) system for MMS(Microgrid Management System) by using RTDS," in *Proc*. *13th International Power Electronics and Motion Control Conference*, Poland, 2008, pp. 2492-2497.

[19] M. H. Khooban, N. Vafamand, T. Dragicevic, M. M. Mardani, and R. Heydari, "Modeling and HiL Real-Time Simulation for the Secondary LFC in Time-Delay Shipboard Microgrids," in *Proc*. *IEEE International Conference on Electrical Systems for Aircraft, Railway, Ship Propulsion, and Road Vehicles & International Transportation Electrification Conference (ESARS-ITEC)*, UK, 2018, pp. 1-5.

[20] K. Prabakar, A. Pratt, D. Krishnamurthy, and A. Maitra, "Hardware-in-the-Loop Test Bed and Test Methodology for Microgrid Controller Evaluation," *IEEE/PES Transmission and Distribution Conference and Exposition (T&D)*, USA, 2018, pp. 1-9.

[21] A. Genić, P. Gartner, D. Medjo and M. Dinić, "Multi-layer hardware-in-the-loop testbed for microgrids," in *Proc*. *International Conference on Smart Systems and Technologies (SST)*, Croatia, 2016, pp. 95-102.

[22] J. Wang, Y. Song, W. Li, J. Guo, and A. Monti, "Development of a Universal Platform for Hardware In-the-Loop Testing of Microgrids," *IEEE Transactions on Industrial Informatics*, vol. 10, no. 4, pp. 2154-2165, Nov. 2014.

[23] K. Prabakar *et al*., "Site-Specific Evaluation of Microgrid Controller Using Controller and Power-Hardware-in-the-Loop," in *Proc*. *IECON 2019 - 45th*

Annual Conference of the IEEE Industrial Electronics Society, Portugal, 2019, pp. 6463-6468.

[24] B. Aluisio *et al*., "Advancements of field tests in PrInCE lab experimental microgrid," in *Proc*. *AEIT International Annual Conference*, Italy, 2018, pp. 1-6.

[25] J. Stevens, H. Vollkommer and D. Klapp, "CERTS Microgrid System Tests," *IEEE Power Engineering Society General Meeting*, USA, 2007, pp. 1-4.

[26] P. Chirapongsananurak, S. Santoso and A. Maitra, "Operating fixed-speed and wide-slip wind turbines in isolated microgrids," *IEEE Power & Energy Society General Meeting*, USA, 2015, pp. 1-5.

[27] C. Wang, J. Li, and Y. Hu, "Frequency Control of Isolated Wind-Diesel Microgrid Power System by Double Equivalent-Input-Disturbance Controllers," *IEEE Access*, vol. 7, pp. 105617-105626, 2019.

[28] M. Patterson, N. F. Macia, and A. M. Kannan, "Hybrid Microgrid Model Based on Solar Photovoltaic Battery Fuel Cell System for Intermittent Load Applications," *IEEE Transactions on Energy Conversion*, vol. 30, no. 1, pp. 359-366, March 2015.

[29] F. Chishti, S. Murshid, and B. Singh, "Development of Wind and Solar Based AC Microgrid With Power Quality Improvement for Local Nonlinear Load Using MLMS," *IEEE Transactions on Industry Applications*, vol. 55, no. 6, pp. 7134-7145, Nov.-Dec. 2019.

[30] M. T. Lawder *et al*., "Battery Energy Storage System (BESS) and Battery Management System (BMS) for Grid-Scale Applications," *Proceedings of the IEEE*, vol. 102, no. 6, pp. 1014-1030, June 2014.

[31] A. T. Elsayed, C. R. Lashway and O. A. Mohammed, "Advanced Battery Management and Diagnostic System for Smart Grid Infrastructure," *IEEE Transactions on Smart Grid*, vol. 7, no. 2, pp. 897-905, March 2016.

[32] O. Adeyemo, P. Idowu, A. Asrari, and J. Khazaei, "Reactive Power Control for Multiple Batteries Connected in Parallel Using Modified Power Factor Method," in *Proc*. *North American Power Symposium (NAPS)*, USA, 2018, pp. 1-6.

[33] L. K. Gan, J. K. H. Shek, and M. A. Mueller, "Modelling and experimentation of grid-forming inverters for standalone hybrid wind-battery systems," in *Proc*. *International Conference on Renewable Energy Research and Applications (ICRERA)*, Italy, 2015, pp. 449-454.

[34] J. Chiasson and B. Vairamohan, "Estimating the state of charge of a battery," *IEEE Transactions on Control Systems Technology*, vol. 13, no. 3, pp. 465-470, May 2005.

[35] M. Farrokhabadi, S. König, C. A. Cañizares, K. Bhattacharya and T. Leibfried, "Battery Energy Storage System Models for Microgrid Stability Analysis and Dynamic Simulation," *IEEE Transactions on Power Systems*, vol. 33, no. 2, pp. 2301-2312, March 2018.

[36] H. Zhao, M. Hong, W. Lin, and K. A. Loparo, "Voltage and Frequency Regulation of Microgrid With Battery Energy Storage Systems," *IEEE Transactions on Smart Grid*, vol. 10, no. 1, pp. 414-424, Jan. 2019.

[37] L. Yang *et al*., "Development of converter based reconfigurable power grid emulator," in *Proc*. *IEEE Energy Conversion Congress and Exposition (ECCE)*, USA, 2014, pp. 3990-3997.

[38] Y. Ma, J. Wang, F. Wang, and L. M. Tolbert, "Converter-based reconfigurable real-time electrical system emulation platform," *Chinese Journal of Electrical Engineering*, vol. 4, no. 1, pp. 20-27, March 2018.

[39] Lin Zhu *et al*., "Adaptive and coordinated oscillation damping control using measurement-driven approach," in *Proc. Power Systems Computation Conference (PSCC)*, Italy, 2016, pp. 1-7.

[40] F. Hu *et al*., "Measurement-based voltage stability assessment and control on CURENT hardware test bed system," in *Proc. IEEE Power and Energy Society General Meeting (PESGM)*, USA, 2016, pp. 1-5.

[41] I. Kosen *et al*., "UPS: Unified PMU-Data Storage System to Enhance T+D PMU Data Usability," *IEEE Transactions on Smart Grid*, vol. 11, no. 1, pp. 739-748, Jan. 2020.

[42] L. Wang *et al*., "Frequency Disturbance Recorder Design and Developments," in *Proc. IEEE Power Engineering Society General Meeting*, Tampa, FL, USA, 2007, pp. 1-7.

[43] L. Yang *et al*., "Three-Phase Power Converter-Based Real-Time Synchronous Generator Emulation," *IEEE Transactions on Power Electronics*, vol. 32, no. 2, pp. 1651-1665, Feb. 2017.

[44] L. Yang *et al*., "Stability analysis of inverter based generator emulator in test-bed for power systems," in *Proc. IEEE Energy Conversion Congress and Exposition*, USA, 2013, pp. 5410-5417.

[45] Y. Ma, W. Cao, L. Yang, F. Wang, and L. M. Tolbert, "Virtual Synchronous Generator Control of Full Converter Wind Turbines With Short-Term Energy Storage," *IEEE Transactions on Industrial Electronics*, vol. 64, no. 11, pp. 8821-8831, Nov. 2017.

[46] W. Cao *et al*., "Two-stage PV inverter system emulator in converter based power grid emulation system," in *Proc. IEEE Energy Conversion Congress and Exposition*, Denver, CO, USA, 2013, pp. 4518-4525.

[47] J. D. Boles, Y. Ma, J. Wang, D. Osipov, L. M. Tolbert, and F. Wang, "Converter-Based Emulation of Battery Energy Storage Systems (BESS) for Grid Applications," *IEEE Transactions on Industry Applications*, vol. 55, no. 4, pp. 4020-4032, July-Aug. 2019.

[48] S. Zhang, B. Liu, S. Zheng, Y. Ma, F. Wang, and L. M. Tolbert, "Development of a Converter-Based Transmission Line Emulator With Three-Phase Short-Circuit Fault Emulation Capability," *IEEE Transactions on Power Electronics*, vol. 33, no. 12, pp. 10215-10228.

[49] J. Wang *et al*., "Static and dynamic power system load emulation in a converter-based reconfigurable power grid emulator," *IEEE Transactions on Power Electronics*, vol. 31, no. 4, pp. 3239-3251, April 20.

[50] Y. Ma, L. Yang, F. Wang, and L. M. Tolbert, "Voltage closed-loop virtual synchronous generator control of full converter wind turbine for grid-connected and stand-alone operation," *in Proc. IEEE Applied Power Electronics Conference and Exposition (APEC)*, USA, 2016, pp. 1261-1266.

[51] F. Bai, L. Zhu, Y. Liu, X. Wang, K. Sun, Y. Ma, M. Patel, E. Farantatos, and N. Bhatt, “Design and implementation of a measurement-based adaptive wide-area damping controller considering time delays,” *Electric Power Systems Research*, vol. 130, pp. 1-9, 2016.

[52] W. Cao, Y. Ma, L. Yang, F. Wang, and L. M. Tolbert, "D–Q Impedance Based Stability Analysis and Parameter Design of Three-Phase Inverter-Based AC Power Systems," *IEEE Transactions on Industrial Electronics*, vol. 64, no. 7, pp. 6017-6028, July 2017.

[53] M. Daowd, N. Omar, P. Van Den Bossche, and J. Van Mierlo, "Passive and active battery balancing comparison based on MATLAB simulation," in *Proc. IEEE Vehicle Power and Propulsion Conference*, USA, 2011, pp. 1-7.

[54] J. Gallardo-Lozano, E. Romero-Cadaval, M.I. Milanes-Montero, and M.A. Guerrero-Martinez, "Battery equalization active methods," *Journal of Power Sources*, 246, pp. 934-949, 2014.

[55] D. Xu, L. Wang, and J. Yang, "Research on Li-ion Battery Management System," in *Proc. International Conference on Electrical and Control Engineering*, China, 2010, pp. 4106-4109.

[56] A. Govindaraj, S. M. Lukic, and A. Emadi, "A novel scheme for optimal paralleling of batteries and ultracapacitors," in *Proc. IEEE Energy Conversion Congress and Exposition*, USA, 2009, pp. 1410-1416.

[57] H. Park, C. Kim, G. Moon, J. Lee, and J. K. Oh, "Two-Stage Cell Balancing Scheme for Hybrid Electric Vehicle Lithium-Ion Battery Strings," in *Proc. IEEE Power Electronics Specialists Conference*, USA, 2007, pp. 273-279.

[58] C. Young, N. Chu, L. Chen, Y. Hsiao, and C. Li, "A Single-Phase Multilevel Inverter With Battery Balancing," *IEEE Transactions on Industrial Electronics*, vol. 60, no. 5, pp. 1972-1978, May 2013.

[59] R. Xiong, J. Cao, Q. Yu, H. He, and F. Sun, "Critical Review on the Battery State of Charge Estimation Methods for Electric Vehicles," *IEEE Access*, vol. 6, pp. 1832-1843, 2018.

[60] Z. He, Z. Yang, X. Cui, and E. Li, "A Method of State-of-Charge Estimation for EV Power Lithium-Ion Battery Using a Novel Adaptive Extended Kalman Filter," *IEEE Transactions on Vehicular Technology*, vol. 69, no. 12, pp. 14618-14630, Dec. 2020.

[61] A. P. Schmidt, M. Bitzer, Á. W. Imre, and L. Guzzella, ‘‘Experiment-driven electrochemical modeling and systematic parameterization for a lithium-ion battery cell,’’ *Journal of Power Sources*, vol. 195, no. 15, pp. 5071–5080, 2010.

[62] S. Lee, J. Kim, J. Lee, and B. H. Cho, ‘‘State-of-charge and capacity estimation of lithium-ion battery using a new open-circuit voltage versus state-of-charge,’’ *Journal of Power Sources*, vol. 185, no. 2, pp. 1367–1373, 2008.

[63] J. Xu, C. C. Mi, B. Cao, and J. Cao, ‘‘A new method to estimate the state of charge of lithium-ion batteries based on the battery impedance model,’’ *Journal of Power Sources*, vol. 233, pp. 277–284, Jul. 2013.

[64] X. Zhao-Xia, Z. Mingke, H. Yu, J. M. Guerrero, and J. C. Vasquez, "Coordinated Primary and Secondary Frequency Support Between Microgrid and Weak Grid," *IEEE Transactions on Sustainable Energy*, vol. 10, no. 4, pp. 1718-1730, Oct. 2019.

[65] I. S. Jha, S. Sen, M. Tiwari, and M. K. Singh, "Control strategy for Frequency Regulation using Battery Energy Storage with optimal utilization," in *Proc. IEEE 6th India International Conference on Power Electronics (IICPE)*, India, 2014, pp. 1-4.

[66] D. Stroe, V. Knap, M. Swierczynski, A. Stroe and R. Teodorescu, "Operation of a Grid-Connected Lithium-Ion Battery Energy Storage System for Primary Frequency Regulation: A Battery Lifetime Perspective," in *IEEE Transactions on Industry Applications*, vol. 53, no. 1, pp. 430-438, Jan.-Feb. 2017.

[67] X. Xu, M. Bishop, D. G. Oikarinen and C. Hao, "Application and modeling of battery energy storage in power systems," *CSEE Journal of Power and Energy Systems*, vol. 2, no. 3, pp. 82-90, Sept. 2016.

[68] J. Gouveia, C. L. Moreira, and J. A. P. Lopes, "Grid-Forming Inverters Sizing in Islanded Power Systems – a stability perspective," in *Proc. International*

Conference on Smart Energy Systems and Technologies (SEST), Portugal, 2019, pp. 1-6.

[69] W. Gao, "Microgrid Control Strategy Based on Battery Energy Storage System-Virtual Synchronous Generator (BESS-VSG)," in *Proc. IEEE Kansas Power and Energy Conference (KPEC)*, USA, 2020, pp. 1-6.

[70] Y. A. I. Mohamed and A. A. Radwan, "Hierarchical Control System for Robust Microgrid Operation and Seamless Mode Transfer in Active Distribution Systems," *IEEE Transactions on Smart Grid*, vol. 2, no. 2, pp. 352-362, June 2011.

[71] I. Serban and C. Marinescu, "Control Strategy of Three-Phase Battery Energy Storage Systems for Frequency Support in Microgrids and with Uninterrupted Supply of Local Loads," *IEEE Transactions on Power Electronics*, vol. 29, no. 9, pp. 5010-5020, Sept. 2014.

[72] Z. Guo, "A harmonic current injection control scheme for active islanding detection of grid-connected inverters," in *Proc. IEEE International Telecommunications Energy Conference (INTELEC)*, Japan, 2015, pp. 1-5.

[73] J. Li, X. Li, Y. Zhang, S. Hao, and Y. Jia, "A Centralized Injection Method for Islanding Detection in Micro-Grids," in *Proc. Asia-Pacific Power and Energy Engineering Conference*, Shanghai, China, 2012, pp. 1-3.

[74] Chen Yunping and Zhangxia, "A study on mathematical model, calculation and physical mechanism of transmission lines with mutual inductance," in *Proc*. *Proceedings. International Conference on Power System Technology*, China, 2002, pp. 2116-2121.

[75] R. T. Naayagi and A. J. Forsyth, "Design of high frequency air-core inductor for DAB converter," in *Proc. IEEE International Conference on Power Electronics, Drives and Energy Systems (PEDES)*, Bengaluru, India, 2012, pp. 1-4.

[76] H. Yin, Y. Ma, X. Hu, Y. Su, J. Glass, F. Wang, Y. Liu, and L. M. Tolbert, " Hierarchical control system for a flexible microgrid with dynamic boundary: design, implementation and testing," *IET Smart Grid,* vol. 2, no. 4, pp. 669-676, 2019.

[77] "IEEE Standard for Interconnection and Interoperability of Distributed Energy Resources with Associated Electric Power Systems Interfaces," *IEEE Std 1547-2018 (Revision of IEEE Std 1547-2003)*, vol., no., pp.1-138, 6 April 2018.

[78] W. Du *et al*., "A Comparative Study of Two Widely Used Grid-Forming Droop Controls on Microgrid Small-Signal Stability," *IEEE Journal of Emerging and Selected Topics in Power Electronics*, vol. 8, no. 2, pp. 963-975, June 2020.

[79] H. Zhang, S. Kim, Q. Sun and J. Zhou, "Distributed Adaptive Virtual Impedance Control for Accurate Reactive Power Sharing Based on Consensus Control in Microgrids," *IEEE Transactions on Smart Grid*, vol. 8, no. 4, pp. 1749-1761, July 2017.

[80] R. Razi, H. Iman-Eini, M. Hamzeh, and S. Bacha, "A Novel Extended Impedance-Power Droop for Accurate Active and Reactive Power Sharing in a Multi-Bus Microgrid With Complex Impedances," *IEEE Transactions on Smart Grid*, vol. 11, no. 5, pp. 3795-3804, Sept. 2020.

[81] D. Li *et al*., "Development of a Converter Based Microgrid Test Platform," in *Proc. IEEE Energy Conversion Congress and Exposition (ECCE)*, USA, 2019, pp. 6294-6300.

VITA

Dingrui Li was born in Xining, Qinghai Province in China. He started his undergraduate study in Tsinghua University in 2013 at Beijing, China. He graduated with a bachelor's degree in Electrical Engineering in 2017. His graduate study in the University of Tennessee, Knoxville began from 2017. He is now a PhD student whose research area focuses on the high voltage power electronics control and power electronics applications in power grids.